

MULTIDIMENSIONAL SEPARATIONS IN COMPLEX BIOLOGICAL MATRICES  
UTILIZING CHROMATOGRAPHY, ION MOBILITY, AND MASS SPECTROMETRY

By

Don E. Davis, Jr.

Dissertation

Submitted to the Faculty of the  
Graduate School of Vanderbilt University  
in partial fulfillment of the requirements

for the degree of

DOCTOR OF PHILOSOPHY

in

Chemistry

May 14<sup>th</sup>, 2021


Nashville, TN

Approved:

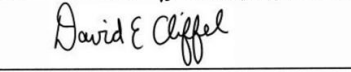
John A. McLean, Ph.D.



David E. Cliffel, Ph.D.



Lauren E. Buchanan, Ph.D.



Jennifer M. Colby, Ph.D.



Date:

3-19-21

3/22/21

3/22/2021

3/20/2021

*This dissertation is dedicated to my Family,  
Tiffany Davis, who has always been my most significant source of inspiration,  
encouragement, and has always kept me on the right path, to my parents, Don Davis, Sr. and  
Marilyn Davis, who have molded me into the man I am today, and to my wife and son, Ashley  
Davis and Don Davis, III., who are my source of complete peace and joy.*

## ACKNOWLEDGEMENTS

I want to thank my dissertation advisor, Dr. John A. McLean, for giving me the opportunity to join the McLean Research Group and allowing me to explore my interests under his direction and guidance throughout the entire process. I am very fortunate to have developed my scientific skills in his lab, featuring the latest innovative analytical technology. In the end, I had a great time and gained an array of marketable skill sets. Thank you for your encouragement, mentorship, expertise, and patience throughout my time in your lab.

Three other insightful professors have also guided my research as my committee members – Dr. David Cliffler, Dr. Lauren Buchanan, and Dr. Jennifer Colby. Their support, insightful questions, and suggestions have improved my critical thinking skills and strengthen my research. Thank you for your time, feedback along the way, and for providing me your differences in perspective, which has helped me see the bigger picture of scientific research and how it all connects.

I would also like to acknowledge Dr. Stacy Sherrod and Dr. Jody May for their numerous editing and mentorship hours for the past six years. I am deeply grateful for your training and advice, which has greatly strengthened my scientific knowledge.

I want to acknowledge my graduate school coaches/mentors, Dr. Renã Robinson and Dr. Don Brunson. Without them, I would not have known how to navigate the gruesome process of graduate school successfully.

I would like to acknowledge the many collaborators who have contributed to my dissertation research: Dr. Stacy Sherrod, Dr. Randi Gant-Branum, Dr. Simona Codreanu, Dr. Jennifer Colby, Dr. Jody May, Ms. Amelia Taylor, Dr. Katrina Leaptrot, Mr. David Koomen, Dr.

Gustavo Cavalcanti, Dr. Monica Padilha, Dr. Henrique Pereira, and Dr. Fiona Harrison. I have learned many new things through our work together.

I want to acknowledge my colleagues in the McLean Research Group for helping me with presentations, proofreading my papers, and enduring countless hours of troubleshooting instrumentation. I wish the best for you throughout life in all aspects. Thank you to those who came before and after me in the McLean Research Group, whom I have learned from and taught throughout the years. Honestly, me teaching others has taught me a great deal about myself. The first person I met in the McLean Research Group, Dr. James Dodds, acclimated me into the world of multidimensional separations using chromatography, ion mobility, and mass spectrometry.

I would not have realized my love for Chemistry without the inspiration and enthusiasm of the outstanding professors at Tougaloo College in Jackson, Mississippi: Dr. Wendy White, Dr. Richard McGinnis, Dr. Bidisha Sengupta, Dr. George Armstrong, Dr. Bianca Garner, Dr. Scharri Walker, Dr. Dexter Whitley, Dr. Pradip Biswas, Dr. Santanu Banerjee, Dr. Rajender Trahan, Dr. Manliang Feng, Dr. Jinghe Mao, and Dr. Lianna Li. Thank you for everything.

I want to acknowledge my extended family and friends who have provided support for me over these past six years. Listening to me speak about my scientific endeavors might not have been that interesting, but you always gave me the best advice and encouragement.

Last but not least, I would like to acknowledge the funding sources for this research: the Vanderbilt Center for Innovative Technology, College of Arts and Sciences, Department of Chemistry, Institute of Chemical Biology, Institute for Integrative Biosystems Research and Education, Vanderbilt-Ingram Cancer Center, Department of Pathology, Microbiology, and Immunology at Vanderbilt University Medical Center, the National Institutes of Health (National Cancer Institutes R03CA222452), the Partnership for Clean Competition (PCC), the Mitchum E.

Warren Fellowship program (Vanderbilt University), and the Graduate Assistantship in Areas of National Need (GAANN) fellowship (Department of Education). Their generous grants funded my research projects.

## TABLE OF CONTENTS

|  | Page |
|--|------|
| DEDICATION.....  | ii   |
| ACKNOWLEDGEMENTS.....  | iii  |
| LIST OF TABLES.....  | ix   |
| LIST OF FIGURES.....   | x    |
| CHAPTER  |      |
| Introduction.....  | 1    |
| State of the Field and Personal Contributions.....   | 1    |
| 1. The Development, Validation, and Application of a Clinical LC-MS/MS Method for the Quantification of Anti-Epileptic Drugs in Human Serum..... | 9    |
| 1.1. Introduction.....   | 9    |
| 1.2. Material and Methods.....   | 12   |
| 1.2.1. Serum Samples.....  | 12   |
| 1.2.2. Chromatographic Conditions.....   | 12   |
| 1.2.3. MS/MS Conditions.....   | 15   |
| 1.2.4. Sample Preparation.....   | 15   |
| 1.2.5. Method Validation.....  | 17   |
| 1.2.6. Precision and Accuracy.....   | 17   |
| 1.2.7. Linearity and LOQ.....  | 17   |
| 1.2.8. Carryover.....  | 18   |
| 1.2.9. Stability.....  | 18   |
| 1.2.10. Recovery.....  | 18   |
| 1.2.11. Matrix Effects.....  | 19   |
| 1.2.12. Selectivity.....   | 19   |
| 1.3. Results of Method Validation.....   | 19   |
| 1.3.1. Linearity and LOQ.....  | 19   |
| 1.3.2. Precision, Accuracy, and Carryover.....   | 20   |
| 1.3.3. Recovery and Matrix Effect.....   | 20   |
| 1.3.4. Selectivity and Stability.....  | 20   |
| 1.3.5. Method Comparison.....  | 23   |
| 1.4. Discussion.....   | 23   |
| 1.5. Conclusions.....  | 27   |
| 1.6. Acknowledgements.....   | 27   |
| 1.7. References.....   | 27   |

|   |    |
|---|----|
| 2. Elucidating Peripheral Amino Acid Changes in Obesity and Alzheimer’s Disease Using Metabolomics Based LC-MS/MS and LC-HRMS/MS..... | 31 |
| 2.1. Introduction.....  | 31 |
| 2.2. Experimental Methods.....  | 34 |
| 2.2.1. Standards and Chemicals.....   | 34 |
| 2.2.2. Human Plasma Samples.....  | 34 |
| 2.2.3. Mice Peripheral Tissue Samples.....  | 35 |
| 2.2.4. Plasma and Liver Sample Preparation.....   | 35 |
| 2.2.5. Chromatographic Conditions.....  | 36 |
| 2.2.6. MS/MS and High-Resolution MS/MS Conditions.....  | 37 |
| 2.2.7. Method Validation.....   | 39 |
| 2.2.8. Method Application.....  | 39 |
| 2.3. Results and Discussion.....  | 42 |
| 2.3.1. Method Validation.....   | 42 |
| 2.3.2. Method Application.....  | 42 |
| 2.4. Conclusions.....   | 49 |
| 2.5. Acknowledgements.....  | 50 |
| 2.6. References.....  | 50 |
| 3. Targeted Strategy to Analyze Anti-Epileptic Drugs in Human Serum by LC-MS/MS and LC-Ion Mobility-MS.....                           | 58 |
| 3.1. Introduction.....  | 58 |
| 3.2. Experimental Methods.....  | 62 |
| 3.2.1. Standards and Chemicals.....   | 62 |
| 3.2.2. Human Serum Samples.....   | 62 |
| 3.2.3. Human Serum Extraction and Preparation.....  | 62 |
| 3.2.4. Chromatographic Conditions.....  | 63 |
| 3.2.5. MS/MS and DTIMS-MS Conditions.....   | 64 |
| 3.2.6. Method Validation.....   | 67 |
| 3.3. Results and Discussion.....  | 68 |
| 3.3.1. LC-MS/MS and FIA-DTIMS-MS.....   | 68 |
| 3.3.2. Method Validation, Comparison, and Application.....  | 70 |
| 3.4. Conclusions.....   | 76 |
| 3.5. Acknowledgements.....  | 77 |
| 3.6. References.....  | 78 |
| 4. Multidimensional Separations of Intact Phase II Steroid Metabolites Utilizing LC-Ion Mobility-MS.....                              | 84 |
| 4.1. Introduction.....  | 84 |
| 4.2. Experimental Methods.....  | 89 |
| 4.2.1. Standards and Chemicals.....   | 89 |
| 4.2.2. Human Urine Extraction and Preparation.....  | 91 |

|   |     |
|---|-----|
| 4.2.3. Chromatographic Conditions.....                                    | 91  |
| 4.2.4. DTIMS-MS Conditions.....   | 93  |
| 4.3. Results and Discussion   |     |
| 4.3.1. LC-IMS-MS.....   | 95  |
| 4.3.2. Isomer Separation.....   | 97  |
| 4.3.3. Mass-Mobility Correlations.....                                    | 99  |
| 4.3.4. Relationships Between CCS, Retention Time, and Mass-to-Charge..... | 100 |
| 4.3.5. AAS in Human Urine.....  | 100 |
| 4.4. Conclusions.....   | 101 |
| 4.5. Acknowledgements.....  | 102 |
| 4.6. References.....  | 102 |
| 5. Perspectives on Emerging and Future Directions.....                    | 117 |
| 5.1. Summary.....   | 117 |
| 5.2. Future Directions.....   | 120 |
| 5.2.1. Chapter 2.....   | 120 |
| 5.2.2. Chapter 3.....   | 120 |
| 5.2.3. Chapter 4.....   | 120 |
| 5.3. Concluding Remarks.....  | 123 |
| 5.4. References.....  | 124 |

## APPENDIX

|   |     |
|---|-----|
| A. References of Adaption for Chapters.....   | 127 |
| B. Supplementary Materials for Chapter 2..... | 128 |
| C. Supplementary Materials for Chapter 3..... | 140 |
| D. Supplementary Materials for Chapter 4..... | 157 |



## LIST OF TABLES

| Table   | Page |
|---|------|
| 0.1. Analytical Figures of Merit for Method Validation.....                         | 3    |
| 1.1. Anti-Epileptic Drugs (AEDs) Analytical Figures of Merit.....                   | 16   |
| 1.2. AEDs Parallel Analysis (LC-UV vs. LC-MS/MS).....                               | 24   |
| 1.3. AEDs Blind Study (LC-UV vs. LC-MS/MS).....                                     | 25   |
| 2.1. Method Validation Results for Targeted Amino Acid Method.....                  | 40   |
| 3.1. AEDs Analytical Figures of Merit.....  | 66   |
| 4.1. Exogenous Anabolic-Androgenic Steroids (AASs) Analytical Figures of Merit..... | 90   |

## LIST OF FIGURES

| Figure   | Page |
|--|------|
| 1.1. LC-MS/MS Analytical Workflow for Anti-Epileptic Drugs (AEDs).....           | 11   |
| 1.2. LC-MS/MS Chromatogram for AEDs with Structures.....                         | 14   |
| 1.3. LC-MS/MS Precision and Accuracy for AEDs.....                               | 21   |
| 1.4. LC-MS/MS Stability for AEDs.....  | 22   |
| 2.1. Mouse Study with HILIC-MS/MS and RPLC-HRMS/MS Analytical Workflows.....     | 33   |
| 2.2. RPLC-HRMS/MS Multivariate Statistical Analyses.....                         | 43   |
| 2.3. Individual Amino Acid Trends Across Diet Groups.....                        | 46   |
| 2.4. Amino Acid Changes Associated with Mitochondrial Dysfunction.....           | 47   |
| 3.1. LC-MS/MS and LC-DTIMS-MS Analytical Workflow for AEDs.....                  | 61   |
| 3.2. LC-MS/MS Chromatograms and LC-DTIMS-MS Drift Times/CCS for AEDs.....        | 65   |
| 3.3. Conformational Space Analysis of AEDs.....                                  | 69   |
| 3.4. LC-DTIMS-MS Analysis of Patient Sample (Theoretical vs. Experimental) ..... | 73   |
| 4.1. Exogenous Anabolic-Androgenic Steroids (AASs) Analytical Workflow.....      | 88   |
| 4.2. Chemical Structures of AASs.....  | 92   |
| 4.3. LC-IMS-MS Analyses of AASs.....   | 94   |
| 4.4. Conformational Space Analysis of AASs.....                                  | 96   |
| 5.1 LC-IMS-MS Analyses Utilizing Ion Multiplexing.....                           | 122  |

## INTRODUCTION

### STATE OF THE FIELD AND PERSONAL CONTRIBUTIONS

Mass spectrometry (MS) has been a rapidly growing analytical technique, especially when analyzing complex biological matrices in metabolomics, clinical applications, anti-doping applications, and routine testing analyses.<sup>1,2</sup> With new MS platforms being developed every year, the resolution of separation by mass analyzers has increased, improving utility tremendously. Even though more fundamental research is being developed for improving the efficiency of mass analyzers, several challenges remain when analyzing complex biological samples. More specifically, when analyzing isomeric species such as structural isomers (constitutional isomers) or stereoisomers. The isomer analysis issue is seen in metabolomics, clinical, anti-doping, and routine testing applications, where laboratories typically operate in regulated environments and get audited by governing agencies like the US food and drug administration (US FDA) or the Clinical Laboratory Improvement Amendments (CLIA). Most of their current analytical techniques can not compensate for issues as specific as isomers. Therefore, to address this daunting issue that is the crux of laboratories, ion mobility techniques in conjunction with liquid chromatography (LC) and MS provide a reasonable solution in separating isomers without adding additional analysis time.

Ion mobility spectrometry (IMS) is a gas-phase separation technique that distinguishes ions based on their size, shape, and charge state.<sup>1-30</sup> The IMS size and shape measurement takes the form of an ion collision cross section (CCS), a coarse-grained area measurement (reported in square angstroms, Å<sup>2</sup>) encompassing the ion size as well as its interaction with the neutral gas.

IMS separates ions based on differences in gas phase electrophoretic mobility. Gas-phase IMS analysis is rapid, typically occurs on a time scale of less than 100 ms per spectrum. In contrast, condensed phase LC-MS is on the time scale of minutes. Therefore, IMS can be included in workflows without compromising analytical throughput, providing an additional separation dimension and an associated molecular descriptor (CCS) to support analyte detection, identification, and minimize false positive/negative results.<sup>1,13</sup> IMS experiments provide a dimension of separation in addition to LC that can be coupled to mass analysis (LC-IMS-MS) to potentially distinguish isomeric interferences and provide further confidence in analyte identification in complex biological samples. Furthermore, IMS can identify analytes not reported in relevant biological samples through a combination of targeted and untargeted analyses because CCS values derived from IMS show utility in improving analyte identification accuracy.

My initial bioanalytical studies, without IMS, show that analyte separations occur with increased LC times (17.5-45 minutes) and yield promising results when combining targeted with untargeted analytical methods (see Chapters 1 and 2). The significance of the work in Chapters 1, 2, and 3 is the use of the FDA Bioanalytical Method Validation and the Clinical & Laboratory Standards Institute (CLSI) LC-MS C62-A guidance documents to aid in method development, validation, and application to complex biological samples (**Table 0.1**).<sup>31,32</sup> However, increased LC times may not be suitable for all laboratories utilizing analytical techniques. LC-MS analyses are susceptible to interferences from chemically similar species, therefore further differentiation and more specific detection techniques (such as LC-MS/MS and LC-IMS-MS) may be necessary for analyte quantification and qualitative studies mainly if structural isomers will be analyzed simultaneously (see Chapter 3).

**Table 0.1.** Analytical figures of merit and acceptance criteria for liquid chromatography-mass spectrometry methods according to FDA bioanalytical method validation and CLSI C62-A guidance documents. <sup>31,32</sup>

| Analytical Figures of Merit                   | Validation Recommendations   | Acceptance Criteria   |
|---|--|---|
| calibration curve (linearity) and sensitivity | <ul style="list-style-type: none"> <li>A blank that is negative for both analytes and internal standards (IS), a negative blank that is negative for analytes but with IS, and at least 6 non-zero standards with IS (calibrator) levels covering the quantification range including the limit of quantification (LOQ)</li> <li>All blanks and calibrators should be in the same matrix as the study samples</li> <li>The concentration-response relationship should fit with the simplest regression model</li> <li>The lowest nonzero standard on the calibration curve defines the sensitivity (LOQ)</li> </ul> | <ul style="list-style-type: none"> <li>Non-zero calibrators should be <math>\pm</math> 15% - 20% of nominal (theoretical) concentrations (this is like accuracy or error% or bias%) in each validation run</li> <li>75% and a minimum of six non-zero calibrator levels should meet the above criteria in each validation run.</li> <li>For the LOQ, the analyte's response should be <math>\geq</math> 5 five times the analytes response of the zero calibrator</li> <li>For the LOQ, the accuracy should be <math>\pm</math> 20% bias%</li> <li>For the LOQ, the precision should be <math>\pm</math> 20% CV%</li> </ul> |
| selectivity and specificity                   | <ul style="list-style-type: none"> <li>the method selectivity should analyze blank samples of the appropriate biological matrix from at least six individual sources</li> <li>The method specificity should be assessed for interference by cross-reacting molecules, concomitant medications, bio-transformed species, etc.</li> </ul>  | <ul style="list-style-type: none"> <li>Blank and zero calibrators should be free of interference at the retention times of the analytes and the IS</li> </ul>   |
| precision and accuracy (P & A)                | <ul style="list-style-type: none"> <li>P &amp; A should be established with at least three independent P &amp; A runs at different QC levels per run (low, medium, and high QCs), and <math>\geq</math> five replicates per QC level</li> <li>This analysis should be done both within-run and between runs</li> </ul>   | <ul style="list-style-type: none"> <li>The run should meet the calibration curve acceptance criteria and include the LLOQ calibrator</li> <li>For the within-run and between run analyses, the accuracy should be 15% - 20% bias%</li> <li>For the within-run and between run analyses, the precision should be 15% - 20% CV%</li> </ul>  |
| recovery                                      | <ul style="list-style-type: none"> <li>Extracted samples concentrations versus extracts of blanks spiked with the analyte post extraction</li> </ul>   | <ul style="list-style-type: none"> <li>The IS is used to account for recovery variance but if the response imprecision is <math>&gt;</math> 15% - 20% CV%, further development is probably needed</li> </ul>  |
| matrix effects                                | <ul style="list-style-type: none"> <li>Extracted blanks spiked with the analyte post extraction versus matrix free samples</li> </ul>  | <ul style="list-style-type: none"> <li>The IS is used to account for matrix effects but if the response imprecision is <math>&gt;</math> 15% - 20% CV%, further development is probably needed</li> </ul>   |
| stability                                     | <ul style="list-style-type: none"> <li>For auto-sampler, bench-top, extract, freeze-thaw, stock solutions or long term stability, perform at least three replicates</li> </ul>   | <ul style="list-style-type: none"> <li>The accuracy should be 15% - 20% bias% or 80% - 120% recovered</li> </ul>  |
| carryover                                     | <ul style="list-style-type: none"> <li>The impact of carryover on the accuracy of the study sample concentrations should be assessed</li> </ul>  | <ul style="list-style-type: none"> <li>Carryover should not exceed 20% of the LOQ</li> </ul>  |

Stereoisomers are typically always more challenging to separate using IMS, especially for ions less than 200 Daltons.<sup>11</sup> However, multidimensional analytical separations such as LC-IMS-MS may be necessary for analyte analyses, particularly for complex sample matrices where numerous constitutional isomers and stereoisomers (phase II steroid metabolites) greater than 350 Daltons are commonly co-existing within a human urine sample (see Chapter 4).<sup>2,21,33</sup>

### **References**

- (1) May, J. C.; McLean, J. A. Ion Mobility-Mass Spectrometry: Time-Dispersive Instrumentation. *Anal. Chem.* **2015**, *87* (3), 1422–1436. <https://doi.org/10.1021/ac504720m>
- (2) Davis, D. E.; Sherrod, S. D.; Gant-Branum, R. L.; Colby, J. M.; McLean, J. A. Targeted Strategy to Analyze Antiepileptic Drugs in Human Serum by LC-MS/MS and LC-Ion Mobility-MS. *Anal. Chem.* **2020**, *92* (21), 14648–14656. <https://doi.org/10.1021/acs.analchem.0c03172>
- (3) May, J. C.; Gant-Branum, R. L.; McLean, J. A. Targeting the Untargeted in Molecular Phenomics with Structurally-Selective Ion Mobility-Mass Spectrometry. *Current Opinion in Biotechnology*. Elsevier Ltd June 1, **2016**, pp 192–197. <https://doi.org/10.1016/j.copbio.2016.04.013>
- (4) Giles, K.; Williams, J. P.; Campuzano, I. Enhancements in Travelling Wave Ion Mobility Resolution. In *Rapid Communications in Mass Spectrometry*; John Wiley & Sons, Ltd, **2011**; Vol. 25, pp 1559–1566. <https://doi.org/10.1002/rcm.5013>
- (5) Pu, Y.; Ridgeway, M. E.; Glaskin, R. S.; Park, M. A.; Costello, C. E.; Lin, C. Separation and Identification of Isomeric Glycans by Selected Accumulation-Trapped Ion Mobility Spectrometry-Electron Activated Dissociation Tandem Mass Spectrometry. *Anal. Chem.* **2016**, *88* (7), 3440–3443. <https://doi.org/10.1021/acs.analchem.6b00041>
- (6) Bijlsma, L.; Berntssen, M. H. G.; Merel, S. A Refined Nontarget Workflow for the Investigation of Metabolites through the Prioritization by in Silico Prediction Tools. *Anal. Chem.* **2019**, *91* (9), 6321–6328. <https://doi.org/10.1021/acs.analchem.9b01218>

- (7) Poland, J. C.; Schrimpe-Rutledge, A. C.; Sherrod, S. D.; Flynn, C. R.; McLean, J. A. Utilizing Untargeted Ion Mobility-Mass Spectrometry to Profile Changes in the Gut Metabolome Following Biliary Diversion Surgery. *Anal. Chem.* **2019**. <https://doi.org/10.1021/acs.analchem.9b02924>
- (8) May, J. C.; Goodwin, C. R.; Lareau, N. M.; Leaptrot, K. L.; Morris, C. B.; Kurulugama, R. T.; Mordehai, A.; Klein, C.; Barry, W.; Darland, E.; Overney, G.; Imatani, K.; Stafford, G. C.; Fjeldsted, J. C.; McLean, J. A. Conformational Ordering of Biomolecules in the Gas Phase: Nitrogen Collision Cross Sections Measured on a Prototype High Resolution Drift Tube Ion Mobility-Mass Spectrometer. *Anal. Chem.* **2014**, *86* (4), 2107–2116. <https://doi.org/10.1021/ac4038448>
- (9) May, J. C.; Dodds, J. N.; Kurulugama, R. T.; Stafford, G. C.; Fjeldsted, J. C.; McLean, J. A. Broadscale Resolving Power Performance of a High Precision Uniform Field Ion Mobility-Mass Spectrometer. *Analyst* **2015**, *140* (20), 6824–6833. <https://doi.org/10.1039/c5an00923e>
- (10) Stow, S. M.; Causon, T. J.; Zheng, X.; Kurulugama, R. T.; Mairinger, T.; May, J. C.; Rennie, E. E.; Baker, E. S.; Smith, R. D.; McLean, J. A.; Hann, S.; Fjeldsted, J. C. An Interlaboratory Evaluation of Drift Tube Ion Mobility-Mass Spectrometry Collision Cross Section Measurements. *Anal. Chem.* **2017**, *89* (17), 9048–9055. <https://doi.org/10.1021/acs.analchem.7b01729>
- (11) Dodds, J. N.; May, J. C.; McLean, J. A. Investigation of the Complete Suite of the Leucine and Isoleucine Isomers: Toward Prediction of Ion Mobility Separation Capabilities. *Anal. Chem.* **2017**, *89* (1), 952–959. <https://doi.org/10.1021/acs.analchem.6b04171>
- (12) Nichols, C. M.; Dodds, J. N.; Rose, B. S.; Picache, J. A.; Morris, C. B.; Codreanu, S. G.; May, J. C.; Sherrod, S. D.; McLean, J. A. Untargeted Molecular Discovery in Primary Metabolism: Collision Cross Section as a Molecular Descriptor in Ion Mobility-Mass Spectrometry. *Anal. Chem.* **2018**, *90* (24), 14484–14492. <https://doi.org/10.1021/acs.analchem.8b04322>
- (13) Dodds, J. N.; Hopkins, Z. R.; Knappe, D. R. U.; Baker, E. S. Rapid Characterization of Per- And Polyfluoroalkyl Substances (PFAS) by Ion Mobility Spectrometry-Mass Spectrometry (IMS-MS). *Anal. Chem.* **2020**, *92* (6), 4427–4435. <https://doi.org/10.1021/acs.analchem.9b05364>

- (14) Picache, J. A.; Rose, B. S.; Balinski, A.; Leaptrot, K. L.; Sherrod, S. D.; May, J. C.; McLean, J. A. Collision Cross Section Compendium to Annotate and Predict Multi-Omic Compound Identities. *Chem. Sci.* **2019**, *10* (4), 983–993. <https://doi.org/10.1039/c8sc04396e>
- (15) Leaptrot, K. L.; May, J. C.; Dodds, J. N.; McLean, J. A. Ion Mobility Conformational Lipid Atlas for High Confidence Lipidomics. *Nat. Commun.* **2019**, *10* (1). <https://doi.org/10.1038/s41467-019-08897-5>
- (16) Chouinard, C. D.; Wei, M. S.; Beekman, C. R.; Kemperman, R. H. J.; Yost, R. A. Ion Mobility in Clinical Analysis: Current Progress and Future Perspectives. *Clinical Chemistry.* **2016**, pp 124–133. <https://doi.org/10.1373/clinchem.2015.238840>
- (17) Harris, R. A.; Leaptrot, K. L.; May, J. C.; McLean, J. A. New Frontiers in Lipidomics Analyses Using Structurally Selective Ion Mobility-Mass Spectrometry. *TrAC - Trends in Analytical Chemistry.* **2019**, pp 316–323. <https://doi.org/10.1016/j.trac.2019.03.031>
- (18) Maddox, S. W.; Fraser Caris, R. H.; Baker, K. L.; Burkus-Matesevac, A.; Peverati, R.; Chouinard, C. D. Ozone-Induced Cleavage of Endocyclic C=C Double Bonds within Steroid Epimers Produces Unique Gas-Phase Conformations. *J. Am. Soc. Mass Spectrom.* **2020**, *31* (2), 411–417. <https://doi.org/10.1021/jasms.9b00058>
- (19) Harris, R. A.; May, J. C.; Stinson, C. A.; Xia, Y.; McLean, J. A. Determining Double Bond Position in Lipids Using Online Ozonolysis Coupled to Liquid Chromatography and Ion Mobility-Mass Spectrometry. *Anal. Chem.* **2018**, *90* (3), 1915–1924. <https://doi.org/10.1021/acs.analchem.7b04007>
- (20) Sherrod, S. D.; McLean, J. A. Systems-Wide High-Dimensional Data Acquisition and Informatics Using Structural Mass Spectrometry Strategies. *Clinical Chemistry.* **2016**, pp 77–83. <https://doi.org/10.1373/clinchem.2015.238261>
- (21) Schrimpe-Rutledge, A. C.; Codreanu, S. G.; Sherrod, S. D.; McLean, J. A. Untargeted Metabolomics Strategies—Challenges and Emerging Directions. *J. Am. Soc. Mass Spectrom.* **2016**, *27* (12), 1897–1905. <https://doi.org/10.1007/s13361-016-1469-y>



- (22) Gabelica, V.; Shvartsburg, A. A.; Afonso, C.; Barran, P.; Benesch, J. L. P.; Bleiholder, C.; Bowers, M. T.; Bilbao, A.; Bush, M. F.; Campbell, J. L.; Campuzano, I. D. G.; Causon, T.; Clowers, B. H.; Creaser, C. S.; De Pauw, E.; Far, J.; Fernandez-Lima, F.; Fjeldsted, J. C.; Giles, K.; Groessl, M.; Hogan, C. J.; Hann, S.; Kim, H. I.; Kurulugama, R. T.; May, J. C.; McLean, J. A.; Pagel, K.; Richardson, K.; Ridgeway, M. E.; Rosu, F.; Sobott, F.; Thalassinou, K.; Valentine, S. J.; Wytenbach, T. Recommendations for Reporting Ion Mobility Mass Spectrometry Measurements. *Mass Spectrom. Rev.* **2019**, *38* (3), 291–320. <https://doi.org/10.1002/mas.21585>
- (23) Dodds, J. N.; Baker, E. S. Ion Mobility Spectrometry: Fundamental Concepts, Instrumentation, Applications, and the Road Ahead. *J. Am. Soc. Mass Spectrom.* **2019**, *30* (11), 2185–2195. <https://doi.org/10.1007/s13361-019-02288-2>
- (24) Viehland, L. A.; Mason, E. A. Gaseous Ion Mobility in Electric Fields of Arbitrary Strength. *Ann. Phys. (N. Y.)* **1975**, *91* (2), 499–533. [https://doi.org/10.1016/0003-4916\(75\)90233-X](https://doi.org/10.1016/0003-4916(75)90233-X).
- (25) Hines, K. M.; Ballard, B. R.; Marshall, D. R.; McLean, J. A. Structural Mass Spectrometry of Tissue Extracts to Distinguish Cancerous and Non-Cancerous Breast Diseases. *Mol. Biosyst.* **2014**, *10* (11), 2827–2837. <https://doi.org/10.1039/c4mb00250d>
- (26) Fenn, L. S.; McLean, J. A. Biomolecular Structural Separations by Ion Mobility-Mass Spectrometry. *Anal. Bioanal. Chem.* **2008**, *391* (3), 905–909. <https://doi.org/10.1007/s00216-008-1951-x>
- (27) Goodwin, C. R.; Fenn, L. S.; Derewacz, D. K.; Bachmann, B. O.; McLean, J. A. Structural Mass Spectrometry: Rapid Methods for Separation and Analysis of Peptide Natural Products. *J. Nat. Prod.* **2012**, *75* (1), 48–53. <https://doi.org/10.1021/np200457r>
- (28) Hines, K. M.; Ross, D. H.; Davidson, K. L.; Bush, M. F.; Xu, L. Large-Scale Structural Characterization of Drug and Drug-Like Compounds by High-Throughput Ion Mobility-Mass Spectrometry. *Anal. Chem.* **2017**, *89* (17), 9023–9030. <https://doi.org/10.1021/acs.analchem.7b01709>

- (29) Mairinger, T.; Causon, T. J.; Hann, S. The Potential of Ion Mobility–Mass Spectrometry for Non-Targeted Metabolomics. *Curr. Opin. Chem. Biol.* **2018**, 42, 9–15. <https://doi.org/10.1016/j.cbpa.2017.10.015>
- (30) Zhang, X.; Quinn, K.; Cruickshank-Quinn, C.; Reisdorph, R.; Reisdorph, N. The Application of Ion Mobility Mass Spectrometry to Metabolomics. *Current Opinion in Chemical Biology*. Elsevier Ltd February 1, **2018**, pp 60–66. <https://doi.org/10.1016/j.cbpa.2017.11.001>
- (31) FDA. Guidance for Industry: Bioanalytical Method Validation. **2018**, No. FDA-2013-D-1020, pp 1-41.
- (32) CLSI. Liquid Chromatography-Mass Spectrometry Methods; Approved Guidelines (C62-A). **2014**, No. 1-56238-977–7, pp 1-71.
- (33) Hernández-Mesa, M.; Le Bizec, B.; Monteau, F.; García-Campaña, A. M.; Dervilly-Pinel, G. Collision Cross Section (CCS) Database: An Additional Measure to Characterize Steroids. *Anal. Chem.* **2018**, 90 (7), 4616–4625. <https://doi.org/10.1021/acs.analchem.7b05117>

## CHAPTER 1

### THE DEVELOPMENT, VALIDATION, AND APPLICATION OF A CLINICAL LC-MS/MS METHOD FOR THE QUANTIFICATION OF ANTI-EPILEPTIC DRUGS IN HUMAN SERUM

#### ***1.1. Introduction***

Epilepsy is one of the most common neurological disorders and is characterized by the long-term risk of recurrent seizures. Anti-epileptic drugs (AEDs) are effective at controlling seizures. However, many patients experience adverse side effects associated with AED usages, such as liver toxicity, tremors, dizziness, nausea, and fatigue.<sup>1,2</sup> AEDs have a narrow therapeutic range. Therefore, serum concentration must be optimized to ensure effectiveness (control/minimize seizures) and minimize adverse side effects.<sup>3-5</sup> AED effectiveness is partially dependent upon patient-specific pharmacokinetics (PK), which include: absorption, distribution, metabolism, and excretion (ADME).<sup>6</sup> Patient-specific PK can influence a clinician's decision on dosage and dosing frequency of AEDs.<sup>3</sup> Therapeutic drug management (TDM) of AEDs requires making iterative drug concentration measurements to ensure a patient's serum AED concentration stays within the therapeutic range.<sup>5,7</sup> This is why method validation is essential for these types of analytical workflows. A TDM workflow for AEDs is essential for optimizing AED treatment for individual patients, a primary tenet of personalized medicine.<sup>8</sup>

Routine clinical TDM is often performed using quantitative immunoassays, where analyte concentration is determined as a function of antibody binding and not through direct molecular identification.<sup>1,2</sup> Immunoassays are generally limited to single drug detection and are susceptible to false positives due to cross-reactivity between the drug target and related metabolites.<sup>9-12</sup> Supplement consumption in the United States has also increased dramatically in recent years,

which may convolute testing by introducing additional interferences.<sup>8,13</sup> Also, new AEDs are routinely developed, which may introduce interferences and complicate quantification of AEDs using less specific methodologies like immunoassays.<sup>1,14,15</sup> Finally, patients are often prescribed more than one AED, which necessitates testing a sample on multiple immunoassays. Thus a single assay offering precise detection of multiple related drugs and drug metabolites, high sensitivity, rapid analytical time, and minimal cost is ideal.<sup>16</sup>

Separation of drugs by liquid chromatography and detection through absorbance at a particular wavelength (LC–UV) or by triple quadrupole mass spectrometry (LC-MS/MS) have also been utilized to quantify AEDs.<sup>16–18</sup> Like immunoassay, LC-UV analyses may also be limited by interferences from chemically similar species (e.g., isobaric or isomeric species with similar polarity and retention times).

Clinical and analytical labs use LC-MS/MS to quantify analytes for numerous reasons, including ruggedness, ease of use, cost, and the ability to perform highly selective multiplexed measurements.<sup>19</sup> Here, we present a reversed-phase liquid chromatography-tandem mass spectrometry (RPLC-MS/MS) method for routine clinical use in quantifying analytes in patient serum (**Figure 1.1.**), validated by the FDA bioanalytical method validation and CLSI C62-A guidance documents.<sup>20,21</sup> This chapter of the dissertation delivers robust quantification of multiple compounds and should prove beneficial for laboratories interested in increasing efficiency and selectivity in routine testing.

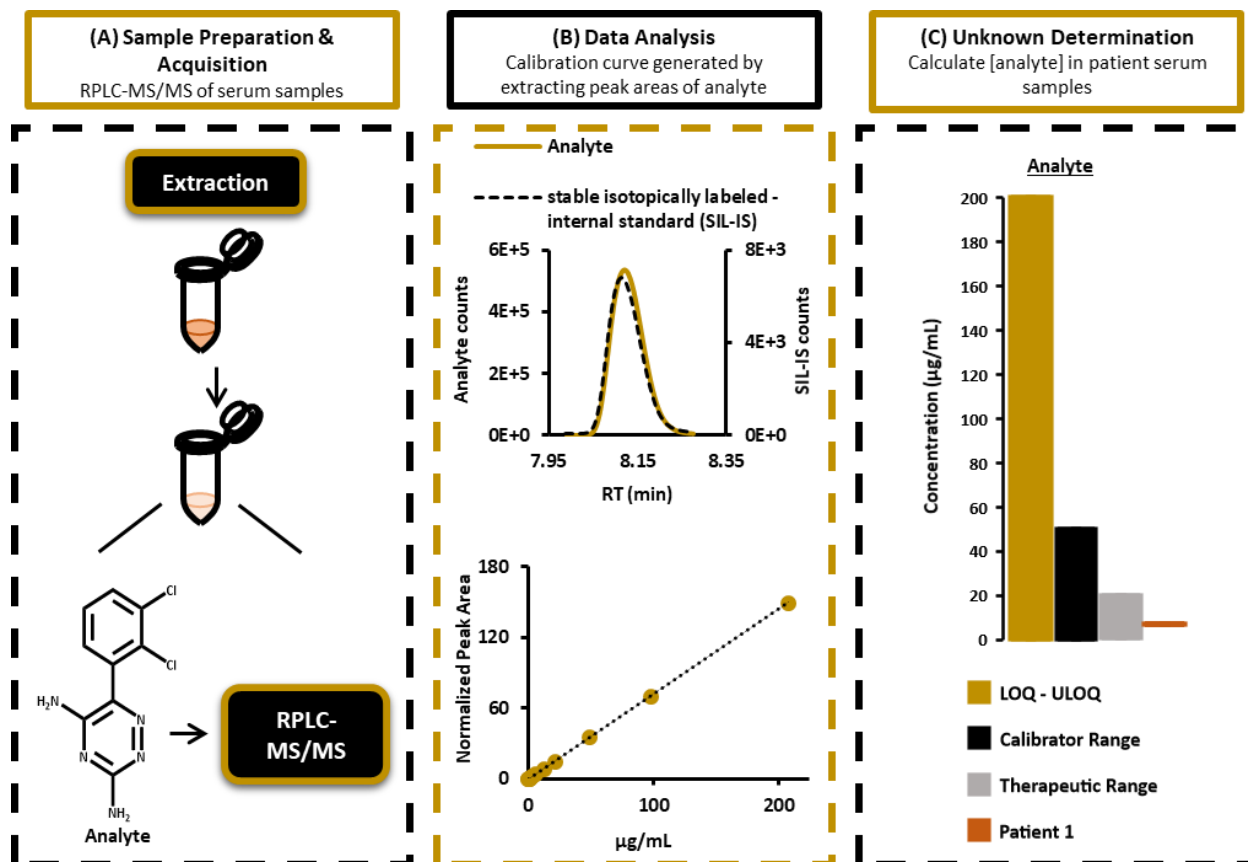


**Figure 1.1.** Workflow for sample preparation & acquisition (A), data analysis (B), and unknown determination of an analyte in patient serum samples (C). This workflow is applied to all analytes in serum but is applicable to any matrix.

## **1.2. Material and Methods**

Levetiracetam, levetiracetam-D<sub>6</sub>, pregabalin, pregabalin-<sup>13</sup>C<sub>3</sub>, gabapentin, gabapentin-<sup>13</sup>C<sub>3</sub>, ethosuximide, primidone, PEMA, zonisamide, zonisamide-<sup>13</sup>C<sub>6</sub>, lamotrigine, lamotrigine-<sup>13</sup>C<sub>1</sub>, <sup>15</sup>N<sub>4</sub>, topiramate, topiramate-D<sub>12</sub>, carbamazepine, carbamazepine epoxide, MHD, MHD-<sup>13</sup>C<sub>6</sub>, oxcarbazepine, and phenytoin were purchased from Sigma-Aldrich (St. Louis, MO, USA). Optima LC/MS grade water, isopropyl alcohol, and methanol were obtained from Fisher Scientific (Hampton, NH, USA). Optima LC/MS grade formic acid and ammonium acetate were obtained from Fisher Scientific (Hampton, NH, USA).

Primary stock solutions of individual AEDs were prepared in methanol at a concentration of 1 mg/mL and stored at -20°C. Stock solutions of the internal standards were also prepared in methanol at a concentration of 100 µg/mL and stored at -20°C (except for lamotrigine-<sup>13</sup>C<sub>1</sub>, <sup>15</sup>N<sub>4</sub>, which was prepared at 500 µg/mL).

### **1.2.1. Serum Samples**

Human drug-free serum and custom-made matrix-matched quality control material (QCs) at low, medium, and high AED concentrations were obtained from UTAK Laboratories Incorporated (Valencia, CA, USA). De-identified, residual serum specimens were obtained from VUMC's clinical toxicology laboratory. These samples were subjected to the extraction protocol described in the sample preparation section.

### **1.2.2. Chromatographic Conditions**

Analysis of AEDs was performed using a 3.0 x 50 mm reverse phase column, ZORBAX Eclipse Plus C18 Rapid Resolution HD 1.8 µm (Agilent Technologies, Santa Clara, CA) with a

2.1 x 5 mm 1.8  $\mu\text{m}$  ZORBAX Eclipse Plus C18 guard column, maintained at 40°C for separation by Ultra High-Pressure Liquid Chromatography (UHPLC, Agilent 1290 Infinity II LC system, Agilent Technologies, Santa Clara, CA). Mobile phase A was comprised of water with 0.1% formic acid and 10 mM ammonium acetate. Mobile Phase B consisted of methanol with 0.1% formic acid and 10 mM ammonium acetate. The UHPLC was directly coupled online to a commercial triple quadrupole mass spectrometer (6470, Agilent Technologies, Santa Clara, CA). A 1  $\mu\text{L}$  sample was injected at a flow rate of 800  $\mu\text{L}/\text{min}$  with the following chromatographic conditions (17.5 minute runtime including purge and equilibration times): mobile phase B was held at 5% for the first 3 minutes for an initial isocratic hold, linearly increased from 5% to 32.5% over 5.5 minutes, linearly increased from 32.5% to 35% over 0.01 minutes, linearly increased from 35% to 100% over 2.48 minutes, and held at 100% for 1.51 minutes to remove contaminants from the column. Mobile phase B returned to 5% by 12.5 minutes and was held at 5% for 5 minutes to re-equilibrate the column. In this method, the initial isocratic hold, final purge, and re-equilibration times were performed to ensure efficient cleaning, minimize carryover and increase column lifetime. Additionally, the injection needle was washed with 60:40 (v:v) isopropyl alcohol: methanol followed by mobile phase starting conditions between every run to ensure minimum carryover. As an example of method development for validation, a representative chromatogram of the 14 AEDs and mobile phase B gradient is outlined in **Figure 1.2**.

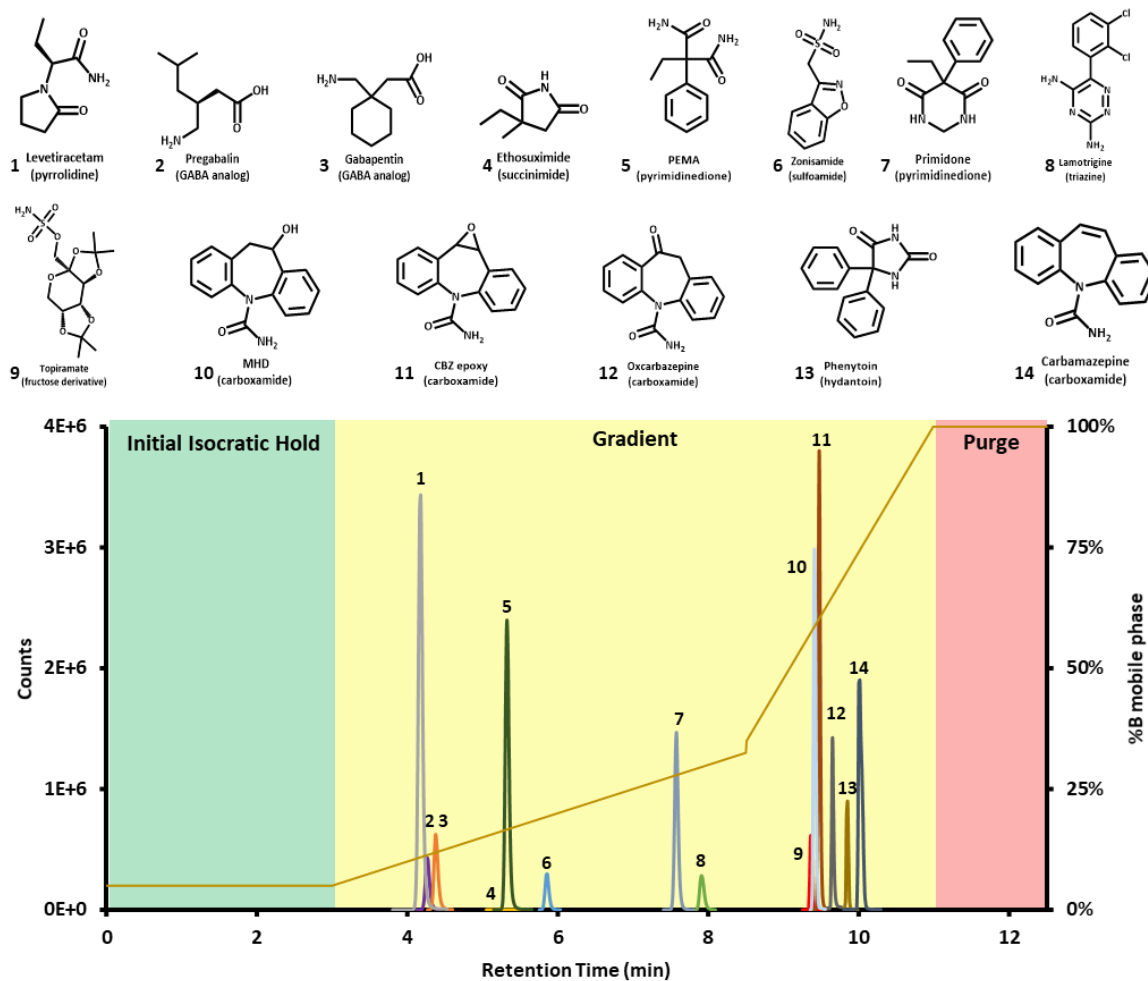


**Figure 1.2.** RPLC chromatogram of 14 AEDs with their chemical structures organized by elution order. The secondary axis represents the %B mobile phase for the LC method. The green box is the initial isocratic hold period, the yellow box is the gradient portion, and the red box is the purge section of this LC method.



### 1.2.3. MS/MS Conditions

All AEDs were analyzed in positive ionization mode using the Jet Stream ESI source (Agilent Technologies, Santa Clara, CA). Nitrogen was used as the nebulizing gas and collision gas. AED transitions were collected using dynamic multiple reaction monitoring (dMRM) or scheduled MRM where the retention time window for each chromatographic peak was set to  $\Delta 2$  min ( $\pm 1$  min) from the expected retention time. Retention times and MRM transitions are listed in **Table 1.1**. Also, **Table 1.1** denotes the dMRM transitions of each AED. Quantifier transitions have characteristic fragments or product ions of AED precursor ions (Quant m/z) used to quantitate serum concentrations. Qualifier ions (Qual m/z) are characteristic fragments or product ions of precursor ions used to assess the assay's quality. Data were acquired using Agilent's MassHunter Workstation Data Acquisition software and analyzed using Skyline (MacCoss Lab)<sup>22,23</sup>, Agilent's MassHunter Quantitative Analysis, MassHunter Qualitative Analysis software, and Microsoft Excel.

### 1.2.4. Sample Preparation

For all samples in this study, protein precipitation was performed in a 1.5-ml polypropylene microcentrifuge tube (Eppendorf, Hauppauge, NY). One mL of  $-20^{\circ}\text{C}$  cooled methanol was added to 100  $\mu\text{L}$  of serum to precipitate proteins. Samples were then vortexed, stored at  $-80^{\circ}\text{C}$  for 1 hour, and centrifuged at 15,000 rpm for 15 min at  $0^{\circ}\text{C}$ . The protein pellet was discarded while the supernatant was transferred, subsequently evaporated *in vacuo*, and stored at  $-80^{\circ}\text{C}$  until analysis. Before analysis, individual samples were reconstituted in 100  $\mu\text{L}$  of mobile phase A. The idea here is to use the most straightforward and quickest sample preparation methods for validation and application purposes.

**Table 1.1.** AEDs with stable isotopically labeled internal standards (SIL-IS), MRM transition list, retention times (min), the limit of quantification (LOQ), therapeutic ranges,<sup>5</sup> recovery, and matrix effects.

| No. | AED   | Q1 (m/z) | Q3 Quant (m/z) | Q3 Qual (m/z) | RT (min) | LOQ (µg/mL) | therapeutic range (µg/mL) | recovery ± %CV        | matrix effect ± %CV    |
|-----|---|----------|----------------|---------------|----------|-------------|---------------------------|-----------------------|------------------------|
| 1   | levetiracetam   | 171      | 154            | 126           | 4.4      | 0.2         | 5 - 40                    | 112% ± 7% at 25 µg/mL | 92% ± 12% at 25 µg/mL  |
|     | levetiracetam - D <sub>6</sub>  | 177      | 160            | 132           | 4.3      |             |                           |                       |                        |
| 2   | pregabalin  | 160      | 142            | 97            | 4.5      | 0.2         | 4 - 20                    | 116% ± 7% at 13 µg/mL | 103% ± 9% at 13 µg/mL  |
|     | pregabalin - <sup>13</sup> C <sub>3</sub>                                 | 163      | 145            | 127           | 4.5      |             |                           |                       |                        |
| 3   | gabapentin  | 172      | 154            | 137           | 4.6      | 0.2         | 2 - 20                    | 120% ± 7% at 13 µg/mL | 104% ± 10% at 13 µg/mL |
|     | gabapentin - <sup>13</sup> C <sub>3</sub>                                 | 175      | 157            | 140           | 4.6      |             |                           |                       |                        |
| 4   | ethosuximide  | 142      | 114            | 72            | 5.4      | 1.4         | 40 - 100                  | 80% ± 18% at 50 µg/mL | 76% ± 11% at 50 µg/mL  |
|     | zonisamide - <sup>13</sup> C <sub>6</sub>                                 | 219      | 138            | 109           | 6.0      |             |                           |                       |                        |
| 5   | PEMA  | 207      | 162            | 119           | 5.5      | 0.2         |                           | 95% ± 7% at 25 µg/mL  | 50% ± 3% at 25 µg/mL   |
|     | zonisamide - <sup>13</sup> C <sub>6</sub>                                 | 219      | 138            | 109           | 6.0      |             |                           |                       |                        |
| 6   | zonisamide  | 213      | 132            | 77            | 6.0      | 0.2         | 10 - 40                   | 114% ± 6% at 25 µg/mL | 100% ± 10% at 25 µg/mL |
|     | zonisamide - <sup>13</sup> C <sub>6</sub>                                 | 219      | 138            | 109           | 6.0      |             |                           |                       |                        |
| 7   | primidone   | 219      | 162            | 119           | 7.7      | 0.2         | 5 - 12                    | 87% ± 8% at 12 µg/mL  | 63% ± 4% at 12 µg/mL   |
|     | lamotrigine - <sup>13</sup> C <sub>1</sub> , <sup>15</sup> N <sub>4</sub> | 262      | 215            | 190           | 8.1      |             |                           |                       |                        |
| 8   | lamotrigine   | 256      | 211            | 145           | 8.1      | 0.2         | 1 - 20                    | 111% ± 7% at 13 µg/mL | 101% ± 10% at 13 µg/mL |
|     | lamotrigine - <sup>13</sup> C <sub>1</sub> , <sup>15</sup> N <sub>4</sub> | 262      | 215            | 190           | 8.1      |             |                           |                       |                        |
| 9   | topiramate  | 362      | 265            | 207           | 9.4      | 0.4         | 10 - 20                   | 52% ± 2% at 13 µg/mL  | 47% ± 4% at 13 µg/mL   |
|     | topiramate - D <sub>12</sub>  | 374      | 276            | 213           | 9.5      |             |                           |                       |                        |
| 10  | MHD   | 255      | 237            | 194           | 9.5      | 0.2         | 10 - 40                   | 104% ± 8% at 25 µg/mL | 98% ± 11% at 25 µg/mL  |
|     | MHD - <sup>13</sup> C <sub>6</sub>  | 261      | 200            | 185           | 9.5      |             |                           |                       |                        |
| 11  | CBZ Epoxy   | 253      | 236            | 210           | 9.6      | 0.1         | 4 - 12                    | 62% ± 6% at 13 µg/mL  | 86% ± 19% at 13 µg/mL  |
|     | MHD - <sup>13</sup> C <sub>6</sub>  | 261      | 200            | 185           | 9.5      |             |                           |                       |                        |
| 12  | oxcarbazepine   | 253      | 180            | 210           | 9.7      | 0.7         | 10 - 40                   | 88% ± 15% at 25 µg/mL | 80% ± 10% at 25 µg/mL  |
|     | MHD - <sup>13</sup> C <sub>6</sub>  | 261      | 200            | 185           | 9.5      |             |                           |                       |                        |
| 13  | phenytoin   | 253      | 104            | 225           | 9.9      | 0.1         | 1 - 2.5                   | 59% ± 6% at 25 µg/mL  | 62% ± 7% at 25 µg/mL   |
|     | MHD - <sup>13</sup> C <sub>6</sub>  | 261      | 200            | 185           | 9.5      |             |                           |                       |                        |
| 14  | carbamazepine   | 237      | 194            | 192           | 10.1     | 0.1         | 4 - 12                    | 60% ± 6% at 13 µg/mL  | 91% ± 3% at 13 µg/mL   |
|     | MHD - <sup>13</sup> C <sub>6</sub>  | 261      | 200            | 185           | 9.5      |             |                           |                       |                        |

### ***1.2.5. Method Validation***

Guidelines established by the FDA bioanalytical method validation and CLSI C62-A guidance documents were used.<sup>20,21</sup> Analytical figures of merit, including the limit of quantification (LOQ), accuracy, precision, carryover, stability, selectivity, recovery, and matrix effect were assessed. The following sections in this chapter explain each analytical figure of merit for validation of AEDs and are meant to be applied to all analytes.

### ***1.2.6. Precision and Accuracy***

Precision and accuracy were obtained for each AED at given QC concentrations (e.g., low, medium, and high) using 5-process replicates. Imprecision was determined by calculating the coefficient of variation (%CV). Bias was determined by calculating % observed relative to the target concentration. Precision and accuracy were evaluated within-run (intraday) and between runs (interday). For intraday studies, a set of calibrators, 5 sets of QCs (n=5 process replicates), and a negative sample for analysis were prepared. For the interday studies, a set of calibrators, 5 sets of QCs (n=5 process replicates), and a negative sample were prepared 24 hours after intraday studies were performed. This analysis of the QC process replicates was used to perform the statistical analysis of precision and accuracy reported in this study.

### ***1.2.7. Linearity and LOQ***

A calibration curve of drug-free human serum from UTAK spiked with AEDs, and internal standards at 12 concentration ranges with 5-process replicates was used to construct a matrix-based calibration curve. Calibration curves were used to assess LOQ. All calibration curves were generated by a linear fit of the analyte/IS area response ratio with 1/x weighting. The LOQ is the

lowest concentration at which quantitative criteria were met, where the quantitative criteria were described as accuracy within +/- 20% and precision within +/- 20%.

#### **1.2.8. Carryover**

Carryover was determined by analyzing blank samples after the injection of the highest concentration samples using 5-process replicates. Carryover is reported if the blank's response is  $\geq 1/5$  of the LOQ's response (blank's response  $\geq \frac{\sim\text{LLOQ response}}{5}$ ).

#### **1.2.9. Stability**

Each analyte's serum stability was evaluated by spiking analytes and internal standards from a fresh stock solution into drug-free serum and exposing the samples to common conditions such as freeze/thaw cycles and short-term temperature fluctuations in the autosampler post-extraction. The conditions of these experiments reflect situations that may be encountered in routine sample handling and analysis. Briefly, analytes were stored at 20°C, thawed at room temperature, extracted, resuspended in mobile phase A, and stored in the autosampler (kept at 4°C) for 48 hours before analysis.

#### **1.2.10. Recovery**

Recovery assesses the extraction efficiency of an analytical method.<sup>20,21</sup> Recovery was assessed in serum (5 process replicates). Extracted standards (e.g., spiked pre-extraction) were compared to the mean peak area of post-extracted serum samples (e.g., spiked post-extraction). This comparison was made using equation 1:

$$\%Recovery = \frac{Peak\ Area\ (spike\ pre\text{-}extraction)}{Peak\ Area\ (spike\ post\text{-}extraction)} \times 100. \text{ (eq. 1)}$$

### **1.2.11. Matrix Effects**

Matrix effects are a direct or indirect interference in response because of other interfering substances in the sample.<sup>20,21</sup> Matrix effects were determined by spiking analytes with internal standards into post extracted serum samples (e.g., spiked post-extraction) (5 process replicates). The post-extract was then compared to the mean peak area of neat standards. This comparison was made using equation 2:

$$\% Matrix\ effect = \frac{Peak\ Area\ (spike\ post\text{-}extraction)}{Peak\ Area\ (neat)} \times 100. \text{ (eq. 2)}$$

### **1.2.12. Selectivity**

Selectivity is the ability of an analytical method to detect and quantify the analyte in the presence of other components in the sample or the ability to differentiate between a blank serum sample and a positive serum sample. Selectivity is determined by extracting analyte negative serum samples from 6 different sources (6 biological replicates).

## **1.3. Results of Method Validation**

### **1.3.1. Linearity and LOQ**

Calibration curves were evaluated using a linear fit with a weighting factor of 1/x. When viewed separately, the correlation coefficient of all calibration curves was greater than 0.985. The accuracy in the observed concentration of calibration curve samples fell within the tolerance, ranging from +/- 20% of the theoretical value. **Table 1.1.** contains individual AED LOQ values.

### ***1.3.2. Precision, Accuracy, and Carryover***

The within-run and between runs precision and accuracy of all AEDs were less than 15% CV and 15% bias, respectively (**Figure 1.3.**). For carryover, no sample blanks were observed to produce a response  $\geq 1/5$  of the LLOQ's response. Therefore, we concluded that no significant carryover was observed for the AEDs presented here.

### ***1.3.3. Recovery and Matrix Effect***

The observed recovery and matrix effects for AEDs in serum are shown in **Table 1.1.** Recovery allows for the assessment of extraction efficiency at various concentrations and satisfies quantitative criteria. In this method, we did not observe any significant matrix effects (e.g., ionization suppression or ionization enhancement). These results suggest that the analytical method reported here minimizes the impacts of endogenous interferences from human serum or concomitant medications.

### ***1.3.4. Selectivity and Stability***

The selectivity in **Figure 1.2.** demonstrates the analytical method's ability to differentiate and quantify analytes simultaneously in the presence of other components in human serum. In these studies, less than +/- 15% quantitative loss or recovery was observed for AEDs after 48 hours of storage at 4°C (**Figure 1.4.**).

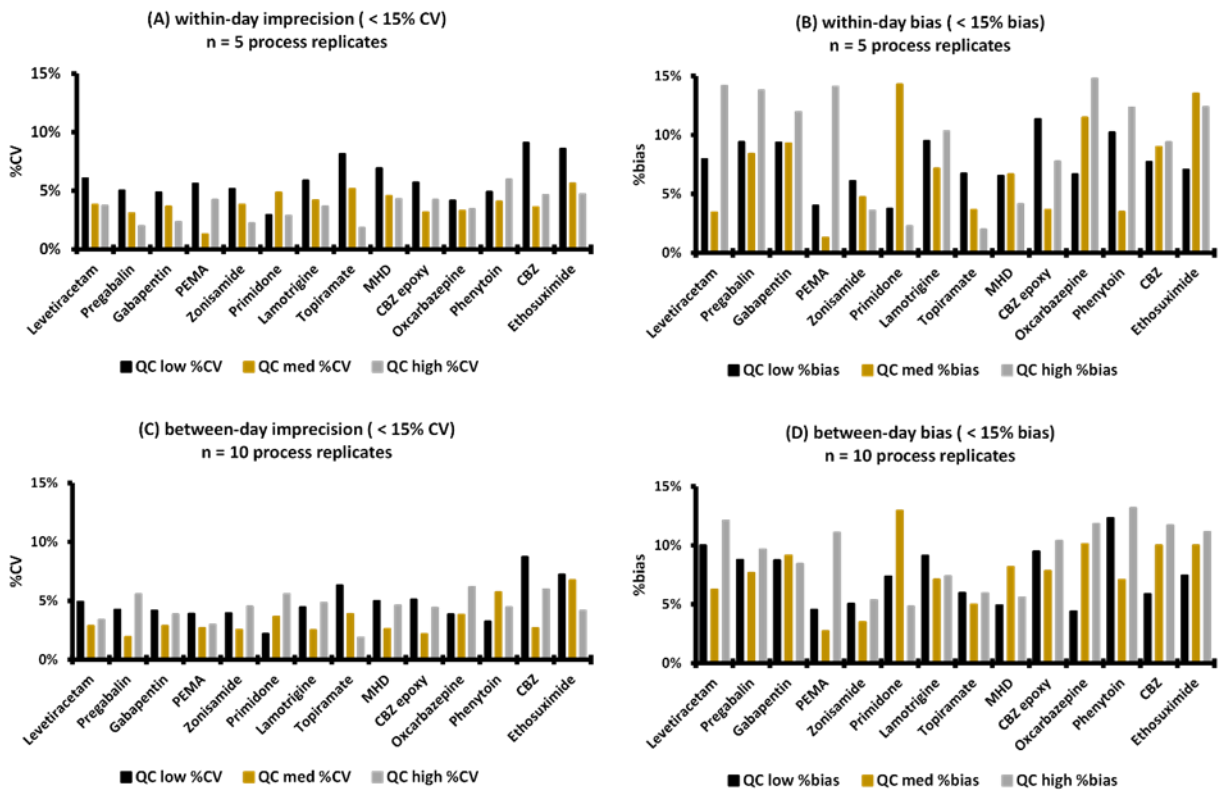


**Figure 1.3.** AED within-day imprecision (A) and bias (B). AED between-day imprecision (C) and bias (D).

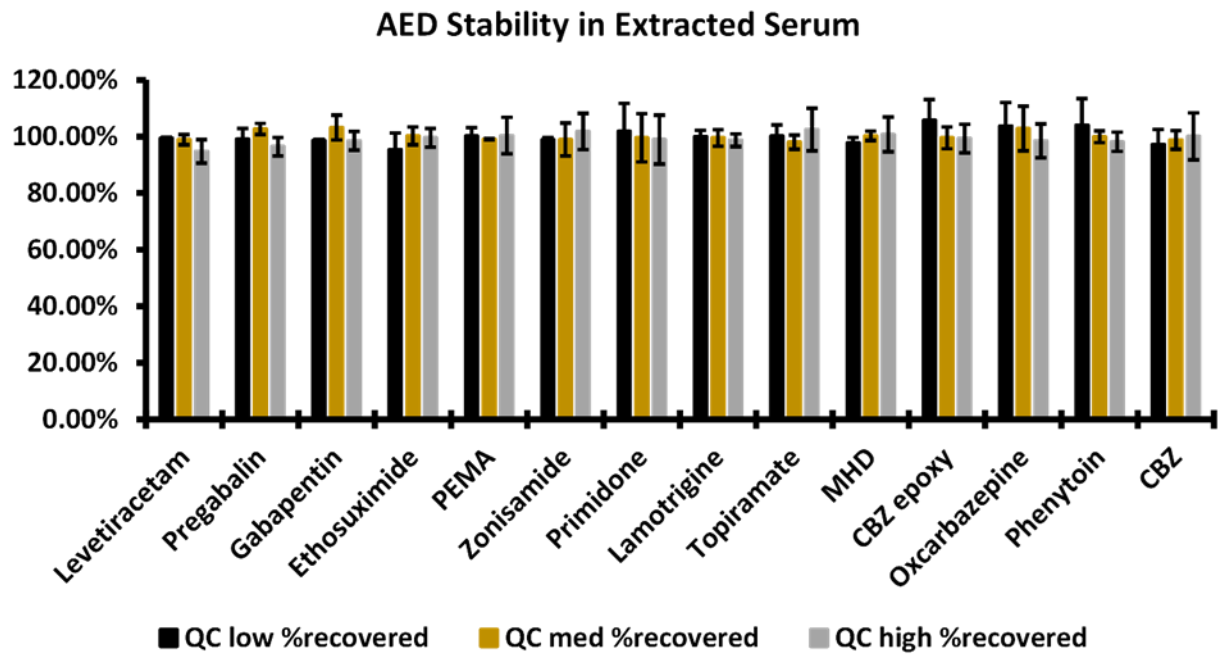


**Figure 1.4.** Stability of AEDs in extracted serum at 4°C after 48 hours (n = 3 technical replicates).



### **1.3.5. Method Comparison**

After successful method validation, the method was compared to another validated LC-UV method. The method was successfully applied to blind testing of 9 contrived samples and 21 residual patient samples from Vanderbilt University Medical Center's (VUMC's) clinical toxicology laboratory. The results of this study are outlined in **Tables 2 and 3**. The RPLC-MS/MS measurements in this study were compared to the clinical toxicology laboratory's LC-UV method, previously validated under the College of American Pathologists' requirements. The analytical figure of merit being compared is the % bias.

### **1.4. Discussion**

An RPLC-MS/MS method was developed and validated to quantify 14 AEDs in serum using FDA bioanalytical method validation and CLSI C62-A guidance documents.<sup>20,21</sup> The 14 AEDs are levetiracetam, pregabalin, gabapentin, ethosuximide, primidone, phenylethylmalonamide (PEMA), zonisamide, lamotrigine, topiramate, carbamazepine, carbamazepine epoxide, monohydroxy derivative of oxcarbazepine (MHD), oxcarbazepine, and phenytoin. The method, which can be tailored to any analyte in any matrix, has minimal sample handling steps and outlines an LC method that allows for separation to occur in less than 10 minutes run time (not including initial isocratic hold, purge, and re-equilibration times).

The analytical procedure's validity was evaluated by determining each analyte's LOQ, precision, accuracy, selectivity, carryover, recovery, matrix effect, and stability. Even though our LOQs for each analyte falls well below individual therapeutic ranges, the QCs analyzed spanned the entire therapeutic range for individual analytes. The determination of each AED's therapeutic range was based on available literature and clinical experience<sup>5</sup>. The within-day and between-day

**Table 1.2.** The developed and validated LC-MS/MS method was compared to VUMC's pre-existing LC-UV method by parallel analysis of serum samples.

| AED        | Parallel Sample # | AEDs          | Expected (µg/mL) | LC-UV (µg/mL) | LC-MS/MS (µg/mL) | LC-UV (%bias) | LC-MS/MS (%bias) |
|------------|-------------------|---------------|------------------|---------------|------------------|---------------|------------------|
| Parallel 1 |                   | pregabalin    | 3.00             | -             | 2.50             | -             | -17%             |
|            |                   | gabapentin    | 1.00             | -             | 1.18             | -             | 18%              |
| Parallel 2 |                   | zonisamide    | 11.0             | 0.00          | 11.0             | -100%         | 0%               |
|            |                   | lamotrigine   | 2.00             | 2.40          | 2.30             | 20%           | 15%              |
|            |                   | levetiracetam | 6.00             | 5.80          | 7.00             | -3%           | 17%              |
| Parallel 3 |                   | ethosuximide  | 55.0             | 11.0          | 17.5             | -80%          | -68%             |
|            |                   | MHD           | 9.00             | 9.00          | 8.50             | 0%            | -6%              |
| Parallel 4 |                   | pregabalin    | 11.0             | -             | 11.2             | -             | 2%               |
|            |                   | gabapentin    | 15.0             | -             | 13.8             | -             | -8%              |
| Parallel 5 |                   | zonisamide    | 26.0             | 26.0          | 25.0             | 0%            | -4%              |
|            |                   | lamotrigine   | 11.0             | 11.0          | 11.0             | 0%            | 0%               |
|            |                   | levetiracetam | 22.0             | 22.8          | 25.2             | 4%            | 15%              |
| Parallel 6 |                   | ethosuximide  | 77.0             | 33.0          | 52.5             | -57%          | -32%             |
|            |                   | MHD           | 24.0             | 23.0          | 26.0             | -4%           | 8%               |
| Parallel 7 |                   | pregabalin    | 30.0             | -             | 29.6             | -             | -1%              |
|            |                   | gabapentin    | 22.0             | -             | 21.9             | -             | 0%               |
| Parallel 8 |                   | zonisamide    | 50.0             | 50.2          | 52.7             | 0%            | 5%               |
|            |                   | lamotrigine   | 26.0             | 22.7          | 27.3             | -13%          | 5%               |
|            |                   | levetiracetam | 40.0             | 37.1          | 42.0             | -7%           | 5%               |
| Parallel 9 |                   | ethosuximide  | 150              | 70.0          | 101.1            | -53%          | -33%             |
|            |                   | MHD           | 45.0             | 45.0          | 50.0             | 0%            | 11%              |

**Table 1.3.** This was a blind study, whereas the concentrations of the serum samples received from VUMC’s clinic were compared to the McLean Lab’s validated LC-MS/MS analysis.

| Patient Sample # | AEDs          | LC – UV (µg/mL) | LC - MS/MS (µg/mL) |
|------------------|---------------|-----------------|--------------------|
| Patient 1        | Lamotrigine   | 12.2            | 10.22              |
|                  | Gabapentin    | no TDM ordered  | 6.47               |
| Patient 2        | Lamotrigine   | 10.6            | 4.96               |
|                  | Levetiracetam | 32.3            | 20.8               |
| Patient 3        | Lamotrigine   | 5.80            | 4.49               |
|                  | Levetiracetam | no TDM ordered  | 20.7               |
| Patient 4        | Lamotrigine   | 10.6            | 8.02               |
| Patient 5        | Lamotrigine   | 10.0            | 8.04               |
|                  | Levetiracetam | 61.5            | 71.0               |
| Patient 6        | Lamotrigine   | 14.2            | 8.58               |
|                  | Levetiracetam | 39.8            | 52.1               |
| Patient 7        | Lamotrigine   | 14.2            | 11.7               |
|                  | Levetiracetam | 39.8            | 40.3               |
| Patient 8        | Ethosuximide  | 145             | 134.8              |
|                  | Zonisamide    | 11.0            | 5.94               |
| Patient 9        | Levetiracetam | no TDM ordered  | 3.2                |
|                  | Pregabalin    | no TDM ordered  | 1.75               |
| Patient 10       | Ethosuximide  | 46.0            | 44.2               |
|                  | Lamotrigine   | no TDM ordered  | 5.18               |
|                  | Zonisamide    | 51.0            | 37.9               |
| Patient 11       | Levetiracetam | no TDM ordered  | 43.9               |
|                  | MHD           | no TDM ordered  | 19.3               |
| Patient 12       | Lamotrigine   | 11.8            | 6.66               |
| Patient 13       | Lamotrigine   | 8.00            | 5.74               |
|                  | Zonisamide    | 14.0            | 9.20               |
| Patient 14       | Zonisamide    | 10.0            | 6.35               |
|                  | Carbamazepine | 4.00            | 1.53               |
| Patient 15       | MHD           | 24.0            | 20.7               |
|                  | Topiramate    | 17.2            | 22.1               |
| Patient 16       | Levetiracetam | no TDM ordered  | 23.8               |
| Patient 17       | Lamotrigine   | 32.7            | 22.6               |
|                  | Levetiracetam | 46.4            | 39.7               |
|                  | Lamotrigine   | < 1.0           | < 1.0              |
| Patient 18       | Levetiracetam | 37.7            | 26.7               |
|                  | Gabapentin    | 6.70            | 4.03               |
| Patient 19       | Ethosuximide  | 75.0            | 73.9               |
| Patient 20       | MHD           | 13.0            | 10.5               |
|                  | Gabapentin    | no TDM ordered  | 1.03               |
| Patient 21       | MHD           | 39.0            | 27.6               |

precision and accuracy for 3 QC levels were < 15% CV and bias, respectively. The selectivity data (**Figure 1.2.**) showed that there were no endogenous interferences. In the carryover study, we determined that the carryover was negligible. Therefore it was not necessary to include blank samples between each concentrated sample. For individual AEDs, the recovery and matrix effects (**Table 1.1.**) were reproducible. In these studies, the stable isotopically labeled internal standards (SILIS) compensated for any issues with recovery or matrix effects by normalizing these internal standards. Finally, the stability study determined that extracted AED samples were stable at 4°C for at least 48 hours.

This method meets the criteria for routine clinical TDM due to sufficient linearity, accuracy, precision, carryover, recovery, matrix effects, selectivity, and stability. Our method was compared to VUMC's toxicology laboratories RPLC-UV method for 30 serum samples (21 patient samples). Many samples contained multiple AEDs. Recovery and accuracy for ethosuximide could be improved by the use of a SILIS of ethosuximide. Seven of the 30 samples contained additional AEDs not detected in the RPLC-UV method (pregabalin and gabapentin, **Table 1.2., Table 1.3.**). With the predicate RPLC-UV method in use at VUMC, a sample containing either of these drugs would need to be further analyzed at a reference laboratory. Also, samples containing carbamazepine would need to be tested using VUMC's immunoassay analyzer. This study demonstrates the utility of using one analytical method with the RPLC-MS/MS method. It streamlines sample handling and allows for a faster time-to-result for patients and physicians. RPLC-MS/MS also provides cost savings for the laboratory, as up to 14 different analyses could be performed in a single simultaneous assay.

### **1.5. Conclusions**

In conclusion, these results outline a developed and validated RPLC-MS/MS bioanalytical method that allows for the simultaneous quantification of 14 analytes (including active metabolites) in serum, according to FDA and CLSI guidelines. Because it is common for patients to be prescribed numerous compounds, many hospital laboratories use a combination of immunoassays, LC-UV, or reference testing to offer a large panel of TDM testing for analytes. The single and quantitative method outlined here would enable laboratories to quantitate 14 analytes simultaneously. The assay is specific, offers baseline separation of isobars/structural isomers, and is necessary to inform therapeutic decision-making for personalized medicine.

### **1.6. Acknowledgements**

This chapter was adapted from work done earlier in Don E. Davis, Jr.'s graduate education. I would like to thank Stacy D. Sherrod, Randi L. Gant-Branum, Jennifer M. Colby, Jody C. May, Simona G. Codreanu, Charles M. Nichols, James N. Dodds, and Andrzej Balinski for their contributions in various stages for advice and technical expertise. Financial support for this research was provided by The National Institutes of Health (National Cancer Institute R03CA222452). This work was supported in part using the Center for Innovative Technology resources at Vanderbilt University and the Department of Pathology, Microbiology, and Immunology at the Vanderbilt University Medical Center.

### **1.7. References**

- (1) Patsalos, P. N.; Spencer, E. P.; Berry, D. J. Therapeutic Drug Monitoring of Antiepileptic Drugs in Epilepsy. *Ther. Drug Monit.* **2018**, *40* (5), 1. <https://doi.org/10.1097/FTD.0000000000000546>

- (2) Patsalos, P. N.; Berry, D. J.; Bourgeois, B. F. D.; Cloyd, J. C.; Glauser, T. A.; Johannessen, S. I.; Leppik, I. E.; Tomson, T.; Perucca, E. Antiepileptic Drugs - Best Practice Guidelines for Therapeutic Drug Monitoring: A Position Paper by the Subcommittee on Therapeutic Drug Monitoring, ILAE Commission on Therapeutic Strategies. *Epilepsia*. **2008**, pp 1239–1276. <https://doi.org/10.1111/j.1528-1167.2008.01561.x>
- (3) Rogawski, M. A.; Löscher, W. The Neurobiology of Antiepileptic Drugs. *Nat. Rev. Neurosci.* **2004**, 5 (7), 553–564. <https://doi.org/10.1038/nrn1430>
- (4) Levy, R. H.; Schmidt, D. Utility of Free Level Monitoring of Antiepileptic Drugs. *Epilepsia* **1985**, 26 (3), 199–205. <https://doi.org/10.1111/j.1528-1157.1985.tb05406.x>
- (5) Louis, E. K. S. Monitoring Antiepileptic Drugs: A Level-Headed Approach. *Curr. Neuropharmacol.* **2009**, 7, 115–119.
- (6) Balestrini, S.; Sisodiya, S. M. Pharmacogenomics in Epilepsy. *Neuroscience Letters*. Elsevier Ireland Ltd **2018**, pp 27–39. <https://doi.org/10.1016/j.neulet.2017.01.014>
- (7) Krasowski, M. D.; McMillin, G. A. Advances in Anti-Epileptic Drug Testing. *Clinica Chimica Acta*. Elsevier B.V. **2014**, pp 224–236. <https://doi.org/10.1016/j.cca.2014.06.002>
- (8) Meador, K. J.; Loring, D. W. Developmental Effects of Antiepileptic Drugs and the Need for Improved Regulations. *Neurology* **2016**, 86 (3), 297–306. <https://doi.org/10.1212/WNL.0000000000002119>
- (9) Shibata, M.; Hashi, S.; Nakanishi, H.; Masuda, S.; Katsura, T.; Yano, I. Detection of 22 Antiepileptic Drugs by Ultra-Performance Liquid Chromatography Coupled with Tandem Mass Spectrometry Applicable to Routine Therapeutic Drug Monitoring. *Biomed. Chromatogr.* **2012**, 26 (12), 1519–1528. <https://doi.org/10.1002/bmc.2726>
- (10) Krasowski, M. D.; Siam, M. G.; Iyer, M.; Ekins, S. Molecular Similarity Methods for Predicting Cross-Reactivity with Therapeutic Drug Monitoring Immunoassays. *Ther. Drug Monit.* **2009**, 31 (3), 337–344. <https://doi.org/10.1097/FTD.0b013e31819c1b83>

- (11) Dasgupta, A. Impact of Interferences Including Metabolite Crossreactivity on Therapeutic Drug Monitoring Results. In *Therapeutic Drug Monitoring*; **2012**; Vol. 34, pp 496–506. <https://doi.org/10.1097/FTD.0b013e318261c2c9>
- (12) Krasowski, M. D.; Siam, M. G.; Iyer, M.; Pizon, A. F.; Giannoutsos, S.; Ekins, S. Chemoinformatic Methods for Predicting Interference in Drug of Abuse/Toxicology Immunoassays. *Clin. Chem.* **2009**, 55 (6), 1203–1213. <https://doi.org/10.1373/clinchem.2008.118638>
- (13) Dasgupta, A. Herbal Supplements and Therapeutic Drug Monitoring: Focus on Digoxin Immunoassays and Interactions with St. John’s Wort. In *Therapeutic Drug Monitoring*; **2008**; Vol. 30, pp 212–217. <https://doi.org/10.1097/FTD.0b013e31816b918f>
- (14) Krasowski, M. D. Therapeutic Drug Monitoring of the Newer Anti-Epilepsy Medications. *Pharmaceuticals*. **2010**, pp 1909–1935. <https://doi.org/10.3390/ph3061908>
- (15) Patsalos, P. N.; Zugman, M.; Lake, C.; James, A.; Ratnaraj, N.; Sander, J. W. Serum Protein Binding of 25 Antiepileptic Drugs in a Routine Clinical Setting: A Comparison of Free Non-Protein-Bound Concentrations. *Epilepsia* **2017**, 58 (7), 1234–1243. <https://doi.org/10.1111/epi.13802>
- (16) D’Urso, A.; Cangemi, G.; Barco, S.; Striano, P.; D’Avolio, A.; de Grazia, U. LC-MS/MS Based Quantification of Nine Antiepileptic Drugs from Dried Sample Spots Device. *Ther. Drug Monit.* **2019**, 1. <https://doi.org/10.1097/FTD.0000000000000600>
- (17) Kuhn, J.; Knabbe, C. Fully Validated Method for Rapid and Simultaneous Measurement of Six Antiepileptic Drugs in Serum and Plasma Using Ultra-Performance Liquid Chromatography-Electrospray Ionization Tandem Mass Spectrometry. *Talanta* **2013**, 110, 71–80. <https://doi.org/10.1016/j.talanta.2013.02.010>
- (18) Zhang, M.; Yin, L.; Wang, T.; Shi, M.; Zhang, Y.; Gu, J.; Zhao, X. A Parallel-Column LC-MS/MS Method for High-Throughput Analysis of Eight Antiepileptic Drugs in Clinical Therapeutic Drug Monitoring. *Chromatographia* **2016**, 80 (1), 137–143. <https://doi.org/10.1007/s10337-016-3196-8>

- (19) Miura, M.; Takahashi, N. Routine Therapeutic Drug Monitoring of Tyrosine Kinase Inhibitors by HPLC-UV or LC-MS/MS Methods. *Drug Metab. Pharmacokinet.* **2016**, *31* (1), 12–20. <https://doi.org/10.1016/j.dmpk.2015.09.002>
- (20) FDA. Guidance for Industry: Bioanalytical Method Validation. **2018**, No. FDA-2013-D-1020, pp 1-41.
- (21) CLSI. Liquid Chromatography-Mass Spectrometry Methods; Approved Guidelines (C62-A). **2014**, No. 1-56238-977–7, pp 1-71.
- (22) Finney, G. L.; Chambers, M.; MacCoss, M. J.; Liebler, D. C.; Shulman, N.; Tomazela, D. M.; Tabb, D. L.; Kern, R.; Frewen, B.; MacLean, B. Skyline: An Open Source Document Editor for Creating and Analyzing Targeted Proteomics Experiments. *Bioinformatics* **2010**, *26* (7), 966–968. <https://doi.org/10.1093/bioinformatics/btq054>
- (23) Shulman, N. J.; Henderson, C. M.; MacLean, B.; Hoofnagle, A. N.; MacCoss, M. J. Skyline Performs as Well as Vendor Software in the Quantitative Analysis of Serum 25-Hydroxy Vitamin D and Vitamin D Binding Globulin. *Clin. Chem.* **2017**, *64* (2), 408–410. <https://doi.org/10.1373/clinchem.2017.282293>



## CHAPTER 2

### ELUCIDATING PERIPHERAL AMINO ACID CHANGES IN OBESITY AND ALZHEIMER'S DISEASE UTILIZING LC-MS/MS AND LC- HRMS/MS

#### **2.1. Introduction**

Alzheimer's disease (AD) is the most prevalent age-associated neurodegenerative disease.<sup>1,2</sup> While AD results from complex interactions among genetic, nutritional, environmental, and aging-associated factors, recent research has shown that obesity and diabetes are risk factors for AD with a high prevalence of both of these conditions in western societies.<sup>3-8</sup> Many brain regions (e.g. hippocampus) are susceptible to glucose and oxygen supply changes because they have high metabolic activity. Such changes under high-fat diet (HFD) conditions are strongly related to accelerated cognitive decline.<sup>9</sup> Chronic peripheral inflammation from an increase in adipose tissue also manifests in the brain and decreases brain white matter (which leads to impaired neuronal connections).<sup>1</sup> Furthermore, a HFD alters hippocampal morphology and synaptic complexity and density, which may offer some explanation for diet-associated cognitive decline in young wild-type animals as well as in AD and aged models.<sup>10-14</sup>

The mitochondrial cascade hypothesis plays a significant role in AD's pathogenesis, precedes amyloid- $\beta$  (A $\beta$ ) plaque formation, and has been observed in mouse AD models.<sup>15-20</sup> Such changes have not been extensively studied in the context of diet-induced obesity in AD. However, evidence suggests that mitochondrial dysfunction, associated with mitochondrial damage and oxidative stress, is triggered by AD neuropathology and HFD feeding.<sup>18</sup> Another possible explanation for mitochondrial dysfunction is an impairment of amino acid degradation pathways, which occurs before the mitochondrial tricarboxylic acid (TCA) cycle.<sup>21</sup> Previous studies using

plasma shows that specific free amino acids are in a state of imbalance in type 2 diabetes and prediabetes.<sup>22-23</sup> Specifically, branched-chain amino acids (BCAAs—leucine, isoleucine, and valine), aromatic amino acids (phenylalanine, tyrosine, and tryptophan), alanine, glycine, proline, and glutamine are related to insulin resistance, irregular glucose levels, and diabetes.<sup>23-26</sup> One specific mechanism for the risk of AD associated with obesity and diabetes is the increase or accumulation of amino acid levels. Elevated levels of BCAAs (leucine, isoleucine, and valine) have been shown to induce neuronal oxidative stress, apoptosis, and mammalian target of rapamycin (mTOR) hyperactivation, which leads to insulin resistance in the brain—representing some of the significant pathophysiological hallmarks of AD.<sup>21,27-28</sup>

Therefore, to further understand the relationship between amino acid metabolism, diet, and AD, we assessed the effect of high fat diet on amino acid levels in liver in a mouse model of AD. Specifically, we addressed whether a cessation of high-fat diet feeding and subsequent weight loss could improve the amino acid imbalances in peripheral tissues or potentially lead to new druggable targets. It is crucial to simultaneously analyze many metabolites to arrive at a more accurate etiologic picture.<sup>21</sup> In this study, targeted and untargeted metabolomics were used to measure the interaction between AD genotype and obesity on amino acid metabolism (**Figure 2.1**). Both targeted and untargeted strategies measure the organism's current biochemical state. We directly assayed specific amino acids to provide absolute quantitative measurement (targeted), since these are highly likely to be impacted by HFD and related obesity.<sup>21,29</sup> We then further utilized an untargeted strategy to provide a global view of all biochemical processes and pathways. A qualitative reversed-phase liquid chromatography-high resolution tandem mass spectrometry (RPLC-HRMS/MS) method was developed for untargeted amino acid analyses and pathway

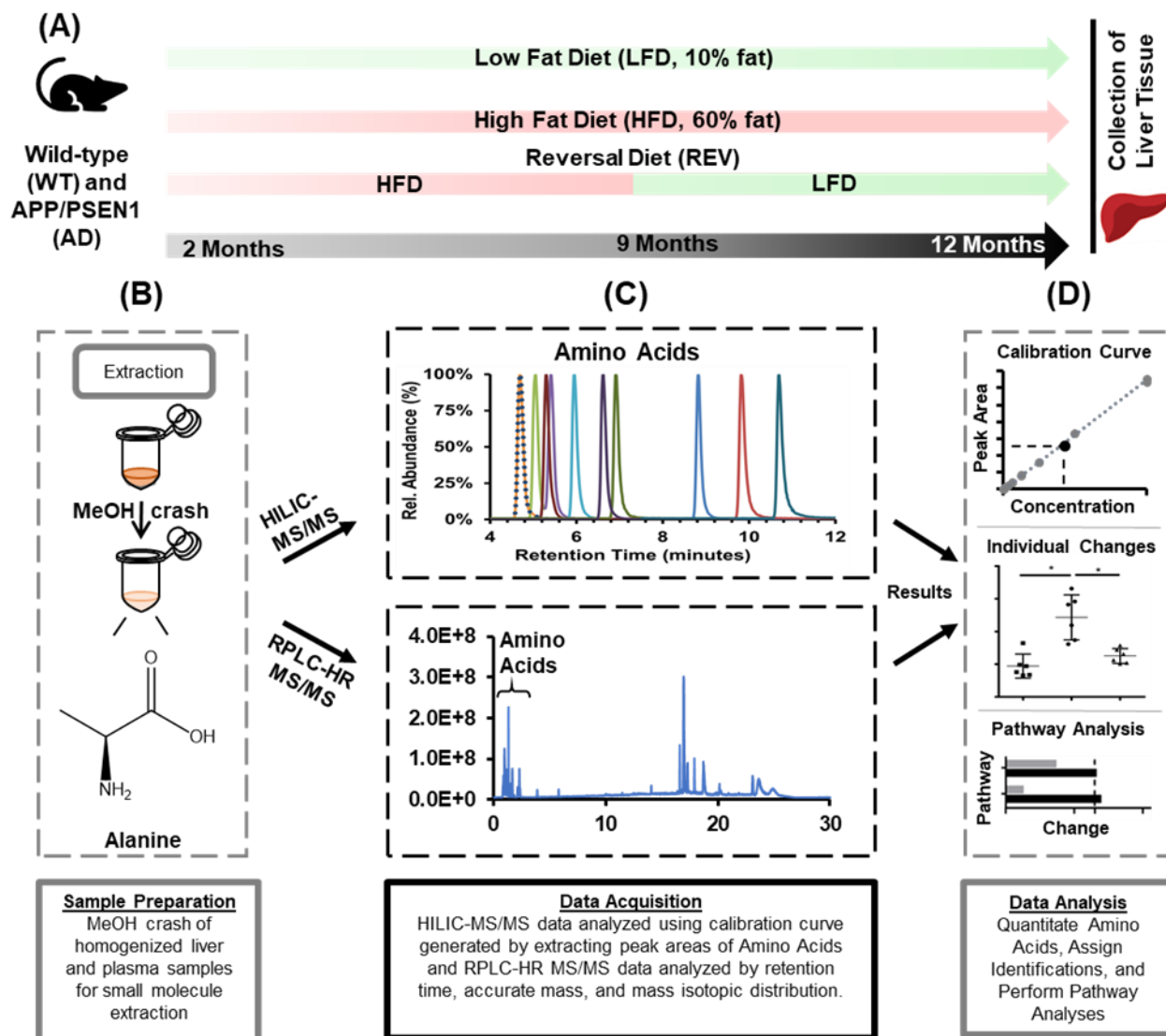


**Figure 2.1.** Mouse study conditions and analytical workflow. (A) WT and APP/PSEN1 mice were split into LFD, HFD, or REV diet groups ( $n=6$  mice per group, 3 male and 3 female). At 12 months of age, tissue was harvested for analysis. Tissues were obtained from a subset of mice included in a previous study.<sup>33</sup> (B) Extraction protocol from harvested liver tissue. Tissue was homogenized, and a cold Methanol (MeOH) protein precipitation was used to eliminate protein interferences. (C) Targeted amino acid extracted ion chromatogram (XIC) (top) using hydrophilic interaction liquid chromatography (HILIC) and untargeted chromatogram (bottom) using reversed-phase liquid chromatography (RPLC). (D) Data analysis workflow. For targeted workflow, amino acids were quantified using the validated targeted method. For untargeted workflow, significantly changed features were annotated, and pathway analysis was performed.

discovery. A quantitative hydrophilic interaction liquid chromatography-triple quadrupole mass spectrometry (HILIC-MS/MS) method was developed and validated<sup>30-32</sup> for targeted amino acid analyses and confirmation of our discovery experiments. Our HILIC-MS/MS and RPLC-HRMS/MS analytical workflow can be used in any analytical setting and should prove beneficial for laboratories interested in increasing confidence in amino acid pathway discovery and validation/confirmation in plasma, serum, liver tissue, urine, or other various matrices.

## **2.2. *Experimental Methods***

### **2.2.1. *Standards and Chemicals***

All amino acids and stable isotopically labeled internal standards (SIL-ISs) were purchased from Millipore Sigma (Burlington, MA), CDN Isotopes (Pointe-Claire, Quebec, CA), or Cambridge Isotope Laboratories (Tewksbury, MA). Optima LC/MS grade water, methanol, ammonium formate, formic acid, and acetonitrile were obtained from Fisher Scientific (Hampton, NH).

### **2.2.2. *Human Plasma Samples***

Pooled human plasma was obtained from the Vanderbilt University Medical Center (VUMC) clinical toxicology laboratory for validated experiments (targeted analyses). Plasma was collected fresh, pooled, and stored at 4°C until aliquoting. Plasma was then aliquoted into 1-mL polypropylene microcentrifuge tubes (Eppendorf, Hauppauge, NY) and frozen at -80°C for long-term storage until use. One aliquot was removed at a time, allowed to thaw at 4°C, and then prepared according to the extraction protocol described in **Figure 2.1.B**.

### ***2.2.3. Mice Peripheral Tissue Samples***

Liver samples from male and female APP<sub>Swe</sub>/PS1<sub>ΔE9</sub> (APP/PSEN1) transgenic mice and wild-type (WT) littermates were collected after sacrifice at 12 months. These mice are a subset of mice for which behavioral and biochemical data have already been published, including weight change and diabetic state as assessed by glucose tolerance tests.<sup>33</sup> Briefly, at 2-months of age, standard lab chow (Purina 5001, 4% kcal/fat) was replaced with either HFD in which 60% kcal are derived from lard, 20% from carbohydrate and 20% from protein, or low-fat diet (LFD) control in which 10% kcal are derived from lard and additional calories are derived from corn starch, with 70% carbohydrate and 20% from protein.<sup>33</sup> For the reversal group (REV), a subset of mice on the HFD was provided with an LFD, at 9.5 months of age, for the study duration.<sup>33</sup> All other mice were maintained on their original experimental diets until the end of the study, an additional 10 weeks.<sup>33</sup> After sacrifice, liver tissue samples were taken and put immediately on dry ice and stored at  $-80^{\circ}\text{C}$  until used in the analytical workflow described herein.<sup>33</sup>

### ***2.2.4. Plasma and Liver Sample Preparation***

For all plasma and liver samples analyzed in these studies, a methanol protein precipitation was performed in a 1.5-mL polypropylene microcentrifuge tube (Eppendorf, Hauppauge, NY). For liver samples, frozen tissues were first individually pulverized using a pestle and mortar followed by lysing in 1mL ice-cold lysis buffer (1:1:2, ACN:MeOH:Ammonium Bicarbonate (0.1M, pH 8.0) (LC-MS grade). Individual samples were sonicated using a probe tip sonicator, 10 pulses, at 30% power, and cooled down on ice between samples. A BCA protein assay was used to determine the protein concentration for each individual sample, and adjusted to a total amount of protein of 200 $\mu\text{g}$  in 200  $\mu\text{L}$  of lysis buffer. For untargeted studies, SIL-ISs, Biotin-D2, and Phenylalanine-

D8, were added to each sample to assess sample processing steps (metabolite extraction and reconstitution). For targeted assays, a mixture of SIL-IS for each amino acid quantified in the method were added (**Table B.1.**). Following lysis and addition of SIL-ISs, protein precipitation was performed by adding 800 $\mu$ L of ice-cold methanol (4x by volume). Samples were incubated at -80°C overnight. Following incubation, samples were centrifuged at 10,000 rpm for 10 min. The supernatant containing metabolites were dried in vacuo, and metabolite extracts were stored frozen at -80°C until ready to use. Prior to mass spectrometry analysis, metabolite extracts were reconstituted in 100  $\mu$ l of acetonitrile/ water (3:97, v/v) with 0.1% FA, and centrifuged for 5 min at 15,000 rpm to remove insoluble material. For untargeted studies, quality control samples were prepared by pooling equal volumes of each sample. SIL-ISs, Tryptophan-D3, Carnitine-D9, Valine-D8 and Inosine-4N15, were added to each sample to assess MS instrument reproducibility for the untargeted analysis (**Table B.3.**). For the targeted method, quality control samples were prepared at the concentrations in **Table B.4.** and SIL-ISs for each amino acid were added to assess the accuracy and precision of quantification.

### **2.2.5. Chromatographic Conditions**

For the HILIC-MS/MS targeted method, shown in **Figure 2.1.**, amino acids were analyzed using a 2.1 x 100 mm zwitterionic hydrophilic interaction liquid chromatography (ZIC-HILIC) column, SeQuant ZIC-HILIC 3.5  $\mu$ m (Merck Millipore, Burlington, MA) with a 2.1 x 2 mm SecurityGaurd ULTRA UHPLC HILIC guard column (Phenomenex, Torrance, CA). The column was maintained at 40°C for separation by ultra high-pressure liquid chromatography (UHPLC, Agilent 1290 Infinity II LC system, Agilent Technologies, Santa Clara, CA). Mobile phase A was comprised of 90/10 (v/v) water/acetonitrile with 5mM ammonium formate. Mobile phase B was

comprised of 90/10 (v/v) acetonitrile/water with 5mM ammonium formate. The UHPLC was directly coupled online to a commercial triple quadrupole mass spectrometer (6470, Agilent Technologies, Santa Clara, CA). A 1  $\mu$ L sample was injected at a flow rate of 200  $\mu$ L/min and was subjected to the chromatographic conditions as follows: mobile phase B was maintained at 95% for the first 1 min, linearly decreased from 95% to 45% over 19 mins, held at 45% for 2 mins, linearly increased from 45% to 95% over 18 mins, and held at 95% for 5 mins for re-equilibration. (gradient length: 45 min). A representative chromatogram of the amino acids quantified is shown in **Figure 2.1.C** and **Appendix B.1**.

High resolution (HR) MS and data-dependent acquisition analyses (MS/MS), shown in **Figure 2.1.**, were performed on a high resolution Q-Exactive HF hybrid quadrupole-Orbitrap mass spectrometer (Thermo Fisher Scientific, Bremen, Germany) equipped with a Vanquish UHPLC binary system and autosampler (Thermo Fisher Scientific, Germany). For the RPLC analysis, metabolite extracts (5 $\mu$ L injection volume) were separated on a Hypersil Gold, 1.9 mm, 2.1mm x 100 mm column (Thermo Fisher) held at 40°C. Liquid chromatography was performed at 250  $\mu$ L/min using solvent A (0.1% formic acid (FA) in water) and solvent B (0.1% FA in acetonitrile) with the following gradient: 5% B for 1 min, 5-50% B over 9 min, 50-70% B over 5 min, 70-95% B over 5 min, 95% B held 2 min, and 95-5% B over 3 min, 5% B held 5 min (gradient length: 30 min).

#### **2.2.6. MS/MS and High-Resolution MS/MS conditions**

For HILIC-MS/MS experiments, amino acids were analyzed in positive ionization mode using the Jet Stream ESI source (Agilent Technologies, Santa Clara, CA). Nitrogen was used as the nebulizing gas and the collision gas. Amino acid transitions were collected using the scheduled

multiple reaction monitoring (MRM) mode. MRM transitions are listed in the supporting information **Table B.1**. Mass spectrometry conditions were optimized on a per-molecule basis for compound dependent parameters (such as fragmentor voltage and collision energy voltage) by flow injection analysis to maximize sensitivity. Data were acquired using Agilent's MassHunter Workstation Data Acquisition software and analyzed using Skyline (Michael MacCoss, University of Washington), Agilent's MassHunter Quantitative Analysis, MassHunter Qualitative Analysis software, and Microsoft Excel.<sup>34-37</sup>

For RPLC-HRMS/MS experiments, full MS analyses were acquired over a mass range of  $m/z$  70-1050 using electrospray ionization positive mode using the previously developed protocol.<sup>38</sup> Full mass scan was used at a resolution of 120,000 with a scan rate of 3.5 Hz. The automatic gain control (AGC) target was set at  $1 \times 10^6$  ions, and maximum ion injection time was at 100 ms. Source ionization parameters were optimized with the spray voltage at 3.0 kV, and other parameters were as follows: transfer temperature at 280 °C; S-Lens level at 40; heater temperature at 325°C; Sheath gas at 40, Aux gas at 10, and sweep gas flow at 1. Tandem mass spectra were acquired using a data dependent scanning mode in which one full MS scan ( $m/z$  70-1050) was followed by 2, 4 or 6 MS/MS scans. MS/MS scans are acquired in profile mode using an isolation width of 1.3  $m/z$ , stepped collision energy (NCE 20, 40), and a dynamic exclusion of 6 s. MS/MS spectra were collected at a resolution of 15000, with an automatic gain control (AGC) target set at  $2 \times 10^5$  ions, and maximum ion injection time of 100 ms. The retention times and peak areas of the isotopically labeled standards were used to assess data quality.



### **2.2.7. Method Validation**

The targeted HILIC-MS/MS amino acid assay was evaluated according to guidelines established by the CLSILC-MS C62-A document and FDA's Guidance for Industry Bioanalytical Method Validation.<sup>30,31</sup> Analytical figures of merit including the limit of quantification (LOQ), linearity (**Table B.2.**), accuracy, precision, carryover, stability, recovery, and matrix effect<sup>39</sup> were assessed, and results of accuracy, precision, matrix effect, and recovery; these data can be viewed in **Table 2.1**. All validation experiments were performed in plasma, except for matrix effect and recovery, which were performed in both plasma and liver tissue to compare extraction and ionization efficiencies between different matrices. The method validation HILIC-MS/MS experiments were used to confirm the amino acid metabolism findings obtained in the untargeted studies.

### **2.2.8. Method Application**

The analytical workflow was applied to 36 mouse liver samples equally split among the six groups (APP/PSEN1-HFD, APP/PSEN1-LFD, APP/PSEN1-REV, WT-HFD, WT-LFD, WT-REV). Mouse liver samples were prepared in batches according to the protocol described above for untargeted and targeted analyses. For the targeted analysis, samples were analyzed in triplicate along with calibrators and quality control samples. Individual amino acids passed accuracy and precision metrics (<15% bias and CV respectively) in quality control samples (n=5/level, where levels correspond to low, medium, high, see **Table B.4.**), except Glutamic Acid, for which the accuracy was -22% and -23% for quality control levels medium and high, respectively. Data were analyzed using Skyline (Michael MacCoss, University of Washington), Agilent's MassHunter Quantitative Analysis, MassHunter Qualitative Analysis software, and Microsoft Excel.<sup>34-37</sup>

**Table 2.1.** Validation results for targeted amino acid method. Accuracy and precision data for amino acids of interest at QC medium levels (**Table B.4.**), n=15 runs across three batches. Percent matrix effect and recovery in plasma ( $n = 5$ ) and liver tissue ( $n = 4$ ) for amino acids of interest at quality control medium concentrations. For matrix effect, 100% represents no matrix effect.

| Amino Acid      | Accuracy (% bias)<br>Plasma | Precision (%CV)<br>Plasma | Matrix Effect (%)<br>Plasma | Recovery (%)<br>Plasma | Matrix Effect (%)<br>Liver Tissue | Recovery (%)<br>Liver Tissue |
|-----------------|-----------------------------|---------------------------|-----------------------------|------------------------|-----------------------------------|------------------------------|
| Alanine         | 0.9                         | 1.3                       | 99                          | 97                     | 104                               | 95                           |
| L-Glutamic Acid | -9.1                        | 31                        | 107                         | 97                     | 100                               | 93                           |
| Glycine         | -0.5                        | 3.8                       | 123                         | 96                     | 103                               | 95                           |
| L-Isoleucine    | 3.5                         | 8.7                       | 79                          | 96                     | 97                                | 96                           |
| L-Leucine       | 3.8                         | 10                        | 102                         | 96                     | 104                               | 94                           |
| L-Methionine    | 0.4                         | 4.9                       | 108                         | 92                     | 104                               | 95                           |
| L-Phenylalanine | 3.4                         | 2.0                       | 89                          | 97                     | 103                               | 95                           |
| L-Threonine     | 2.9                         | 1.8                       | 96                          | 97                     | 105                               | 95                           |
| L-Tryptophan    | 2.4                         | 1.3                       | 115                         | 92                     | 106                               | 96                           |
| L-Tyrosine      | 0.9                         | 1.4                       | 116                         | 98                     | 102                               | 94                           |
| L-Valine        | -1.5                        | 3.3                       | 100                         | 96                     | 103                               | 95                           |

Statistical analyses were analyzed using GraphPad Prism (version 8.0); we utilized t-tests with Bonferroni corrections for multiple comparisons.

Untargeted RPLC-HRMS/MS raw data were imported, processed, normalized, and reviewed using Progenesis QI v.2.1 (Non-linear Dynamics, Newcastle, UK). All MS and MS/MS sample runs were aligned against a quality control (pooled) reference run, and peak picking was performed on individual aligned runs to create an aggregate data set. Unique ions (retention time and m/z pairs) were grouped (a sum of the abundances of unique ions) using both adduct and isotope deconvolutions to generate unique ‘features’ (retention time and m/z pairs) representative of unannotated metabolites. Data were normalized to all features using Progenesis QI. Compounds with <25% coefficient of variance (%CV) were retained for further analysis. Variance stabilized measurements achieved through log normalization were used with Progenesis QI to calculate p-values by one-way analysis of variance (ANOVA) test and adjusted p-values (Q-values). Significantly changed metabolites were chosen with the criteria Q-value <0.05 and |FC| > 1.5.

Tentative and putative identifications were determined within Progenesis QI using accurate mass measurements (<5 ppm error), isotope distribution similarity, and fragmentation spectrum matching based on database searches against Human Metabolome Database (HMDB)<sup>40</sup>, METLIN<sup>41</sup>, the National Institute of Standards and Technology (NIST) database<sup>42</sup>, and an in-house library. In these experiments, the level system for metabolite identification confidence was utilized.<sup>43</sup> Briefly, many annotations were considered to be tentative (level 3, L3) and/or putative (level 2, L2); in numerous circumstances a top candidate cannot be prioritized. Thus annotations may represent families of molecules that cannot be distinguished. The biostatistical analysis was performed in Progenesis QI 2.0, and pathway analysis was done using MetaboAnalyst 4.0, and Mummichog 2.0.<sup>44-50</sup>

## **2.3. Results and Discussion**

### **2.3.1. Method Validation**

We did not observe significant matrix effects (i.e., ionization suppression or ionization enhancement matrix effect > 20%) for 10/11 amino acids of interest. Glycine was the only amino acid with a slightly higher matrix effect (23%), though this did not affect its %CV or %bias significantly (>15%). In this method, all amino acids were recovery greater than 90%. Matrix effect and recovery were comparable in the two matrices studied. All amino acids analyzed met the acceptance criteria for precision and accuracy (<15% CV and <15% bias, respectively), except glutamic acid. Glutamic acid's precision and accuracy study was performed before a SIL-IS was acquired for Glutamic Acid, and it was normalized to a neighboring SIL-IS with an inexact retention time match. For Glutamic Acid, precision exceeded 15% CV in initial validation experiments. However, the glutamic acid SIL-IS with an exact retention time was used for quantification runs, which showed appropriate precision. These results suggest that the analytical method reported here minimizes endogenous interferences, allowing for reliable and reproducible quantification of the amino acids.

### **2.3.2. Method Application**

From the untargeted metabolomics analyses, >3000 metabolites were detected in the liver samples. Many metabolites (typically >500) were observed to be statistically significant ( $p \leq 0.05$  and fold change  $\geq |1.5|$ ) in numerous pairwise comparisons related to genotype (WT vs. APP/PSEN1) and/or diet (HFD vs. LFD and HFD vs. REV), as seen in the supporting information

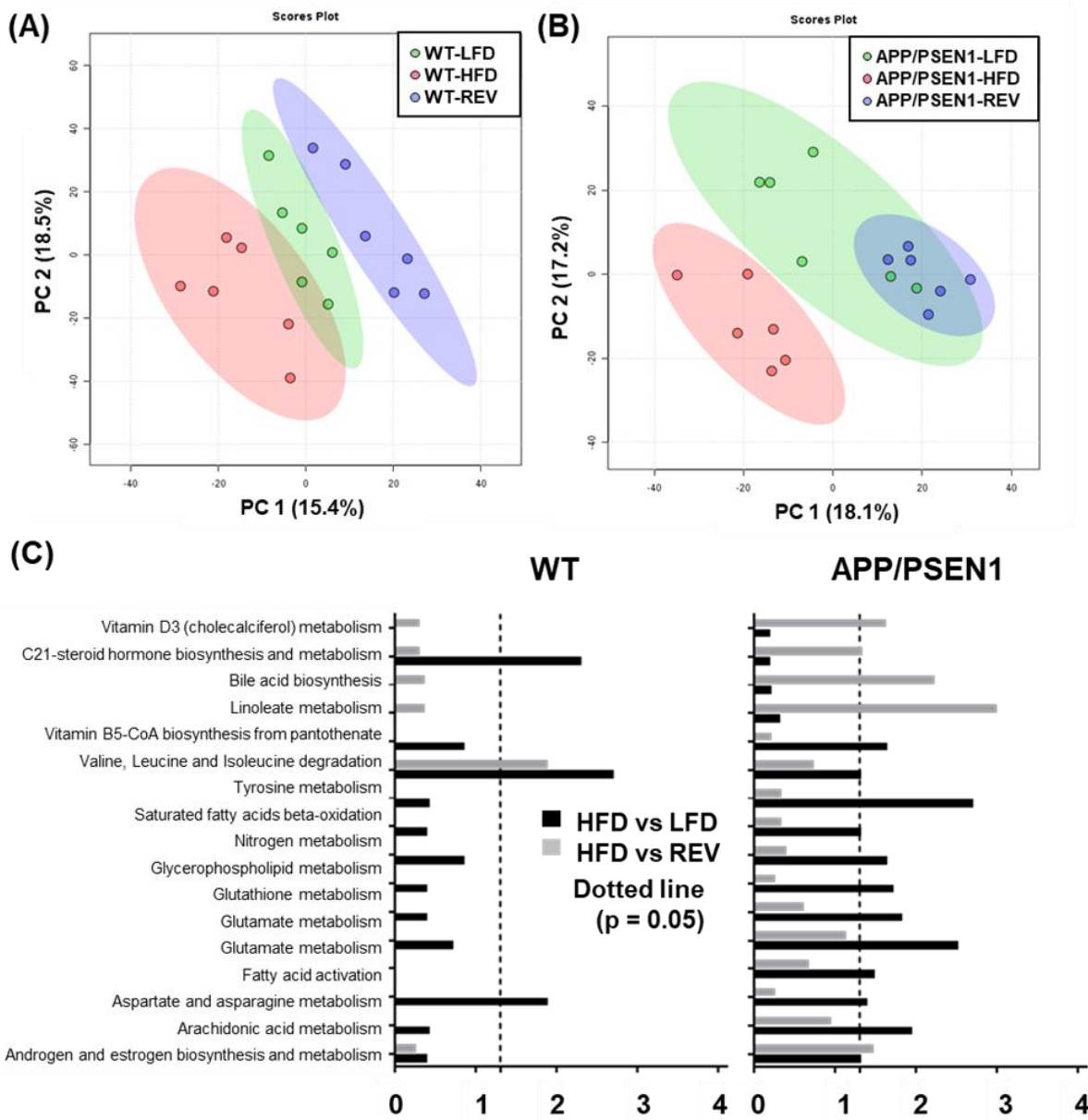


**Figure 2.2.** Multivariate statistical analyses to distinguish amino acid metabolism phenotypes between groups. Separation and metabolic profile classification between A) the three diet groups of WT mice by Partial Least Squares-Discriminant Analysis (PLS-DA) with PC1 describing 15.4% of the variation and PC2 describing 18.5%, B) the three diet groups of APP/PSEN1 mice by PLS-DA with PC1 describing 18.1% of the variation and PC2 describing 17.2%, and C) significant pathways in APP/PSEN1 mice between LFD/HFD and HFD/REV by Mummichog analysis on significant features ( $p < 0.050000$ ). Individual pathways are significant if  $p < 0.05$  for each of the pairwise comparisons.

**Table B.5.** A global view of the multi-dimensional data illustrates that liver tissue differences were observed between mice genotypes and diet conditions. Partial Least Squares-Discriminant Analysis (PLS-DA), displayed in **Figure 2.2.A and B**, highlight global changes between diet groups for each genotype. Notably, minimal overlap is observed between the LFD and HFD groups of each genotype, highlighting the distinct metabolic changes induced by HFD feeding. In WT mice, the REV diet group does not overlap with other groups, while in APP/PSEN1 mice, the REV groups overlap with the LFD group. This signifies that both the initial response to HFD and the potential for a subsequent rescue of effects by removal of HFD differ between the APP/PSEN1 and wild-type animals.

Using differential meta-analysis of the individual pairwise comparisons, the peripheral metabolites and metabolic pathways changed based on diet were determined, specifically those which were partially or fully reversible. In APP/PSEN1 mice, the pathways valine, leucine, and isoleucine degradation, tyrosine metabolism, nitrogen metabolism, glutathione metabolism, glutamate metabolism, and aspartate and arginine metabolism were all found to be distinctly different between LFD and HFD (assessed by Mummichog analysis with a p-value of less than 0.05 considered significant, **Table B.6.**). These pathways are found to be adversely affected by HFD and together may be indicative of mitochondrial dysfunction as these amino acid metabolism pathways feed into the mitochondrial TCA cycle.<sup>21,51</sup> Changes in some of the same pathways are also shown for wild-type mice (compared in **Figure 2.2.C**), highlighting that fewer of the same pathways were dysregulated under HFD conditions. Some pathways show similar changes while others show changes exacerbated by AD, which illuminated the unique changes caused by AD. This data illustrates a more sensitive metabolic response in AD mice based on diet changes than when compared to WT mice.

In addition to looking at dysregulated pathways, the levels of individual amino acids were monitored through the developed and validated targeted method. Upon calculating amino acid concentrations (for targeted analysis) and normalized abundance ratios (for untargeted analysis) in each sample, sample groups were compared (**Tables S7 and S8**, respectively). Multiple amino acids, including alanine, glutamic acid, leucine, isoleucine, and phenylalanine, were significantly increased in APP/PSEN1 mice on HFD compared to LFD. Absolute and relative abundance concentration levels of amino acids for mice on the REV diet were more similar to LFD levels demonstrating the partially reversible effect that diet has on specific amino acid concentrations in liver (**Figure 2.3**). The same trends were observed in both targeted and untargeted analyses, experiments that were prepared in separate batches (at different times) and used different chromatographic and mass spectrometry methods, indicating the reproducibility of the results. Again, while similar trends were seen in WT mice, there are fewer significant changes in individual amino acids and pathways, highlighting the combined effect of obesity and AD on amino acid metabolism and further supports mitochondrial dysfunction is an impairment of amino acid degradation pathways.

These dysregulated peripheral pathways include numerous amino acid pathways directly linked to the TCA cycle and mitochondrial dysfunction (**Figure 2.4**).<sup>16,21</sup> In a normal state, the amino acids feed into the citric acid cycle in the mitochondria in various locations to provide energy for the organism (**Figure 2.4**). When looking at the differences in metabolism between the LFD and HFD APP/PSEN1 mice, many pathways involving these amino acids were significantly altered, such as glutamate and glutamine metabolism and valine, leucine, and isoleucine degradation. These dysregulated peripheral pathways are directly linked to the TCA cycle and

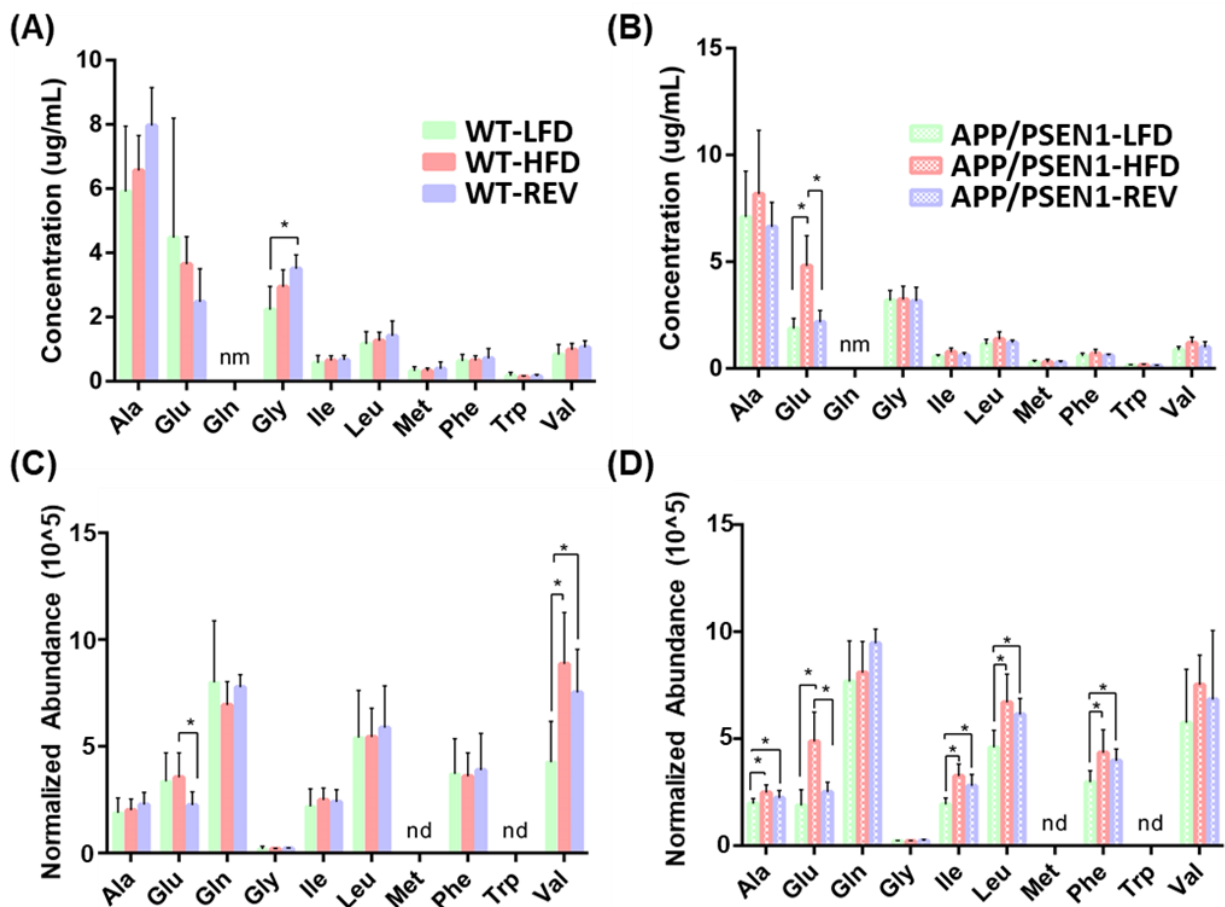


**Figure 2.3.** Individual amino acid trends from untargeted and targeted data acquisition across diet groups for APP/PSEN1 and WT mice. A) and B), represent wild-type and APP/PSEN1 comparisons, from targeted analysis, with significance calculated by unpaired t-tests followed by Bonferroni corrections for multiple comparisons, respectively. C) and D), respectively, show WT and APP/PSEN1 comparisons untargeted analysis, with significance calculated by ANOVA followed by correction for multiple comparisons. \* indicated p-value <0.05. nm=not measured by targeted method, nd=not detected by untargeted method.



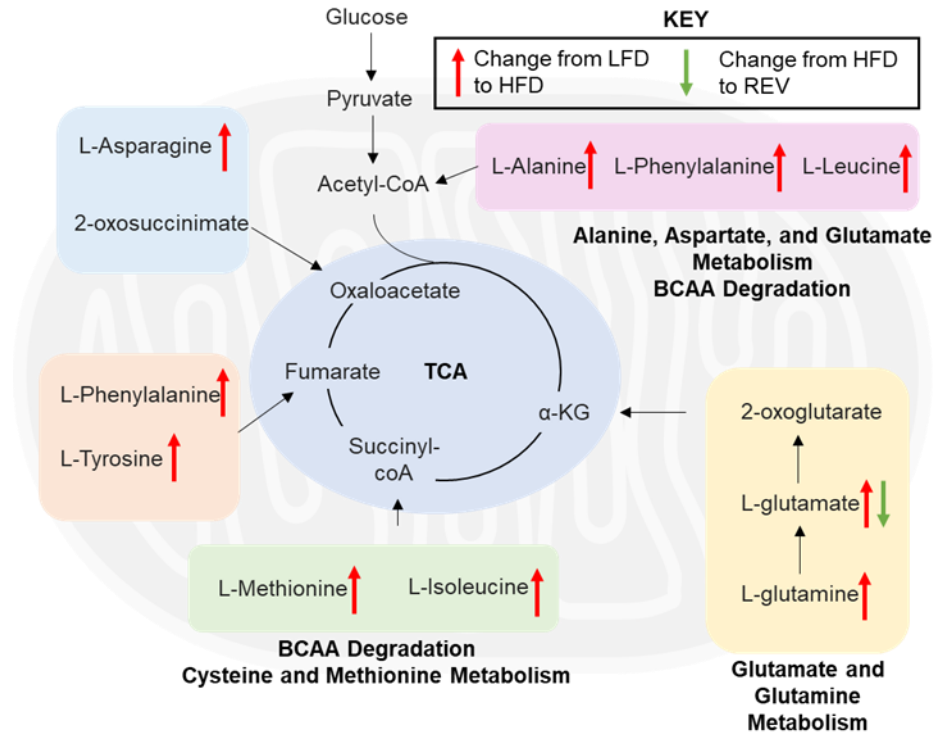


**Figure 2.4.** Amino acid changes indicate mitochondrial dysfunction. Altered pathways feed into the tricarboxylic acid cycle (TCA) in the mitochondria and thus contribute to mitochondrial dysfunction. Red arrow represents significant increase from low fat diet to high fat diet in APP/PSEN1 mice, and green arrow represents significant decrease from high fat diet to reversal diet in APP/PSEN1 mice.

mitochondrial dysfunction, which can directly impact the pathogenesis of AD. These results suggest that the HFD may contribute to AD pathogenesis by further contributing to this mitochondrial dysfunction.<sup>16,21,52</sup> For several individual amino acids within these pathways, the same trend emerges of increasing amino acid levels in HFD compared to LFD, with decreases in the REV diet mice compared to HFD. This pattern was more pronounced in the APP/PSEN1 mice than in the WT mice. These reversibility trends support the hypothesis that mice with APP/PSEN1 mutations are more sensitive to diet conditions and that the metabolic dysregulation that follows from exposure to HFD has the potential to be reversed. Significantly increased changes in amino acid levels in APP/PSEN1 and following HFD suggested that the worsening cognitive decline seen in transgenic mice on HFD could be caused by enhanced mitochondrial dysfunction.<sup>33</sup> Furthermore, the trends in amino acid metabolism follow the same pattern of results observed in cognitive impairment in these mice. HFD impaired performance on several hippocampal-dependent behavioral tasks compounding phenotypic deficits due to APP/PSEN1 mutations.<sup>33</sup> Performance was, however, improved in mice under the REV conditions compared to HFD only mice.<sup>33</sup> Together, the data support the mitochondrial cascade hypothesis and strongly suggest that HFD may contribute to worsening AD by promoting enhanced mitochondrial dysfunction, already seen in HFD conditions.<sup>21</sup>

Overall, these findings suggest that obesity combined with AD further enhances cognitive impairment, possibly through aggravated mitochondrial dysfunction that manifests as altered amino acid metabolism. Critically, there may be potential for reversal of deficits that are induced by dietary intake. Furthermore, given how closely the patterns of data we observed reflected behavioral and biochemical data already collected from these mice<sup>33</sup> our data suggest that peripheral tissue can be used to understand the metabolic changes occurring in the WT and

APP/PSEN1 mouse models. Specific peripheral metabolic pathways are affected by both diet and phenotype. This data also shows promise in reversing amino acid metabolism effects that contribute to AD through diet alteration. The unique amino acid metabolism profiles of normal, wild-type aging mice and APP/PSEN1 genetically modified AD mice were measured and compared using targeted and untargeted metabolomics. It was found that a significant number of amino acid metabolism pathways were dysregulated, specifically between the APP/PSEN1-LFD and APP/PSEN1-HFD groups. These pathways feed into the TCA cycle for amino acid metabolism and degradation, and thus imbalances in these pathways lead to mitochondrial dysfunction. This mitochondrial dysfunction has been observed before in obese and AD conditions.<sup>21,52</sup> Therefore, our results conclude that HFD contributes to AD through mitochondrial dysfunction in a semi-reversible manner.

#### **2.4. Conclusions**

AD and obesity are both very prevalent conditions. Because obesity during mid-life has been linked to future AD and obesity has an unique metabolic signature, it is essential to understand the combined metabolic effects when obesity and AD occur concurrently. The targeted and untargeted analyses highlighted how AD further promotes metabolic dysregulation seen in obesity, proven by the fact that significantly more changes are observed in amino acid metabolism pathways between LFD and HFD conditions in APP/PSEN1 mice.<sup>53</sup> More pathways are significantly altered in APP/PSEN1 mice than wild-type mice under the same diet conditions. While amino acid imbalances are routinely observed in HFD conditions, increases in individual amino acids are more pronounced when coupled with AD.<sup>22,23</sup> Furthermore, the partial reversibility of many altered pathways and molecules highlights that diet change can mitigate metabolic effects

of AD. Our analytical workflow shows similar amino acid metabolism trends despite using entirely different chromatographic and mass spectrometry platforms. The analytical workflow allows for a robust determination of amino acid trends caused by biological changes rather than analytical variations. Future work should now focus on studying larger classes of biomolecules involved in mitochondrial dysfunction, such as lipids and carnitines.

## **2.5. Acknowledgements**

This chapter contains the submitted research article: Amelia L. Taylor, Don E. Davis, Jr., Simona G. Codreanu, Stacy D. Sherrod, Fiona E. Harrison, and John A. McLean, “Elucidating Peripheral Amino Acid Changes in Obesity and Alzheimer’s Disease Using Metabolomics,” *Analytical Chemistry*, **2021**.

The authors would like to thank Jennifer Colby for her contributions in various stages for advice and technical expertise. A.L.T was supported by the SyBBURE Searle Undergraduate Research Program at Vanderbilt University. Financial support for aspects of this research was provided by The National Institutes of Health (National Cancer Institute R03CA222452). This work was supported in part using the resources of the Center for Innovative Technology at Vanderbilt University.

## **2.6. References**

- (1) Reitz, C.; Brayne, C.; Mayeux, R. Epidemiology of Alzheimer Disease. *Nat. Rev. Neurol.* **2011**, *7* (3), 137–152. <https://doi.org/10.1038/nrneurol.2011.2>
- (2) Prince M, Comas-Herrera A, Knapp M, Guerchet M, Karagiannidou M. World Alzheimer report 2016. Improving health care for people living with dementia: coverage, quality and costs now and in the future. *Alzheimer's Disease International*, **2016**.

- (3) Ogden, C. L.; Carroll, M. D.; Kit, B. K.; Flegal, K. M. Prevalence of Childhood and Adult Obesity in the United States, 2011-2012. *JAMA* **2014**, *311* (8), 806–814. <https://doi.org/10.1001/jama.2014.732>
- (4) Gustafson, D.; Rothenberg, E.; Blennow, K.; Steen, B.; Skoog, I. An 18-Year Follow-up of Overweight and Risk of Alzheimer Disease. *Arch. Intern. Med.* **2003**, *163* (13), 1524–1528. <https://doi.org/10.1001/archinte.163.13.1524>
- (5) Profenno, L. A.; Porsteinsson, A. P.; Faraone, S. V. Meta-Analysis of Alzheimer’s Disease Risk with Obesity, Diabetes, and Related Disorders. *Biol. Psychiatry* **2010**, *67* (6), 505–512. <https://doi.org/10.1016/j.biopsych.2009.02.013>
- (6) Beydoun, M. A.; Beydoun, H. A.; Wang, Y. Obesity and Central Obesity as Risk Factors for Incident Dementia and Its Subtypes: A Systematic Review and Meta-Analysis. *Obes. Rev. Off. J. Int. Assoc. Study Obes.* **2008**, *9* (3), 204–218. <https://doi.org/10.1111/j.1467-789X.2008.00473.x>
- (7) Whitmer, R. A.; Gunderson, E. P.; Quesenberry, C. P.; Zhou, J.; Yaffe, K. Body Mass Index in Midlife and Risk of Alzheimer Disease and Vascular Dementia. *Curr. Alzheimer Res.* **2007**, *4* (2), 103–109. <https://doi.org/10.2174/156720507780362047>
- (8) Borenstein, A. R.; Copenhaver, C. I.; Mortimer, J. A. Early-Life Risk Factors for Alzheimer Disease. *Alzheimer Dis. Assoc. Disord.* **2006**, *20* (1), 63–72. <https://doi.org/10.1097/01.wad.0000201854.62116.d7>
- (9) Hendrix, J. A.; Bateman, R. J.; Brashear, H. R.; Duggan, C.; Carrillo, M. C.; Bain, L. J.; DeMattos, R.; Katz, R. G.; Ostrowitzki, S.; Siemers, E.; Sperling, R.; Vitolo, O. V. Challenges, Solutions, and Recommendations for Alzheimer’s Disease Combination Therapy. *Alzheimers Dement. J. Alzheimers Assoc.* **2016**, *12* (5), 623–630. <https://doi.org/10.1016/j.jalz.2016.02.007>
- (10) Bocarsly, M. E.; Fasolino, M.; Kane, G. A.; LaMarca, E. A.; Kirschen, G. W.; Karatsoreos, I. N.; McEwen, B. S.; Gould, E. Obesity Diminishes Synaptic Markers, Alters Microglial Morphology, and Impairs Cognitive Function. *PNAS Proc. Natl. Acad. Sci. U. S. Am.* **2015**, *112* (51), 15731–15736.

- (11) Freeman, L. R.; Haley-Zitlin, V.; Stevens, C.; Granholm, A.-C. Diet-Induced Effects on Neuronal and Glial Elements in the Middle-Aged Rat Hippocampus. *Nutr. Neurosci.* **2011**, *14* (1), 32–44. <https://doi.org/10.1179/174313211X12966635733358>
- (12) Sah, S. K.; Lee, C.; Jang, J.-H.; Park, G. H. Effect of High-Fat Diet on Cognitive Impairment in Triple-Transgenic Mice Model of Alzheimer’s Disease. *Biochem. Biophys. Res. Commun.* **2017**, *493* (1), 731–736. <https://doi.org/10.1016/j.bbrc.2017.08.122>
- (13) Granholm, A.-C.; Bimonte-Nelson, H. A.; Moore, A. B.; Nelson, M. E.; Freeman, L. R.; Sambamurti, K. Effects of a Saturated Fat and High Cholesterol Diet on Memory and Hippocampal Morphology in the Middle-Aged Rat. *J. Alzheimers Dis. JAD* **2008**, *14* (2), 133–145. <https://doi.org/10.3233/jad-2008-14202>
- (14) Denver, P.; Gault, V. A.; McClean, P. L. Sustained High-Fat Diet Modulates Inflammation, Insulin Signalling and Cognition in Mice and a Modified Xenin Peptide Ameliorates Neuropathology in a Chronic High-Fat Model. *Diabetes Obes. Metab.* **2018**, *20* (5), 1166–1175. <https://doi.org/10.1111/dom.13210>
- (15) Kondo, T.; Asai, M.; Tsukita, K.; Kutoku, Y.; Ohsawa, Y.; Sunada, Y.; Imamura, K.; Egawa, N.; Yahata, N.; Okita, K.; Takahashi, K.; Asaka, I.; Aoi, T.; Watanabe, A.; Watanabe, K.; Kadoya, C.; Nakano, R.; Watanabe, D.; Maruyama, K.; Hori, O.; Hibino, S.; Choshi, T.; Nakahata, T.; Hioki, H.; Kaneko, T.; Naitoh, M.; Yoshikawa, K.; Yamawaki, S.; Suzuki, S.; Hata, R.; Ueno, S.-I.; Seki, T.; Kobayashi, K.; Toda, T.; Murakami, K.; Irie, K.; Klein, W. L.; Mori, H.; Asada, T.; Takahashi, R.; Iwata, N.; Yamanaka, S.; Inoue, H. Modeling Alzheimer’s Disease with iPSCs Reveals Stress Phenotypes Associated with Intracellular A $\beta$  and Differential Drug Responsiveness. *Cell Stem Cell* **2013**, *12* (4), 487–496. <https://doi.org/10.1016/j.stem.2013.01.009>
- (16) Tönnies, E.; Trushina, E. Oxidative Stress, Synaptic Dysfunction, and Alzheimer’s Disease. *J. Alzheimers Dis. JAD* **2017**, *57* (4), 1105–1121. <https://doi.org/10.3233/JAD-161088>
- (17) Nunomura, A.; Perry, G.; Aliev, G.; Hirai, K.; Takeda, A.; Balraj, E. K.; Jones, P. K.; Ghanbari, H.; Wataya, T.; Shimohama, S.; Chiba, S.; Atwood, C. S.; Petersen, R. B.; Smith, M. A. Oxidative

- Damage Is the Earliest Event in Alzheimer Disease. *J. Neuropathol. Exp. Neurol.* **2001**, *60* (8), 759–767. <https://doi.org/10.1093/jnen/60.8.759>
- (18) Swerdlow, R. H.; Burns, J. M.; Khan, S. M. The Alzheimer's Disease Mitochondrial Cascade Hypothesis: Progress and Perspectives. *Biochim. Biophys. Acta* **2014**, *1842* (8), 1219–1231. <https://doi.org/10.1016/j.bbadis.2013.09.010>
- (19) Hawkins, K. E.; Duchen, M. Modelling Mitochondrial Dysfunction in Alzheimer's Disease Using Human Induced Pluripotent Stem Cells. *World J. Stem Cells* **2019**, *11* (5), 236–253. <https://doi.org/10.4252/wjsc.v11.i5.236>
- (20) Martins, I. V. A.; Rivers-Auty, J.; Allan, S. M.; Lawrence, C. B. Mitochondrial Abnormalities and Synaptic Loss Underlie Memory Deficits Seen in Mouse Models of Obesity and Alzheimer's Disease. *J. Alzheimers Dis.* **2016**, *55* (3), 915–932. <https://doi.org/10.3233/JAD-160640>
- (21) Bagheri, M.; Djazayeri, A.; Farzadfar, F.; Qi, L.; Yekaninejad, M. S.; Aslibekyan, S.; Chamari, M.; Hassani, H.; Koletzko, B.; Uhl, O. Plasma Metabolomic Profiling of Amino Acids and Polar Lipids in Iranian Obese Adults. *Lipids Health Dis.* **2019**, *18* (1), 94. <https://doi.org/10.1186/s12944-019-1037-0>
- (22) Yamakado, M.; Nagao, K.; Imaizumi, A.; Tani, M.; Toda, A.; Tanaka, T.; Jinzu, H.; Miyano, H.; Yamamoto, H.; Daimon, T.; Horimoto, K.; Ishizaka, Y. Plasma Free Amino Acid Profiles Predict Four-Year Risk of Developing Diabetes, Metabolic Syndrome, Dyslipidemia, and Hypertension in Japanese Population. *Sci. Rep.* **2015**, *5*, 11918. <https://doi.org/10.1038/srep11918>
- (23) Wang, T. J.; Larson, M. G.; Vasan, R. S.; Cheng, S.; Rhee, E. P.; McCabe, E.; Lewis, G. D.; Fox, C. S.; Jacques, P. F.; Fernandez, C.; O'Donnell, C. J.; Carr, S. A.; Mootha, V. K.; Florez, J. C.; Souza, A.; Melander, O.; Clish, C. B.; Gerszten, R. E. Metabolite Profiles and the Risk of Developing Diabetes. *Nat. Med.* **2011**, *17* (4), 448–453. <https://doi.org/10.1038/nm.2307>
- (24) Tillin, T.; Hughes, A. D.; Wang, Q.; Würtz, P.; Ala-Korpela, M.; Sattar, N.; Forouhi, N. G.; Godsland, I. F.; Eastwood, S. V.; McKeigue, P. M.; Chaturvedi, N. Diabetes Risk and Amino Acid Profiles: Cross-Sectional and Prospective Analyses of Ethnicity, Amino Acids and Diabetes in a

- South Asian and European Cohort from the SABRE (Southall And Brent REvisited) Study. *Diabetologia* **2015**, *58* (5), 968–979. <https://doi.org/10.1007/s00125-015-3517-8>
- (25) Würtz, P.; Soininen, P.; Kangas, A. J.; Rönnemaa, T.; Lehtimäki, T.; Kähönen, M.; Viikari, J. S.; Raitakari, O. T.; Ala-Korpela, M. Branched-Chain and Aromatic Amino Acids Are Predictors of Insulin Resistance in Young Adults. *Diabetes Care* **2013**, *36* (3), 648–655. <https://doi.org/10.2337/dc12-0895>
- (26) Tai, E. S.; Tan, M. L. S.; Stevens, R. D.; Low, Y. L.; Muehlbauer, M. J.; Goh, D. L. M.; Ilkayeva, O. R.; Wenner, B. R.; Bain, J. R.; Lee, J. J. M.; Lim, S. C.; Khoo, C. M.; Shah, S. H.; Newgard, C. B. Insulin Resistance Is Associated with a Metabolic Profile of Altered Protein Metabolism in Chinese and Asian-Indian Men. *Diabetologia* **2010**, *53* (4), 757–767. <https://doi.org/10.1007/s00125-009-1637-8>
- (27) Siddik, M. A. B.; Shin, A. C. Recent Progress on Branched-Chain Amino Acids in Obesity, Diabetes, and Beyond. *Endocrinol. Metab.* **2019**, *34* (3), 234–246. <https://doi.org/10.3803/EnM.2019.34.3.234>
- (28) Li, H.; Ye, D.; Xie, W.; Hua, F.; Yang, Y.; Wu, J.; Gu, A.; Ren, Y.; Mao, K. Defect of Branched-Chain Amino Acid Metabolism Promotes the Development of Alzheimer’s Disease by Targeting the MTOR Signaling. *Biosci. Rep.* **2018**, *38* (4). <https://doi.org/10.1042/BSR20180127>
- (29) Libert, D. M.; Nowacki, A. S.; Natowicz, M. R. Metabolomic Analysis of Obesity, Metabolic Syndrome, and Type 2 Diabetes: Amino Acid and Acylcarnitine Levels Change along a Spectrum of Metabolic Wellness. *PeerJ* **2018**, *6*. <https://doi.org/10.7717/peerj.5410>
- (30) Clinical and Laboratory Standards Institute. Liquid Chromatography-Mass Spectrometry Methods; Approved Guidelines (C62-A). **2014**, No. 1-56238-977–7, pp 1-71.
- (31) US Food and Drug Administration. Guidance for Industry: Bioanalytical Method Validation. **2018**, No. FDA-2013-D-1020, pp 1-41.



- (32) Davis, D. E.; Sherrod, S. D.; Gant-Branum, R. L.; Colby, J. M.; McLean, J. A. Targeted Strategy to Analyze Antiepileptic Drugs in Human Serum by LC-MS/MS and LC-Ion Mobility-MS. *Anal. Chem.* **2020**, *92* (21), 14648–14656. <https://doi.org/10.1021/acs.analchem.0c03172>
- (33) Walker, J. M.; Dixit, S.; Saulsberry, A. C.; May, J. M.; Harrison, F. E. Reversal of High Fat Diet-Induced Obesity Improves Glucose Tolerance, Inflammatory Response,  $\beta$ -Amyloid Accumulation and Cognitive Decline in the APP/PSEN1 Mouse Model of Alzheimer's Disease. *Neurobiol. Dis.* **2017**, *100*, 87–98. <https://doi.org/10.1016/j.nbd.2017.01.004>
- (34) MacLean, B.; Tomazela, D. M.; Shulman, N.; Chambers, M.; Finney, G. L.; Frewen, B.; Kern, R.; Tabb, D. L.; Liebler, D. C.; MacCoss, M. J. Skyline: An Open Source Document Editor for Creating and Analyzing Targeted Proteomics Experiments. *Bioinforma. Oxf. Engl.* **2010**, *26* (7), 966–968. <https://doi.org/10.1093/bioinformatics/btq054>
- (35) MacLean, B. X.; Pratt, B. S.; Egertson, J. D.; MacCoss, M. J.; Smith, R. D.; Baker, E. S. Using Skyline to Analyze Data-Containing Liquid Chromatography, Ion Mobility Spectrometry, and Mass Spectrometry Dimensions. *J. Am. Soc. Mass Spectrom.* **2018**, *29* (11), 2182–2188. <https://doi.org/10.1007/s13361-018-2028-5>
- (36) Henderson, C. M.; Shulman, N. J.; MacLean, B.; MacCoss, M. J.; Hoofnagle, A. N. Skyline Performs as Well as Vendor Software in the Quantitative Analysis of Serum 25-Hydroxy Vitamin D and Vitamin D Binding Globulin. *Clin. Chem.* **2018**, *64* (2), 408–410. <https://doi.org/10.1373/clinchem.2017.282293>
- (37) Pino, L. K.; Searle, B. C.; Bollinger, J. G.; Nunn, B.; MacLean, B.; MacCoss, M. J. The Skyline Ecosystem: Informatics for Quantitative Mass Spectrometry Proteomics. *Mass Spectrom. Rev.* **2020**, *39* (3), 229–244. <https://doi.org/10.1002/mas.21540>
- (38) Popay, T. M.; Wang, J.; Adams, C. M.; Howard, G. C.; Codreanu, S. G.; Sherrod, S. D.; McLean, J. A.; Thomas, L. R.; Lorey, S. L.; Machida, Y. J.; Weissmiller, A. M.; Eischen, C. M.; Liu, Q.; Tansey, W. P. MYC Regulates Ribosome Biogenesis and Mitochondrial Gene Expression

- Programs through Its Interaction with Host Cell Factor-1. *eLife* **2021**, *10*, e60191.  
<https://doi.org/10.7554/eLife.60191>
- (39) Matuszewski, B. K.; Constanzer, M. L.; Chavez-Eng, C. M. Matrix Effect in Quantitative LC/MS/MS Analyses of Biological Fluids: A Method for Determination of Finasteride in Human Plasma at Picogram Per Milliliter Concentrations. *Anal. Chem.* **1998**, *70* (5), 882–889.  
<https://doi.org/10.1021/ac971078+>
- (40) Wishart, D. S.; Jewison, T.; Guo, A. C.; Wilson, M.; Knox, C.; Liu, Y.; Djoumbou, Y.; Mandal, R.; Aziat, F.; Dong, E.; Bouatra, S.; Sinelnikov, I.; Arndt, D.; Xia, J.; Liu, P.; Yallou, F.; Bjorn Dahl, T.; Perez-Pineiro, R.; Eisner, R.; Allen, F.; Neveu, V.; Greiner, R.; Scalbert, A. HMDB 3.0--The Human Metabolome Database in 2013. *Nucleic Acids Res.* **2013**, *41* (D1), D801-807.  
<https://doi.org/10.1093/nar/gks1065>
- (41) Smith, C. A.; O'Maille, G.; Want, E. J.; Qin, C.; Trauger, S. A.; Brandon, T. R.; Custodio, D. E.; Abagyan, R.; Siuzdak, G. METLIN: A Metabolite Mass Spectral Database. *Ther. Drug Monit.* **2005**, *27* (6), 747–751. <https://doi.org/10.1097/01.ftd.0000179845.53213.39>
- (42) Powell, C. J.; Jablonski, A.; Salvat, F.; Lee, A. Y. NIST Electron Elastic-Scattering Cross-Section Database, Version 4.0; *NIST NSRDS 64*; National Institute of Standards and Technology **2016**.  
<https://doi.org/10.6028/NIST.NSRDS.64>
- (43) Schrimpe-Rutledge, A. C.; Codreanu, S. G.; Sherrod, S. D.; McLean, J. A. Untargeted Metabolomics Strategies-Challenges and Emerging Directions. *J. Am. Soc. Mass Spectrom.* **2016**, *27* (12), 1897–1905. <https://doi.org/10.1007/s13361-016-1469-y>
- (44) Chong, J.; Wishart, D. S.; Xia, J. Using MetaboAnalyst 4.0 for Comprehensive and Integrative Metabolomics Data Analysis. *Curr. Protoc. Bioinforma.* **2019**, *68* (1), e86.  
<https://doi.org/10.1002/cpbi.86>
- (45) Li, S.; Park, Y.; Duraisingham, S.; Strobel, F. H.; Khan, N.; Soltow, Q. A.; Jones, D. P.; Pulendran, B. Predicting Network Activity from High Throughput Metabolomics. *PLOS Comput. Biol.* **2013**, *9* (7), e1003123. <https://doi.org/10.1371/journal.pcbi.1003123>

- (46) Lazzaro, S.; Ogrinc, N.; Lamont, L.; Vecchio, G.; Pappalardo, G.; Heeren, R. M. A. Ion Mobility Spectrometry Combined with Multivariate Statistical Analysis: Revealing the Effects of a Drug Candidate for Alzheimer's Disease on A $\beta$ 1-40 Peptide Early Assembly. *Anal. Bioanal. Chem.* **2019**, *411* (24), 6353–6363. <https://doi.org/10.1007/s00216-019-02030-7>
- (47) Ellis, B. M.; Fischer, C. N.; Martin, L. B.; Bachmann, B. O.; McLean, J. A. Spatiochemically Profiling Microbial Interactions with Membrane Scaffolded Desorption Electrospray Ionization-Ion Mobility-Imaging Mass Spectrometry and Unsupervised Segmentation. *Anal. Chem.* **2019**, *91* (21), 13703–13711. <https://doi.org/10.1021/acs.analchem.9b02992>
- (48) Hoffmann, N.; Rein, J.; Sachsenberg, T.; Hartler, J.; Haug, K.; Mayer, G.; Alka, O.; Dayalan, S.; Pearce, J. T. M.; Rocca-Serra, P.; Qi, D.; Eisenacher, M.; Perez-Riverol, Y.; Vizcaíno, J. A.; Salek, R. M.; Neumann, S.; Jones, A. R. MzTab-M: A Data Standard for Sharing Quantitative Results in Mass Spectrometry Metabolomics. *Anal. Chem.* **2019**, *91* (5), 3302–3310. <https://doi.org/10.1021/acs.analchem.8b04310>
- (49) Chong, J.; Soufan, O.; Li, C.; Caraus, I.; Li, S.; Bourque, G.; Wishart, D. S.; Xia, J. MetaboAnalyst 4.0: Towards More Transparent and Integrative Metabolomics Analysis. *Nucleic Acids Res.* **2018**, *46*, W486–W494. <https://doi.org/10.1093/nar/gky310>
- (50) Xia, J.; Broadhurst, D. I.; Wilson, M.; Wishart, D. S. Translational Biomarker Discovery in Clinical Metabolomics: An Introductory Tutorial. *Metabolomics* **2013**, *9* (2), 280–299. <https://doi.org/10.1007/s11306-012-0482-9>
- (51) Spinelli, J. B.; Haigis, M. C. The Multifaceted Contributions of Mitochondria to Cellular Metabolism. *Nat. Cell Biol.* **2018**, *20* (7), 745–754. <https://doi.org/10.1038/s41556-018-0124-1>.
- (52) Beal, M. F. Mitochondrial Dysfunction in Neurodegenerative Diseases. *Biochim. Biophys. Acta* **1998**, *1366* (1–2), 211–223. [https://doi.org/10.1016/s0005-2728\(98\)00114-5](https://doi.org/10.1016/s0005-2728(98)00114-5)
- (53) Adams, S. H. Emerging Perspectives on Essential Amino Acid Metabolism in Obesity and the Insulin-Resistant State. *Adv. Nutr.* **2011**, *2* (6), 445–456. <https://doi.org/10.3945/an.111.000737>

## CHAPTER 3

### TARGETED STRATEGY TO ANALYZE ANTI-EPILEPTIC DRUGS IN HUMAN SERUM BY LC-MS/MS AND LC-ION MOBILITY-MS

#### **3.1. Introduction**

Epilepsy is a common neurological disorder characterized by a long-term risk of recurrent seizures. Anti-epileptic drugs (AEDs) are mood stabilizers not only effective at controlling seizures but also treating schizophrenia, depression, and bipolar disorder.<sup>1-4</sup> However, many patients experience adverse side effects associated with AED usage, such as Stevens-Johnson syndrome, toxic epidermal necrolysis, liver toxicity, tremors, dizziness, nausea, and fatigue.<sup>5-7</sup> AEDs have a narrow therapeutic range, therefore the serum concentration of AEDs must be optimized to ensure effectiveness (control/minimize seizures) and minimize negative side effects.<sup>8-10</sup> AED effectiveness is partially dependent upon patient specific pharmacokinetics (PK), which include: absorption, distribution, metabolism, and excretion (ADME).<sup>11</sup> Patient specific PK can influence a clinician's decision on dosage and dosing frequency of AEDs.<sup>8</sup> Therapeutic drug management (TDM) requires iterative measurements of AEDs in serum to ensure a patient's AED concentration is within the therapeutic range.<sup>10,12</sup> Developing a workflow with high precision, accuracy, sensitivity, and selectivity is essential for optimizing AED treatment for individual patients, a primary tenet of personalized medicine.<sup>13</sup>

Routine clinical TDM is often performed using quantitative immunoassays, where analyte concentration is determined as a function of antibody binding, and not through direct molecular measurements.<sup>5,6</sup> Immunoassays are generally limited to single drug detection and are susceptible to false positives as a result of cross-reactivity between the drug target (e.g., carbamazepine or

CBZ) and related metabolites (e.g., carbamazepine-10,11 epoxide or CBZ epoxy).<sup>14-17</sup> Supplement consumption in the United States and across the globe has also increased dramatically in recent years, which may convolute testing by introducing additional interferences.<sup>13,18</sup> In addition, new AEDs are routinely developed, which may complicate the quantification of AEDs using less selective methodologies like immunoassays.<sup>5,19,20</sup> Finally, patients are often prescribed more than one AED, which necessitates testing a single sample using multiple different immunoassays. However, the need for performing multiple tests on a single sample impedes cost effectiveness.<sup>21-24</sup> Thus, an analytical workflow offering highly specific detection of multiple related drugs and drug metabolites with high sensitivity and selectivity is ideal.<sup>25</sup>

Separation of drugs by liquid chromatography and detection via absorbance at a particular wavelength (LC-UV) or by tandem mass spectrometry (LC-MS/MS) have been utilized, as alternatives to immunoassays, to quantify AEDs.<sup>25-27</sup> However, LC-UV analyses are also susceptible to interferences from chemically similar species. Further differentiation and more specific detection techniques (such as triple-quadrupole MS/MS and LC-DTIMS-MS) may be necessary for AED quantification studies, particularly if structural isomers will be analyzed simultaneously.<sup>12</sup> In addition to LC-MS/MS, LC-DTIMS-MS has become an important analytical technique for characterizing drugs and drug metabolites simultaneously by molecular structure and weight.<sup>28-34</sup> Clinical and analytical labs have utilized LC-MS/MS methods for the quantification of AEDs in serum for numerous reasons, including ruggedness, ease of use, and cost.<sup>35</sup> LC-MS/MS methods have been developed for quantification of AEDs from different biological matrices such as dried plasma spots, plasma, and serum.<sup>25-27,36</sup>

In these studies, a complementary approach of AED analysis utilizing LC-DTIMS-MS was investigated to determine if additional structural information for individual AEDs increases

confidence in selectivity. Briefly, DTIMS experiments provide an additional dimension of separation in addition to LC that can be coupled to mass analysis to potentially distinguish isobaric interferences and provide further confidence in AED identification in human serum. Furthermore, LC-DTIMS-MS experiments have the potential to identify AEDs not reported in clinically relevant samples, through a combination of targeted quantitation by LC-MS/MS and semi-targeted (restricted to coverage over AED ranges of interest) LC-DTIMS-MS. The LC-triple quadrupole-MS/MS and LC-DTIMS-MS workflow described herein offers both quantitative and qualitative analytical methods for AEDs in human serum.

Here we present an LC-MS/MS and LC-DTIMS-MS workflow that can be used in any analytical setting, including clinical, for the quantification and qualification of 14 AEDs in patient serum (**Figure 3.1**). In accordance with the Clinical and Laboratory Standards Institute (CLSI) LC-MS guidelines (C62-A)<sup>37</sup> and US Food and Drug Administration (FDA) guidelines (Bioanalytical Method Guidance for Industry Validation),<sup>38</sup> the quantitative LC-MS/MS method was assessed for method verification and validation. A second qualitative method for AED identification was performed using LC-DTIMS-MS to assess selectivity. Collision cross section (CCS) values, which are derived from DTIMS, show utility in improving the accuracy of small molecule AED identifications. The qualitative method for AEDs was performed using an LC-DTIMS-MS assay, building upon an approach detailed elsewhere.<sup>39</sup> Taken together, these methods deliver robust quantification and qualification results for 14 AEDs and should prove beneficial for laboratories interested in increasing efficiency, sensitivity, and selectivity in AED testing.

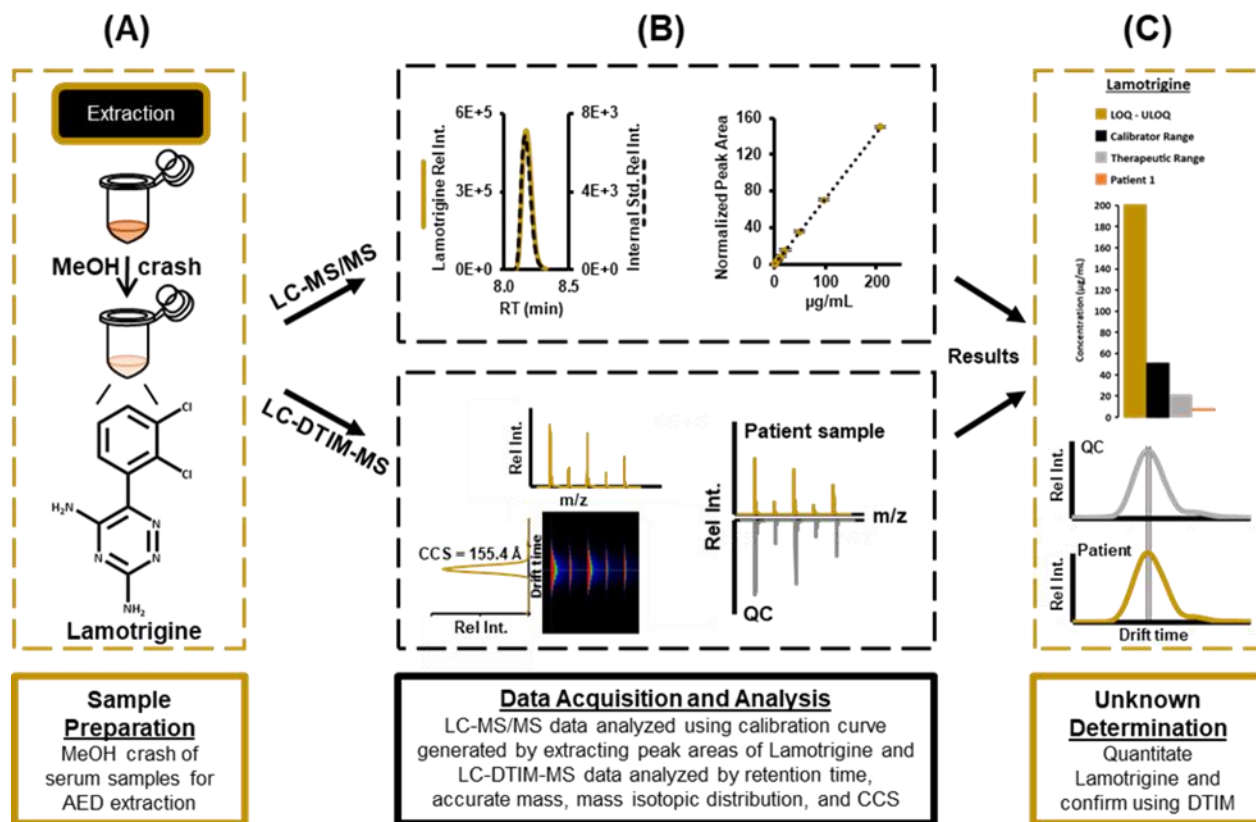


**Figure 3.1.** Workflow for LC-MS/MS and LC-DTIMS-MS analysis beginning with (A) sample preparation, (B) data acquisition and analysis, and (C) unknown determination of AEDs in epileptic patient serum samples. In this study, a validated LC-MS/MS method provides quantitative AED concentrations, and the LC-DTIMS-MS method allowed for structural analysis and isomer discrimination.

## **3.2. Experimental Methods**

### **3.2.1. Standards and Chemicals**

All AEDs and SIL-ISs were purchased from Sigma-Aldrich (St. Louis, MO, USA). Optima LC/MS grade water, isopropyl alcohol, and methanol were obtained from Fisher Scientific (Hampton, NH, USA). Optima LC/MS grade formic acid and ammonium acetate were obtained from Fisher Scientific (Hampton, NH, USA).

### **3.2.2. Human Serum Samples**

Human drug-free serum and matrix matched 3<sup>rd</sup> party verified quality control (QC) material at low, medium, and high AED concentrations were obtained from UTAK Laboratories Incorporated (hereafter referred to as 3<sup>rd</sup> party QC samples, Valencia, CA, USA). QC and calibrator concentrations are outlined in **Table C.1. and Table C.3.**, respectively. Calibrators are samples used for linearity and/or the calibration curve. De-identified, residual serum specimens were obtained from VUMC's clinical toxicology laboratory in accordance with Institutional Review Board approval (IRB #172021). These samples were subjected to the extraction protocol described in **Figure 3.1.**

### **3.2.3. Human Serum Extraction and Preparation**

For all samples analyzed in these studies, a protein precipitation was performed in a 1.5-ml polypropylene microcentrifuge tube (Eppendorf, Hauppauge, NY).



### 3.2.4. *Chromatographic Conditions*

For the LC-MS/MS method, AEDs were analyzed using a 3.0 x 50 mm reverse phase column, ZORBAX Eclipse Plus C18 Rapid Resolution HD 1.8  $\mu\text{m}$  (Agilent Technologies, Santa Clara, CA) with a 2.1 x 5 mm 1.8  $\mu\text{m}$  ZORBAX Eclipse Plus C18 guard column, maintained at 40°C for separation by Ultra High-Pressure Liquid Chromatography (UHPLC, Agilent 1290 Infinity II system, Agilent Technologies, Santa Clara, CA). Mobile phase A consisted of water with 0.1% formic acid and 10 mM ammonium acetate. Mobile Phase B consisted of methanol with 0.1% formic acid and 10 mM ammonium acetate. The UHPLC was directly coupled online to a commercial triple quadrupole mass spectrometer (6470, Agilent Technologies, Santa Clara, CA).

For the LC-DTIMS-MS experiments, an UHPLC (Agilent 1290 Infinity I LC system, Agilent Technologies, Santa Clara, CA) was directly coupled online to a commercial DTIMS-MS (6560, Agilent Technologies, Santa Clara, Ca) using the same column and mobile phases as described above.

For both LC-MS/MS and LC-DTIMS-MS methods, a 1  $\mu\text{L}$  sample was injected at a flow rate of 800  $\mu\text{L}/\text{min}$  and was analyzed using the following chromatographic conditions (17.5 minute runtime including purge and equilibration times): mobile phase B was maintained at 5% for the first 3 minutes for an initial isocratic hold, linearly increased from 5% to 32.5% over 5.5 minutes, linearly increased again from 32.5% to 35% over 0.01 minutes, linearly increased a final time from 35% to 100% over 2.48 minutes, and held at 100% for 1.51 minutes. Mobile phase B returned to 5% by 12.5 minutes and was held at 5% for 5 minutes to re-equilibrate the column. In this method, the initial isocratic hold, final purge, and re-equilibration times were performed to ensure efficient cleaning, minimize carryover, and preserve column integrity. Additionally, the injection needle was washed with 60:40 (v:v) isopropanol: methanol followed by mobile phase

starting conditions between every run to minimize carryover. A representative chromatogram of the 14 AEDs and mobile phase B gradient is shown in **Figure 3.2.A**.

### **3.2.5. MS/MS and DTIMS-MS Conditions**

For LC-MS/MS experiments, AEDs were analyzed in positive ionization mode using the Jet Stream ESI source (Agilent Technologies, Santa Clara, CA) coupled to a triple-quadrupole mass spectrometer (6470, Agilent Technologies). Nitrogen was used as both the nebulizing gas and the collision gas. AED transitions were collected using scheduled multiple reaction monitoring (MRM) with a  $\Delta$  2 min ( $\pm$  1 min) retention time window for each chromatographic peak. MRM transitions are listed in **Table 3.1**. Mass spectrometry conditions were optimized on a per-molecule basis, including compound dependent parameters (e.g., fragmentor voltage, collision energy voltage, and cell accelerator voltage) by flow injection analysis (FIA) to maximize sensitivity. **Table 3.1** also denotes the stable isotopically labeled internal standards (SIL-IS) used for normalization, transitions, limits of quantification (LOQs), therapeutic ranges, recovery, and matrix effect. MHD- $^{13}\text{C}_6$  was used for CBZ, CBZ epoxy, phenytoin, and oxcarbazepine normalization owing to its similar RT and structural properties. Quantifier transitions (Quant m/z) are characteristic fragments or product ions of AED precursor ions used to quantitate AED concentrations. Representative chromatograms of AEDs and SIL-ISs at individual LOQs is available in the supporting information **Figure C.1**. Data were acquired using Agilent's MassHunter Workstation Data Acquisition software and analyzed using Skyline (MacCoss Lab),<sup>40,41</sup> Agilent's MassHunter Quantitative Analysis, MassHunter Qualitative Analysis software, Microsoft PowerPoint, and Microsoft Excel.

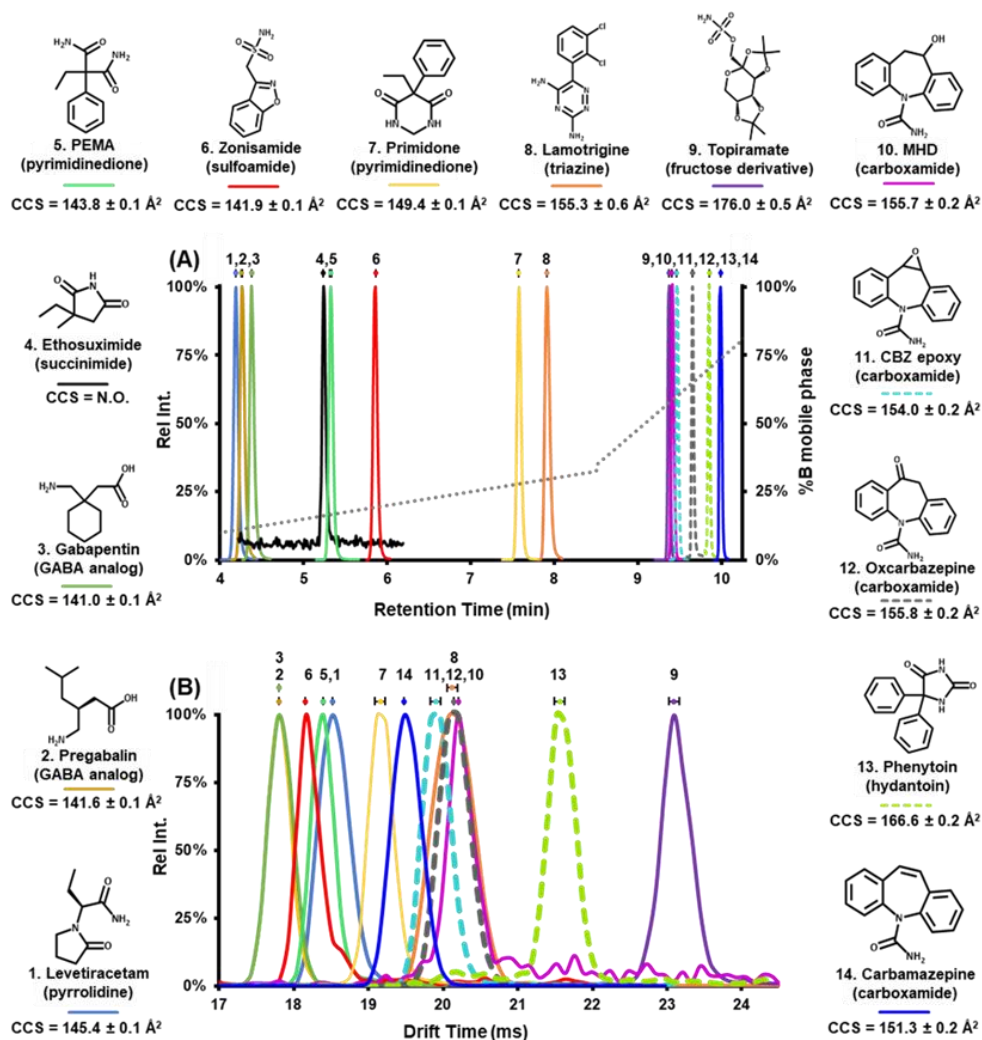


**Figure 3.2.** Structures of the 14 AEDs annotated with experimental CCS measurements. (A) LC-MS/MS analysis showing an LC chromatogram (minutes) of 14 AEDs in pooled human serum (quality control low). Dashed chromatograms are the 3 constitutional isomeric AEDs ( $C_{15}H_{12}N_2O_2$ , 253.0977 Da). The dotted grey line represents %B mobile phase gradient. Standard error bars ( $n = 3$  process replicates) represents overlapping of retention times, and in this LC method all AED retention times were shown to be statistically significant and distinct. (B) Flow injection analysis (FIA)-ion mobility-MS showing experimental DTIMS spectra (milliseconds) of 13 AED neat standards in the gas phase. Standard error bars ( $n = 3$  technical replicates) were used to demonstrate overlapping drift times. Pregabalin/gabapentin and lamotrigine/MHD/oxcarbazepine exhibit non-statistically significant different drift times. Dashed drift times represent the 3 constitutional isomeric AEDs ( $C_{15}H_{12}N_2O_2$ , 253.0977 Da) and all three have statistically significant distinct drift times, thus can be separated from each other in drift time space. It is important to note that AEDs that have similar retention times (e.g., topiramate and MHD) have different baseline resolved drift times. These data illustrate the utility in using both drift time and retention time measurements.

**Table 3.1.** AED MRM transition list, limit of quantification (LOQ), therapeutic range, recovery, and matrix effects.

| No. | AED   | Q1<br>m/z | Q3<br>m/z | LOQ<br>µg/mL | Therapeutic range<br>µg/mL | Recovery<br>+/- %CV | Matrix effect<br>+/- %CV |
|-----|---|-----------|-----------|--------------|----------------------------|---------------------|--------------------------|
| 1   | Levetiracetam   | 171       | 154       | 0.2          | 5 - 40                     | 112% +/- 7%         | 92% +/- 12%              |
|     | Levetiracetam - D <sub>6</sub>                              | 177       | 160       |              |                            | at 25 µg/mL         | at 25 µg/mL              |
| 2   | Pregabalin  | 160       | 142       | 0.2          | 4 - 20                     | 116% +/- 7%         | 103% +/- 9%              |
|     | Pregabalin - <sup>13</sup> C <sub>3</sub>                   | 163       | 145       |              |                            | at 13 µg/mL         | at 13 µg/mL              |
| 3   | Gabapentin  | 172       | 154       | 0.2          | 2 - 20                     | 120% +/- 7%         | 104% +/- 10%             |
|     | Gabapentin - <sup>13</sup> C <sub>3</sub>                   | 175       | 157       |              |                            | at 13 µg/mL         | at 13 µg/mL              |
| 4   | Ethosuximide  | 142       | 114       | 6.3          | 40 - 100                   | 80% +/- 18%         | 76% +/- 11%              |
|     | Zonisamide - <sup>13</sup> C <sub>6</sub>                   | 219       | 138       |              |                            | at 50 µg/mL         | at 50 µg/mL              |
| 5   | PEMA  | 207       | 162       | 0.2          |                            | 95% +/- 7%          | 50% +/- 3%               |
|     | Zonisamide - <sup>13</sup> C <sub>6</sub>                   | 219       | 138       |              |                            | at 25 µg/mL         | at 25 µg/mL              |
| 6   | Zonisamide  | 213       | 132       | 0.2          | 10 - 40                    | 114% +/- 6%         | 100% +/- 10%             |
|     | Zonisamide - <sup>13</sup> C <sub>6</sub>                   | 219       | 138       |              |                            | at 25 µg/mL         | at 25 µg/mL              |
| 7   | Primidone   | 219       | 162       | 0.2          | 5 - 12                     | 87% +/- 8%          | 63% +/- 4%               |
|     | Lamotrigine - <sup>13</sup> C, <sup>15</sup> N <sub>4</sub> | 262       | 215       |              |                            | at 12 µg/mL         | at 12 µg/mL              |
| 8   | Lamotrigine   | 256       | 211       | 0.2          | 1 - 20                     | 111% +/- 7%         | 101% +/- 10%             |
|     | Lamotrigine - <sup>13</sup> C, <sup>15</sup> N <sub>4</sub> | 262       | 215       |              |                            | at 13 µg/mL         | at 13 µg/mL              |
| 9   | Topiramate  | 362       | 265       | 0.4          | 10 - 20                    | 52% +/- 2%          | 47% +/- 4%               |
|     | Topiramate - D <sub>12</sub>                                | 374       | 276       |              |                            | at 13 µg/mL         | at 13 µg/mL              |
| 10  | MHD   | 255       | 237       | 0.2          | 10 - 40                    | 104% +/- 8%         | 98% +/- 11%              |
|     | MHD - <sup>13</sup> C <sub>6</sub>                          | 261       | 200       |              |                            | at 25 µg/mL         | at 25 µg/mL              |
| 11  | CBZ Epoxy   | 253       | 236       | 0.1          | 4 - 12                     | 62% +/- 6%          | 86% +/- 19%              |
|     | MHD - <sup>13</sup> C <sub>6</sub>                          | 261       | 200       |              |                            | at 13 µg/mL         | at 13 µg/mL              |
| 12  | Oxcarbazepine   | 253       | 180       | 0.7          | 10 - 40                    | 88% +/- 15%         | 80% +/- 10%              |
|     | MHD - <sup>13</sup> C <sub>6</sub>                          | 261       | 200       |              |                            | at 25 µg/mL         | at 25 µg/mL              |
| 13  | Phenytoin   | 253       | 104       | 0.8          | 1 - 2.5                    | 59% +/- 6%          | 62% +/- 7%               |
|     | MHD - <sup>13</sup> C <sub>6</sub>                          | 261       | 200       |              |                            | at 25 µg/mL         | at 25 µg/mL              |
| 14  | Carbamazepine   | 237       | 194       | 0.1          | 4 - 12                     | 60% +/- 6%          | 91% +/- 3%               |
|     | MHD - <sup>13</sup> C <sub>6</sub>                          | 261       | 200       |              |                            | at 13 µg/mL         | at 13 µg/mL              |

For FIA-DTIMS-MS and LC-DTIMS-MS analysis, AEDs were analyzed in positive ionization mode using the Jet Stream ESI source (Agilent Technologies, Santa Clara, CA) coupled to a DTIMS mass spectrometer (6560, Agilent Technologies) using previously described instrumental settings and methods.<sup>39,42-45</sup> Briefly, the LC-DTIMS-MS method consisted of a single-field drift time analysis using nitrogen drift gas with the drift tube at a temperature of 30°C, a pressure of 4.0 Torr, and an electric field of 17.3 V/ cm for 30 s. For LC-DTIMS-MS analyses, a calibrated single field CCS method was used to calculate CCS values via the Mason-Schamp equation.<sup>39</sup> Data was analyzed using MassHunter Qualitative Analysis software, MassHunter IM-MS Browser, and Microsoft Excel. A representative plot of the 13 AED ion mobility profiles is shown in **Figure 3.2.B**. The primary measurement dimension of drift time is used rather than collision cross section to overlay the different mass species without alterations in expected ion mobility resolving power (i.e. changes in peak width arising from non-linear conversion from drift time to cross section).

### **3.2.6. Method Validation**

Guidelines established by the FDA Guidance for Industry Bioanalytical Method Validation were used to validate the LC-MS/MS AED assay.<sup>37,38</sup> Analytical figures of merit including LOQ, accuracy, precision, carryover, stability, selectivity, recovery, and matrix effect were assessed. We did not perform dilution effects and partial volume validation studies because none of the clinical samples were diluted as received. The full volume of samples (100µL) was used for analysis.

### 3.3. Results and Discussion

#### 3.3.1. LC-MS/MS and FIA-DTIMS-MS

The range of retention times (minutes) from LC-MS/MS and ion mobility drift times (milliseconds) from FIA-DTIMS-MS are shown in **Figure 3.2.A** and **Figure 3.2.B**, respectively. Collectively, these data demonstrate the structural diversity amongst the AEDs/anticonvulsants outlined in these studies. Under these conditions, ethosuximide was not observed using the FIA-DTIMS-MS method where we observed an LOQ for this AED approximately one order of magnitude higher in concentration than all other AEDs in this study (as shown in **Figure C.1**). Chromatographically, all AEDs were shown to display statistically significant separation with minimal overlapping retention times (**Figure 3.2.B**). For those AEDs that did not exhibit baseline separation chromatographically, the data show that there were statistically significant distinct mobility profiles with baseline separation for two AEDs, topiramate and MHD (**Figure 3.2.A** and **Figure 3.2.B**). Structural isomers (CBZ epoxy, oxcarbazepine, and phenytoin) demonstrated statistically significant separation in both chromatographic and ion mobility profiles (**Figure 3.2**). Separation of structurally isomeric AEDs, such as CBZ epoxy, oxcarbazepine, and phenytoin (identical chemical formulas), can also be observed in **Figure 3.3** in which these three AEDs have the same isotopic  $m/z$  but different CCS values. The structural diversity of AEDs is also shown in **Figure 3.3**, these data exemplify the presence of unique best fit trendlines with  $\pm$  10% deviation from the best fit line for 13 AEDs. The deviation demonstrates the structural properties of AEDs and lays the groundwork for using CCS AED measurements as an identifier in untargeted and/or targeted studies.<sup>34</sup> Taken together, these data strengthen the confidence in identifying which AEDs a particular patient is taking through internal validation of workflows and

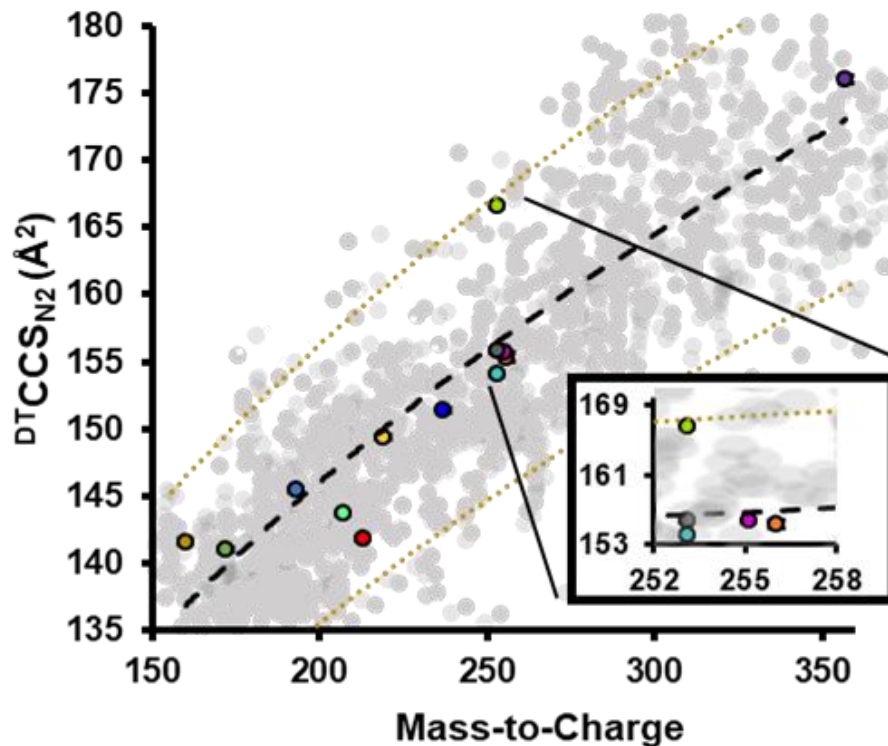


**Figure 3.3.** Conformational space analysis showing  $^{DT}CCS_{N_2}$  values for the AEDs investigated using FIA-DTIMS-MS with neat standards. Included is a black dashed trendline representing the best fit line of the data fit to a power function. Also shown (in gold) are dashed lines representing  $\pm 10\%$  deviation from the best fit line. Measured AEDs were within  $\pm 10\%$  of the best fit line. Error bars represent standard errors and are for most values within the scale of the marker ( $n=3$  technical replicates). The grey data points represent  $\sim 1700$  entries available in the CCS compendium over this CCS and  $m/z$  range. These data span multiple classes of compounds.<sup>34</sup>

also affords the ability to characterize potentially unknown or known structurally similar drugs or drug-like compounds that may be in a patient's serum/plasma sample as chromatographically coeluting interferences. Such situations can complicate accurate quantification of the clinical panel,<sup>33</sup> which ultimately may lead to treatment decisions for a particular patient that might be different with improved accuracy.

### 3.3.2. *Method Validation, Comparison, and Application*

For individual AEDs, the recovery and matrix effect studies (**Table 3.1.** and **Figure C.6.**) showed high reproducibility (< 20% CV). Recovery studies for topiramate, phenytoin, CBZ, and CBZ epoxy were < 80%. However, the QC samples for these molecules did meet the acceptability criteria for precision and accuracy (< 15 %CV and < 15 %bias, respectively), therefore the extraction did not negatively affect reproducibility (**Figure C.2.**). We did not observe any significant matrix effects for 9 out of the 14 AEDs (*i.e.*, ionization suppression or ionization enhancement matrix effect > 80%). Fortunately, the SIL-IS of these AEDs successfully compensated for recovery and/or matrix effects, therefore the matrix effect values were > 80% (e.g. levetiracetam, pregabalin, gabapentin, zonisamide, lamotrigine, MHD, and oxcarbazepine).<sup>46</sup> Five of the AEDs exhibited a matrix effect < 80% (topiramate, ethosuximide, PEMA, primidone, and phenytoin). For these AEDs, we were unable to use the exact SIL-IS and therefore their recoveries and/or matrix effects were < 80%.<sup>46</sup> The SIL-IS used for oxcarbazepine was a physiochemical mimic (MHD-<sup>13</sup>C<sub>6</sub>); the calculated recovery and matrix effect studies were > 80%. On the other hand, the SIL-IS used for topiramate has 12 deuterons causing it to display an isotopic effect and elute earlier (<5 sec) than topiramate (owing to hydrogen-deuterium exchange). Because of these shifts in elution time, we observed < 80% recovery and matrix effect for topirimate.<sup>47-49</sup>



We anticipate that using either carbon-13 or nitrogen-15 SIL-ISs for AEDs exhibiting recoveries and/or matrix effects < 80% could resolve these findings that were observed in complex human serum samples.<sup>37</sup> In these studies, a verified 3<sup>rd</sup> party vendor provided the quality control samples; these samples were used to assess and validate precision, accuracy, recovery, and matrix effects. These results demonstrate that the LC-MS/MS quantitative method described herein is fit for purpose. Taken together, these results suggest that the analytical method reported here minimizes the impacts of endogenous interferences from human serum and/or from concomitant medications and allows for both reliable and reproducible quantification of the 14 AEDs.

The developed LC-MS/MS method meets the criteria for routine clinical TDM owing to the results of the linearity, accuracy, precision, carryover, recovery, matrix effects, selectivity, and stability studies. The LOQ was established and adequately brackets the therapeutic range via linearity studies (**Table 3.1.** and **Table C.2.**). Precision and accuracy of all AEDs in 3<sup>rd</sup> party QCs were < 15% CV and 15% bias (**Figure C.2.**). There was no significant carryover (**Figure C.5.**), instability (**Figure C.4.**), recovery (**Table 3.1.**), and matrix effects (**Table 3.1.**) that negatively impacted the quantification of all 14 AEDs.

The quantitative LC-MS/MS measurements were compared to Vanderbilt University Medical Center (VUMC) clinical toxicology laboratory's LC-UV measurements, many samples of which contained multiple AEDs (9 contrived samples - **Table C.4.** and 21 patient samples - **Figure C.3.**). The data obtained indicate that the method presented here is comparable to the validated LC-UV method. Of the 30 samples analyzed, ~23% of the samples contained additional AEDs that were not reported in the LC-UV method (these AEDs include levetiracetam, lamotrigine, MHD, pregabalin, and gabapentin), but were identified using the workflows described herein. Furthermore, the LC-UV method was unable to distinguish pregabalin and gabapentin from

each other and required a 3<sup>rd</sup> party LC-MS/MS laboratory for analysis. **Figure C.3.A** shows and compares the data generated from the same 21 samples but analyzed using these methods: the LC-MS/MS and LC-DTIMS-MS method developed herein, LC-UV measurements, 3<sup>rd</sup> party LC-MS/MS analyses (pregabalin and gabapentin), and an immunoassay (CBZ). We performed LC-DTIMS-MS analyses to identify AEDs that were present in individual patients but not reported (**Figure C.3.B**). To assess the utility of the DTIMS dimension in identifying targeted analytes and/or selectivity, **Figure 3.4** illustrates the theoretical isotope distribution patterns for 3 AEDs (generated from a single patient sample analyzed in the same batch) as well as data obtained when extracting (1) MS only dimension, (2) LC-MS dimensions, (3) DTIMS-MS dimensions, and (4) combined LC-DTIMS-MS dimensions. These data collectively illustrate that orthogonal separation tools, such as <sup>DT</sup>CCS<sub>N2</sub> measurements, provide additional selectivity and confidence in analyte identification. Specifically, the LC-DTIMS-MS data separated concomitant interferences and increased confidence in AED identification for all 3 AEDs. These data also show the ability of the DTIMS dimension to remove concomitant species otherwise not separated in the LC and MS dimension (see zonisamide, **Figure 3.4**).

By integrating the LC-MS/MS and LC-DTIMS-MS workflows, the process for monitoring AEDs is simplified and provides additional clinical information. Since TDM quantification was not ordered for levetiracetam, lamotrigine, and MHD these were not reported in the clinical samples but monitored in the present work as they are continually included in the workflow. Furthermore, carbamazepine would be tested using an immunoassay method and through always incorporating carbamazepine in these workflows could remove the time and expense related to performing an additional antibody-based testing platform from these processes.

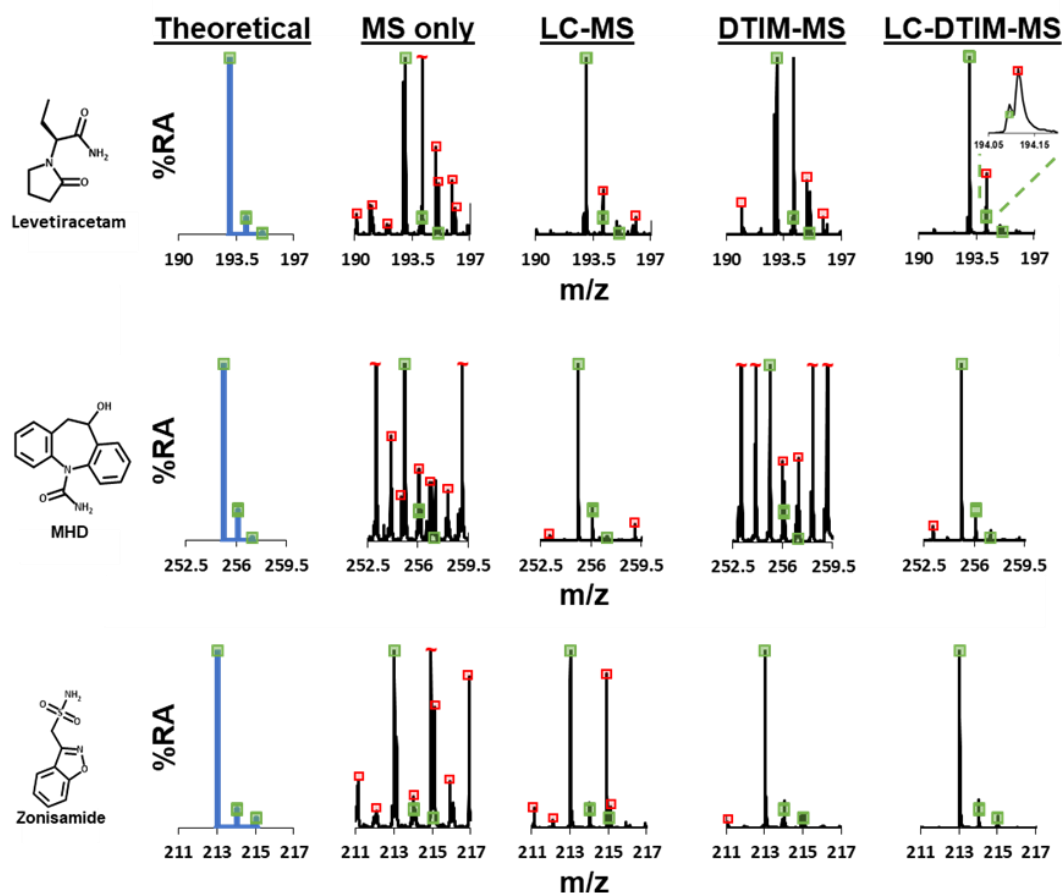


**Figure 3.4.** Isotope distribution patterns for three AEDs (levetiracetam, MHD, and zonisamide) from a single patient serum sample (patient 11) analyzed by LC-DTIMS-MS but mass spectrum were extracted for the listed specific dimensions. The MS only dimension extracted the entire chromatogram and ion mobility spectrum. The LC-MS dimension extracted the AED chromatograms for levetiracetam, MHD, and zonisamide while the entire ion mobility spectrum was extracted. The DTIMS-MS dimension extracted the entire chromatogram while AED ion mobility spectrum for levetiracetam, MHD, and zonisamide were extracted. The LC-DTIMS-MS dimension extracted the AED chromatograms and ion mobility spectrum for levetiracetam, MHD, and zonisamide. The green boxes represent theoretical mass isotopic distribution matches ( $\pm 5\%$  height deviation) and can be used to increase confidence in AED assignment. The mass spectra for MS only, LC-MS, DTIMS-MS and LC-DTIMS-MS also show red boxes. These red boxes represent isotopic distribution mismatches or concomitant interferences that were observed in the complex sample. In this data, numerous interference peaks were observed in the MS only dimension. The separation power by both LC and DTIMS dimensions filtered numerous interference peaks from the AED of interest, especially when these separation dimensions were combined.

Importantly, the qualitative aspects of the LC-DTIMS-MS analyses directly complement the quantitative LC-MS/MS results. While it is possible to potentially combine both workflows onto a single LC-DTIMS-MS instrument, these instruments are typically outfitted with a time-of-flight mass analyzer rather than using a triple quadrupole configuration for fundamental sampling reasons described elsewhere.<sup>43</sup> To draw benchmark comparisons with conventional validated triple quadrupole MS/MS methods, which are the gold standard in routine testing laboratories, we chose to separate the quantitative and qualitative aspects of both triple quadrupole MS/MS and DTIMS-MS platforms, respectively. Our goal is to demonstrate the unique capabilities that DTIMS-MS offer for resolving interferences while having a wide breadth of molecular coverage. In this work we demonstrate the viability of DTIMS-MS for clinical and routine testing laboratories and benchmark against standardized methodologies using triple quadrupole MS/MS methods.

The results in **Figures 2, 3, 4, and S3** show that the use of DTIMS as a molecular descriptor in addition to accurate mass and retention time for AEDs and AED structural isomer analyses has great potential for rapidly characterizing and identifying structurally similar AEDs. **Figure 3.3.** presents a scatter plot of CCS versus  $m/z$  with 13 AEDs shown in color and the gray background points being entries over this CCS and  $m/z$  range in the Unified CCS compendium, which could be considered potential endogenous biological background.<sup>34,42</sup> This type of 2D DTIMS-MS projection as conformational space analysis is indicative of differences in gas-phase molecular packing efficiency, which is related to molecular structure.<sup>42</sup> Previously, the community has shown individual biomolecular classes such as oligonucleotides, carbohydrates, peptides, and lipids occupy distinct regions in conformational space.<sup>50</sup> However, in the small molecule/metabolite region of conformation space these distinctions are much less pronounced. This appears to also be the case for the AEDs or anticonvulsants.<sup>33,39</sup> Nevertheless, the results in **Figure 3.3.** illustrate that

each of the AEDs and structural isomer or isobaric AEDs were separated from each other in conformational space based on their structural properties (e.g., the isobars CBZ epoxy, oxcarbazepine, and phenytoin). CBZ epoxy and oxcarbazepine are both carboxamides and phenytoin is a hydantoin (**Figure 3.2.**). Both CBZ epoxy and oxcarbazepine structures correspond to constrained dibenzazepine structures resulting in more compact collision cross sections. The phenytoin structure is characterized by unconstrained phenyl moieties which yield a higher degree of freedom and likely results in the larger observed collision cross section across the three isomers. Further support for this observation is noted in that the two phenyl functional groups in phenytoin are not coplanar. The structural differences between the two carboxamides is the epoxide group on CBZ epoxy and the ketone group on oxcarbazepine. As these 3 AEDs have the same chemical formula and are isobaric, it is these functional group differences that provide for structural separation via DTIMS ( $^{DT}CCS_{N_2} = 154.0 \text{ \AA}^2$ ,  $^{DT}CCS_{N_2} = 155.8 \text{ \AA}^2$ , and  $^{DT}CCS_{N_2} = 166.6 \text{ \AA}^2$ , for CBZ epoxy, oxcarbazepine, and phenytoin, respectively). These structural separations of isobaric AEDs occur within the time scale of traditional liquid chromatographic and ion mobility techniques.<sup>51</sup>

To further show the utility of the ion mobility separation capabilities, we analyzed a single patient sample which contained levetiracetam, MHD, and zonisamide (**Figure 3.4.**). This data shows the mass spectra from the complex patient sample when analyzed using filtering from the four different modes of separation, specifically: MS only separation, LC-MS separation, DTIMS-MS separation, and integrated LC-DTIMS-MS separation. Individual mass spectra were compared to the theoretical isotopic distribution for each of these drugs. Mass spectra generated using the LC-MS dimension successfully removed numerous interferences when compared to DTIMS-MS (see levetiracetam and MHD, specifically). The DTIMS-MS dimension mass spectra for

zonisamide removed concomitant species that the LC-MS dimension was unable to separate. The combined LC-DTIMS-MS analyses yielded the least number of concomitant species and provides relatively interference free mass spectra. The qualitative LC-DTIMS-MS results shown in this manuscript demonstrate that measured AED CCS values in human serum samples can be matched to pre-existing CCS values from AED standards. These data allow for an increase in confidence in annotated features.<sup>52</sup> Specifically, **Figure C.3.B** shows data generated from AED QCs and patient samples with drift time alignments of levetiracetam, lamotrigine, zonisamide, pregabalin, and MHD where the QCs (n = 3) confirms the identifications of the patient samples (n = 1) and thus show the ability for LC-DTIMS-MS to increase confidence in identifications. These results also highlight the benefits of adding the DTIMS dimension in studying complex samples. Moreover, the CCS values for the AEDs measured in this work can be readily incorporated into existing CCS libraries for inclusion into targeted and/or untargeted LC-DTIMS-MS workflows. As CCS values have been previously shown to be highly reproducible (< 1.0% difference in an interlab study)<sup>39</sup>, CCS values for the 13 AEDs observed in our FIA-DTIMS-MS analyses can be used as reference values for other laboratories. Utilizing database CCS matching provides additional molecular confidence in annotating features in targeted and/or untargeted studies, especially when combined with other molecular descriptors such as mass defect, isotope ratio patterning, and fragmentation methods.<sup>34,52-55</sup>

### **3.4. Conclusions**

Polypharmacy is common for epileptic patients and many hospital laboratories use a combination of immunoassays, LC-UV, and/or LC-MS/MS assays for TDM testing of AEDs. The single, multiplexed, quantitative LC-MS/MS method outlined here would enable laboratories to

simultaneously quantitate 14 AEDs when in-house mass spectrometry platforms are available. The qualitative LC-DTIMS-MS analysis utilized accurate mass measurement and CCS values for improved confidence in identifications generated from the LC-MS/MS method, and additionally increased confidence in identifying AEDs previously unreported in patient samples. The tradeoff between breadth and depth in molecular characterization utilizing DTIMS-MS methods is the reduction in sensitivity over targeted triple quadrupole MS/MS (MRM) methodologies. A unique advantage of DTIMS-MS methods is the ability to perform simultaneous MS/MS experiments for all species on the timescale of the chromatography and ion mobility dimensions. The quantitative and qualitative assays presented here are specific and offer quantitative separation of structural isobaric isomers (e.g., CBZ epoxy, oxcarbazepine, and phenytoin) that should enable therapeutic decisions to be made with higher confidence.

### **3.5. Acknowledgements**

This chapter is published in the ACS journal of Analytical Chemistry and has been reproduced with the permission of the publisher and my co-authors Stacy D. Sherrod, Randi L. Gant-Branum, Jennifer M. Colby, and John A. McLean: Davis, D. E., et. al.; Targeted Strategy to Analyze Antiepileptic Drugs in Human Serum by LC-MS/MS and LC-Ion Mobility-MS. *Anal. Chem.* **2020**, *92* (21), 14648–14656. <https://doi.org/10.1021/acs.analchem.0c03172>.

I would like to thank Jody C. May, Simona G. Codreanu, Charles M. Nichols, James N. Dodds, and Andrzej Balinski for contributions in various stages for advice and technical expertise. Financial support for aspects of this research was provided by The National Institutes of Health (National Cancer Institute R03CA222452). This work was supported in part using the resources of the Center for Innovative Technology at Vanderbilt University.

### 3.6. References

- (1) Brandt, C.; Fueratsch, N.; Boehme, V.; Kramme, C.; Pieridou, M.; Villagran, A.; Woermann, F.; Pohlmann-Eden, B. Development of Psychosis in Patients with Epilepsy Treated with Lamotrigine: Report of Six Cases and Review of the Literature. *Epilepsy Behav.* **2007**, *11* (1), 133–139.
- (2) Gupta, M. A.; Pur, D. R.; Vujcic, B.; Gupta, A. K. Use of Antiepileptic Mood Stabilizers in Dermatology. *Clin. Dermatol.* **2018**, *36* (6), 756–764.
- (3) Prabhavalkar, K. S.; Poovanpallil, N. B.; Bhatt, L. K. Management of Bipolar Depression with Lamotrigine: An Antiepileptic Mood Stabilizer. *Front. Pharmacol.* **2015**, *6* (OCT), 1–11.
- (4) Spina, E.; Perugi, G. Antiepileptic Drugs: Indications Other than Epilepsy. *Epileptic Disord.* **2004**, *6* (2), 57–75.
- (5) Patsalos, P. N.; Spencer, E. P.; Berry, D. J. Therapeutic Drug Monitoring of Antiepileptic Drugs in Epilepsy. *Ther. Drug Monit.* **2018**, *40* (5), 1.
- (6) Patsalos, P. N.; Berry, D. J.; Bourgeois, B. F. D.; Cloyd, J. C.; Glauser, T. A.; Johannessen, S. I.; Leppik, I. E.; Tomson, T.; Perucca, E. Antiepileptic Drugs - Best Practice Guidelines for Therapeutic Drug Monitoring: A Position Paper by the Subcommittee on Therapeutic Drug Monitoring, ILAE Commission on Therapeutic Strategies. *Epilepsia.* **2008**, pp 1239–1276.
- (7) Inada, A.; Oyama, S.; Niinomi, I.; Wakabayashi, T.; Iwanaga, K.; Hosohata, K. Association of Stevens-Johnson Syndrome and Toxic Epidermal Necrolysis with Antiepileptic Drugs in Pediatric Patients: Subgroup Analysis Based on a Japanese Spontaneous Database. *J. Clin. Pharm. Ther.* **2019**, 1–5.
- (8) Rogawski, M. A.; Löscher, W. The Neurobiology of Antiepileptic Drugs. *Nat. Rev. Neurosci.* **2004**, *5* (7), 553–564.
- (9) Levy, R. H.; Schmidt, D. Utility of Free Level Monitoring of Antiepileptic Drugs. *Epilepsia* **1985**, *26* (3), 199–205.
- (10) Louis, E. K. S. Monitoring Antiepileptic Drugs: A Level-Headed Approach. *Curr. Neuropharmacol.* **2009**, *7*, 115–119.



- (11) Balestrini, S.; Sisodiya, S. M. Pharmacogenomics in Epilepsy. *Neurosci. Lett.* **2018**, *667*, 27–39.
- (12) Krasowski, M. D.; McMillin, G. A. Advances in Anti-Epileptic Drug Testing. *Clin. Chim. Acta.* **2014**, *436*, 224–236.
- (13) Meador, K. J.; Loring, D. W. Developmental Effects of Antiepileptic Drugs and the Need for Improved Regulations. *Neurology* **2016**, *86* (3), 297–306.
- (14) Shibata, M.; Hashi, S.; Nakanishi, H.; Masuda, S.; Katsura, T.; Yano, I. Detection of 22 Antiepileptic Drugs by Ultra-Performance Liquid Chromatography Coupled with Tandem Mass Spectrometry Applicable to Routine Therapeutic Drug Monitoring. *Biomed. Chromatogr.* **2012**, *26* (12), 1519–1528.
- (15) Krasowski, M. D.; Siam, M. G.; Iyer, M.; Ekins, S. Molecular Similarity Methods for Predicting Cross-Reactivity with Therapeutic Drug Monitoring Immunoassays. *Ther. Drug Monit.* **2009**, *31* (3), 337–344.
- (16) Dasgupta, A. Impact of Interferences Including Metabolite Crossreactivity on Therapeutic Drug Monitoring Results. *Ther. Drug Monit.* **2012**, *34*, 496–506.
- (17) Krasowski, M. D.; Siam, M. G.; Iyer, M.; Pizon, A. F.; Giannoutsos, S.; Ekins, S. Chemoinformatic Methods for Predicting Interference in Drug of Abuse/Toxicology Immunoassays. *Clin. Chem.* **2009**, *55* (6), 1203–1213.
- (18) Dasgupta, A. Herbal Supplements and Therapeutic Drug Monitoring: Focus on Digoxin Immunoassays and Interactions with St. John’s Wort. *Ther. Drug Monit.* **2008**, *30*, 212–217.
- (19) Krasowski, M. D. Therapeutic Drug Monitoring of the Newer Anti-Epilepsy Medications. *Pharmaceuticals.* **2010**, pp 1909–1935.
- (20) Patsalos, P. N.; Zugman, M.; Lake, C.; James, A.; Ratnaraj, N.; Sander, J. W. Serum Protein Binding of 25 Antiepileptic Drugs in a Routine Clinical Setting: A Comparison of Free Non-Protein-Bound Concentrations. *Epilepsia* **2017**, *58* (7), 1234–1243.

- (21) Alexander, H. B.; Broshek, D. K.; Quigg, M. Quality of Life in Adults with Epilepsy Is Associated with Anticonvulsant Polypharmacy Independent of Seizure Status. *Epilepsy Behav.* **2018**, *78*, 96–99.
- (22) Baftiu, A.; Feet, S. A.; Larsson, P. G.; Burns, M. L.; Henning, O.; Sætre, E.; Molden, E.; Granas, A. G.; Johannessen, S. I.; Landmark, C. J. Utilisation and Polypharmacy Aspects of Antiepileptic Drugs in Elderly versus Younger Patients with Epilepsy: A Pharmacoepidemiological Study of CNS-Active Drugs in Norway, 2004-2015. *Epilepsy Res.* **2018**, *139* (October 2017), 35–42.
- (23) Bjorke, A. B.; Nome, C. G.; Falk, R. S.; Gjerstad, L.; Taubøll, E.; Heuser, K. Evaluation of Long-Term Antiepileptic Drug Use in Patients with Temporal Lobe Epilepsy: Assessment of Risk Factors for Drug Resistance and Polypharmacy. *Seizure* **2018**, *61* (June), 63–70.
- (24) Beiske, G. A. G.; Holmøy, T.; Beiske, A. G.; Johannessen, S. I.; Johannessen Landmark, C. Antiepileptic and Antidepressive Polypharmacy in Patients with Multiple Sclerosis. *Mult. Scler. Int.* **2015**, 1–7.
- (25) D’Urso, A.; Cangemi, G.; Barco, S.; Striano, P.; D’Avolio, A.; de Grazia, U. LC-MS/MS Based Quantification of Nine Antiepileptic Drugs from Dried Sample Spots Device. *Ther. Drug Monit.* **2019**, *41* (3), 331-339.
- (26) Kuhn, J.; Knabbe, C. Fully Validated Method for Rapid and Simultaneous Measurement of Six Antiepileptic Drugs in Serum and Plasma Using Ultra-Performance Liquid Chromatography-Electrospray Ionization Tandem Mass Spectrometry. *Talanta* **2013**, *110*, 71–80.
- (27) Zhang, M.; Yin, L.; Wang, T.; Shi, M.; Zhang, Y.; Gu, J.; Zhao, X. A Parallel-Column LC–MS/MS Method for High-Throughput Analysis of Eight Antiepileptic Drugs in Clinical Therapeutic Drug Monitoring. *Chromatographia* **2016**, *80* (1), 137–143.
- (28) May, J. C.; Goodwin, C. R.; McLean, J. A. Ion Mobility-Mass Spectrometry Strategies for Untargeted Systems, Synthetic, and Chemical Biology. *Curr. Opin. Biotechnol.* **2015**, 117–121.
- (29) Chouinard, C. D.; Wei, M. S.; Beekman, C. R.; Kemperman, R. H. J.; Yost, R. A. Ion Mobility in Clinical Analysis: Current Progress and Future Perspectives. *Clin. Chem.* **2016**, 124–133.

- (30) Sherrod, S. D.; McLean, J. A. Systems-Wide High-Dimensional Data Acquisition and Informatics Using Structural Mass Spectrometry Strategies. *Clin. Chem.* **2016**, 77–83.
- (31) May, J. C.; Gant-Branum, R. L.; McLean, J. A. Targeting the Untargeted in Molecular Phenomics with Structurally-Selective Ion Mobility-Mass Spectrometry. *Curr. Opin. Biotechnol.* **2016**, 192–197.
- (32) Dodds, J. N.; May, J. C.; McLean, J. A. Correlating Resolving Power, Resolution, and Collision Cross Section: Unifying Cross-Platform Assessment of Separation Efficiency in Ion Mobility Spectrometry. *Anal. Chem.* **2017**, 89 (22), 12176–12184.
- (33) Hines, K. M.; Ross, D. H.; Davidson, K. L.; Bush, M. F.; Xu, L. Large-Scale Structural Characterization of Drug and Drug-Like Compounds by High-Throughput Ion Mobility-Mass Spectrometry. *Anal. Chem.* **2017**, 89 (17), 9023–9030.
- (34) Picache, J. A.; Rose, B. S.; Balinski, A.; Leaptrot, K. L.; Sherrod, S. D.; May, J. C.; McLean, J. A. Collision Cross Section Compendium to Annotate and Predict Multi-Omic Compound Identities. *Chem. Sci.* **2019**, 10 (4), 983–993.
- (35) Miura, M.; Takahashi, N. Routine Therapeutic Drug Monitoring of Tyrosine Kinase Inhibitors by HPLC-UV or LC-MS/MS Methods. *Drug Metab. Pharmacokinet.* **2016**, 31 (1), 12–20.
- (36) Farouk, F.; ElKady, E. F.; Azzazy, H. M. E. Simultaneous UPLC-MS/MS Determination of Antiepileptic Agents for Dose Adjustment. *Biomed. Chromatogr.* **2017**, 31 (7), 1–9.
- (37) Clinical and Laboratory Standards Institute. Liquid Chromatography-Mass Spectrometry Methods; Approved Guidelines (C62-A). **2014**, No. 1-56238-977-7, pp 1-71.
- (38) US Food and Drug Administration. Guidance for Industry: Bioanalytical Method Validation. **2018**, No. FDA-2013-D-1020, pp 1-41.
- (39) Stow, S. M.; Causon, T. J.; Zheng, X.; Kurulugama, R. T.; Mairinger, T.; May, J. C.; Rennie, E. E.; Baker, E. S.; Smith, R. D.; McLean, J. A.; et al. An Interlaboratory Evaluation of Drift Tube Ion Mobility-Mass Spectrometry Collision Cross Section Measurements. *Anal. Chem.* **2017**, 89 (17), 9048–9055.

- (40) Finney, G. L.; Chambers, M.; MacCoss, M. J.; Liebler, D. C.; Shulman, N.; Tomazela, D. M.; Tabb, D. L.; Kern, R.; Frewen, B.; MacLean, B. Skyline: An Open Source Document Editor for Creating and Analyzing Targeted Proteomics Experiments. *Bioinformatics*, **2010**, *26* (7), 966–968.
- (41) Shulman, N. J.; Henderson, C. M.; MacLean, B.; Hoofnagle, A. N.; MacCoss, M. J. Skyline Performs as Well as Vendor Software in the Quantitative Analysis of Serum 25-Hydroxy Vitamin D and Vitamin D Binding Globulin. *Clin. Chem.* **2017**, *64* (2), 408–410.
- (42) May, J. C.; Goodwin, C. R.; Lareau, N. M.; Leaptrot, K. L.; Morris, C. B.; Kurulugama, R. T.; Mordehai, A.; Klein, C.; Barry, W.; Darland, E.; et al. Conformational Ordering of Biomolecules in the Gas Phase: Nitrogen Collision Cross Sections Measured on a Prototype High Resolution Drift Tube Ion Mobility-Mass Spectrometer. *Anal. Chem.* **2014**, *86* (4), 2107–2116.
- (43) May, J. C.; McLean, J. A. Ion Mobility-Mass Spectrometry: Time-Dispersive Instrumentation. *Anal. Chem.* **2015**, *87* (3), 1422–1436.
- (44) May, J. C.; McLean, J. A. Advanced Multidimensional Separations in Mass Spectrometry: Navigating the Big Data Deluge. *Annu. Rev. Anal. Chem.* **2016**, *9* (1), 387–409.
- (45) Dodds, J. N.; May, J. C.; McLean, J. A. Investigation of the Complete Suite of the Leucine and Isoleucine Isomers: Toward Prediction of Ion Mobility Separation Capabilities. *Anal. Chem.* **2017**, *89* (1), 952–959.
- (46) Matuszewski, B. K.; Constanzer, M. L.; Chavez-Eng, C. M. Strategies for the Assessment of Matrix Effect in Quantitative Bioanalytical Methods Based on HPLC-MS/MS. *Anal. Chem.* **2003**, *75* (13), 3019–3030.
- (47) Tanaka, N.; Thornton, E. R. Structural and Isotopic Effects in Hydrophobic Binding Measured by High-Pressure Liquid Chromatography. A Stable and Highly Precise Model for Hydrophobic Interactions in Biomembranes. *J. Am. Chem. Soc.* **1977**, *99* (22), 7300–7307.
- (48) Reed, D. R.; Kass, S. R. Hydrogen-Deuterium Exchange at Non-Labile Sites: A New Reaction Facet with Broad Implications for Structural and Dynamic Determinations. *J. Am. Soc. Mass Spectrom.* **2001**, *12* (11), 1163–1168.

- (49) Wang, S.; Cyronak, M.; Yang, E. Does a Stable Isotopically Labeled Internal Standard Always Correct Analyte Response?. A Matrix Effect Study on a LC/MS/MS Method for the Determination of Carvedilol Enantiomers in Human Plasma. *J. Pharm. Biomed. Anal.* **2007**, *43* (2), 701–707.
- (50) Fenn, L. S.; Kliman, M.; Mahsut, A.; Zhao, S. R.; McLean, J. A. Characterizing Ion Mobility-Mass Spectrometry Conformation Space for the Analysis of Complex Biological Samples. *Anal. Bioanal. Chem.* **2009**, *394* (1), 235–244.
- (51) Nichols, C. M.; Dodds, J. N.; Rose, B. S.; Picache, J. A.; Morris, C. B.; Codreanu, S. G.; May, J. C.; Sherrod, S. D.; McLean, J. A. Untargeted Molecular Discovery in Primary Metabolism: Collision Cross Section as a Molecular Descriptor in Ion Mobility-Mass Spectrometry. *Anal. Chem.* **2018**, *90* (24), 14484–14492.
- (52) Dodds, J. N.; Hopkins, Z. R.; Knappe, D. R. U.; Baker, E. S. Rapid Characterization of Per- and Polyfluoroalkyl Substances (PFAS) by Ion Mobility Spectrometry-Mass Spectrometry (IMS-MS). *Anal. Chem.* **2020**, *92* (6), 4427–4435.
- (53) Poland, J. C.; Schrimpe-Rutledge, A. C.; Sherrod, S. D.; Flynn, C. R.; McLean, J. A. Utilizing Untargeted Ion Mobility-Mass Spectrometry to Profile Changes in the Gut Metabolome Following Biliary Diversion Surgery. *Anal. Chem.* **2019**, *91* (22), 14417-14423.
- (54) Harris, R. A.; Leaptrot, K. L.; May, J. C.; McLean, J. A. New Frontiers in Lipidomics Analyses Using Structurally Selective Ion Mobility-Mass Spectrometry. *Trends Analyt. Chem.* **2019**, *116*, 316–323.
- (55) Leaptrot, K. L.; May, J. C.; Dodds, J. N.; McLean, J. A. Ion Mobility Conformational Lipid Atlas for High Confidence Lipidomics. *Nat. Commun.* **2019**, *10* (1), article no. 985.

## CHAPTER 4

### MULTIDIMENSIONAL SEPARATIONS OF INTACT PHASE II STEROID METABOLITES UTILIZING LC-ION MOBILITY-MS

#### **4.1. Introduction**

Exogenous anabolic-androgenic steroids (AASs) are performance enhancement drugs obtained by structural modifications of testosterone. AASs are the most reported prohibited substances in competitive sports.<sup>1-4</sup> Urine sampling is the matrix of choice for testing the presence of AAS because many steroid metabolites are eliminated through urine. These metabolites are typically targeted due to their slow elimination rate in the urinary system. This long elimination time allows drug testing laboratories to detect them over an extended period. Furthermore, urine is a non-invasive sample collection strategy. Usually, two phases of metabolism occur for AASs in urine to inactivate the drug and facilitate its elimination from the body by converting AAS into more polar compounds.<sup>1</sup> Phase I reactions mainly include oxidation and reduction, making them more suitable for phase II reactions. The most common phase II reactions are conjugation with sulfonic acid and glucuronic acid. Both phase I and phase II reactions are enzyme-controlled.<sup>1,5,6</sup>

Routine analyses of AAS metabolites often use indirect methods such as hydrolysis of phase II metabolites, followed by liquid-liquid extraction and derivatization reactions for increased volatility and thermal stability for GC-MS/MS detection.<sup>1,7</sup> Sensitivity challenges in atmospheric pressure ionization (API) methods have been extensively described for the aglycone counterparts of AASs.<sup>8,9</sup> Thus, the sensitivity required in drug testing is difficult to achieve. More recent work has demonstrated that AAS phase II metabolites can be analyzed directly via LC-MS/MS due to their moderate acidity.<sup>1,10-13</sup> Indeed, the LC-MS/MS strategy has been shown suitable to determine

hydrolysis resistant glucuronide metabolites.<sup>14</sup> Nevertheless, this approach does not provide intact steroid structural characterization but only unspecific fragment ions observed in their ESI MS2 spectra. Derivatization reactions are also sometimes used for LC-MS/MS analyses to overcome fragmentation issues.<sup>15</sup> Unfortunately, the sample preparation for derivatization reactions is time-consuming and can yield multiple derivative products.<sup>15</sup>

Despite these challenges, the best targets to track AAS misuse in sports are those eliminated in urine over extended time periods. These are usually referred to as AAS long-term metabolites (LTMs). These LTMs were a turning point in AASs characterization through expanding the detection window of AASs in anti-doping analyses.<sup>1,16</sup> Discovering novel LTMs of AAS with improved analytical capabilities has led to and will continue to provide significant improvements in anti-doping detection.<sup>1,16-21</sup> For example, dehydrochloromethyltestosterone's (DHCMT) estimated detection window without its LTM is 8-18 days, but through inclusion of its LTM this window can be expanded to *ca.* 250 days.<sup>16,17,19-21</sup>

Recently, new LTMs have been described in the sulfate fraction, but current methods can not detect these metabolites in a high-throughput manner. Exhaustive and inefficient chemical hydrolysis reactions are required to achieve the desirable un-sulfated derivative for MS analyses.<sup>22</sup> GC-MS/MS analyses have been utilized for detecting the sulfate metabolites to avoid the inconveniences described above. The degradation products of non-hydrolyzed sulfated metabolites are detected, instead.<sup>23</sup> This approach is not reliable since these degradation products are generated in the GC injection port, and are difficult to control.

A further compounding complication is that the chemical and isomeric diversity of AAS metabolites result in numerous isobaric peaks in the LC-MS/MS or LC-MS/MS (HRMS) analyses, especially considering the high occurrence of coeluting interferences in human urine.<sup>24,25</sup> To date,

several different analytical strategies have been utilized to characterize AAS and related metabolites.<sup>11,16–20,22,23,26–35</sup> Traditionally, these techniques consist of GC-MS/MS, LC-MS/MS, and/or LC-MS/MS (HRMS). However, inherent issues are apparent with phase II steroid metabolites selectivity due to poor fragmentation in API sources and tandem mass spectrometry described by previous studies.<sup>15,24,36</sup> More selective and sensitive analytical methods that are capable of addressing sample complexity and throughput are needed in doping control laboratories to discover novel markers and address the ongoing misuse of AASs.<sup>6,16,37</sup>

Ion mobility spectrometry (IMS) is a gas-phase separation technique that distinguishes ions based on their size, shape, and charge state.<sup>38–66</sup> The IMS size and shape measurement takes the form of an ion collision cross section (CCS), which is a coarse-grained surface area measurement (reported in square angstroms, Å<sup>2</sup>) encompassing the ion size as well as its interaction with the neutral gas. IMS separates ions based on differences in gas phase electrophoretic mobility, while in contrast, GC and LC separations are basically based on differences in analyte boiling point and polarity, respectively. Gas-phase IMS analyses are rapid, typically occurring on a time scale of less than 100 ms per spectrum, whereas condensed phase LC-MS is on the time scale of minutes. Therefore, IMS can be included in existing anti-doping workflows without compromising analytical throughput, providing an additional separation dimension and an associated molecular descriptor (CCS) to support analyte detection and identification.<sup>38,50</sup> Previously, IMS has been utilized to characterize AAS, phase I metabolites, and phase II metabolites.<sup>24,54,67–72</sup> The IMS techniques, such as field asymmetric IMS (FAIMS), traveling wave IMS (TWIMS), and drift tube IMS (DTIMS), each have been utilized for AAS analyses, although they each have different principles of operation.<sup>50,67–74</sup> The Yost research group investigated the effect of cation adducts on FAIMS using AAS isomers. Their principle findings were that separation of isomeric AASs



utilizing Group 1 cation adducts is possible with no increase in analysis time and no additional instrumentation beyond the FAIMS system, which is useful for high-throughput screening.<sup>71</sup> Hernández-Mesa et al. have successfully cross-validated the first TWIMS database for steroids in calves urine and obtained CCS values within 2% of those values contained in literature databases.<sup>68</sup> The Chouinard group has demonstrated the application of the Paternò-Büchi reaction for structural modification of steroid isomers, prompting improved identification by DTIMS, which is promising due to the simplicity, low cost, and relatively high efficiency of the Paternò-Büchi reaction.<sup>67</sup>

Online, multidimensional analytical separations such as liquid chromatography-ion mobility-mass spectrometry (LC-IMS-MS) may be necessary for AAS analyses, particularly for complex sample matrices where numerous isobaric compounds (e.g., nominal mass interferences and structural isomers of the analyte(s)) can be common.<sup>24,57,75</sup> In addition to LC-MS/MS (HRMS) and GC-MS/MS, LC-IMS-MS has become an essential analytical technique for characterizing metabolites simultaneously by molecular structure and weight.<sup>49,52,63,66,75–77</sup>

In this work, we describe an LC-IMS-MS workflow based on DTIMS that can be utilized to support anti-doping efforts to identify relevant and essential AAS phase II intact metabolites in human urine (**Figure 4.1.**). Collision cross section (CCS) values derived from DTIMS show utility in improving the confidence in assigning small-molecule AAS identifications. Broadly, the mobility-mass correlations are used to identify other metabolites with similar structural properties that can be targeted in further analyses. The combined LC-IMS-MS workflow described here delivers reliable and accurate qualification results for AAS phase II metabolites and should prove beneficial for laboratories interested in increasing efficiency and accuracy in anti-doping analyses.

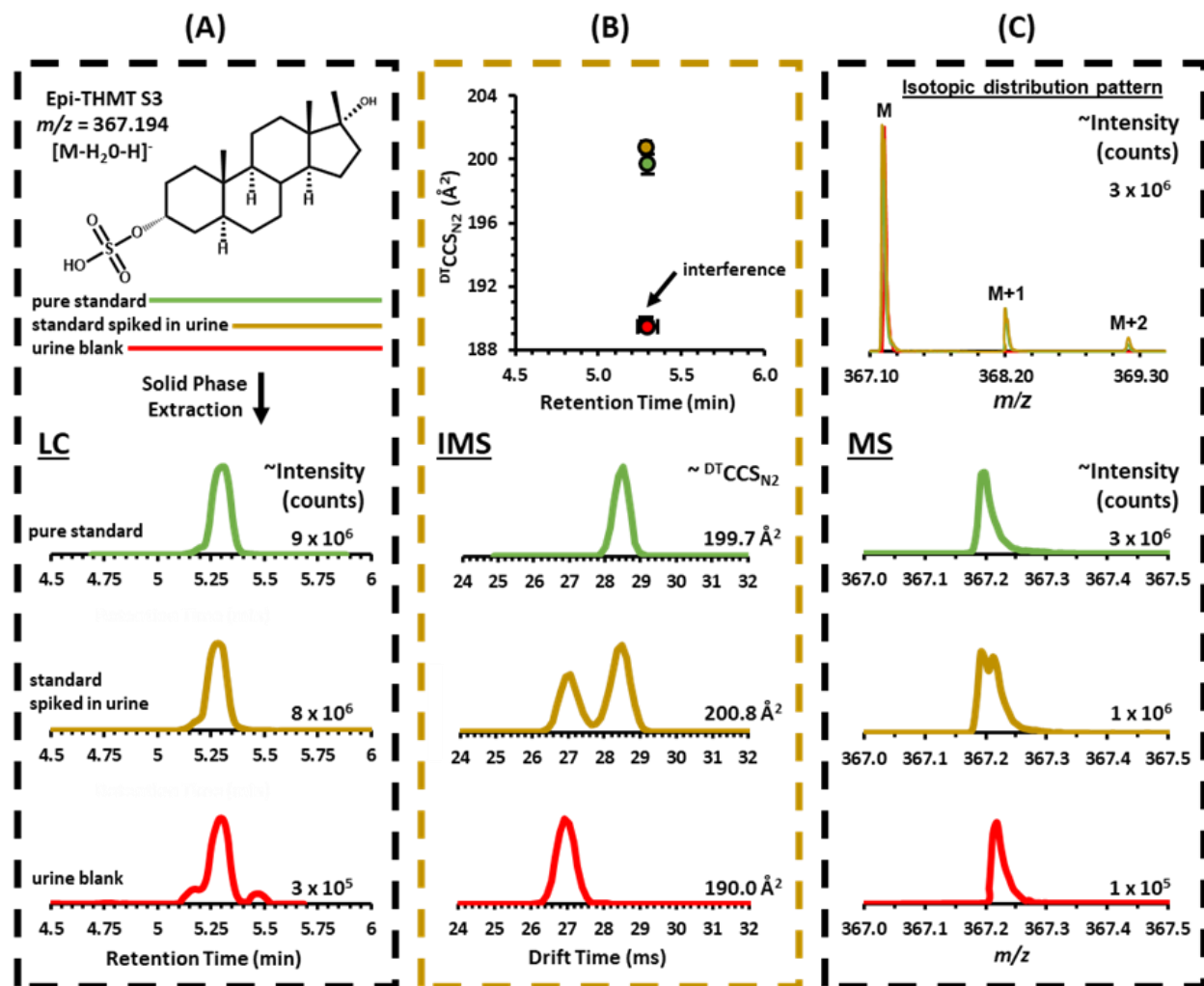


**Figure 4.1.** The anabolic-androgenic steroids (AASs) analytical workflow for the liquid chromatography (LC)-ion mobility (IMS)-mass spectrometry (MS) method with 17-methyltestosterone sulfate metabolite 3 (Epi-THMT S3 as  $[M-H_2O-H]^-$  found in **Figure D.1.**) as an example using the 10 minute LC method (**Table D.1.**). (A) EPI-THMT S3's chemical structure, color coordination legend, sample preparation, LC chromatograms relative intensity vs. retention time in minutes (min) as extracted ion chromatograms (EIC) for 367.1930  $m/z$ . (B) Comparison of collision cross section (CCS) values vs. retention time (min), drift time relative intensity vs. IM spectra in milliseconds (ms). (C) HRMS mass spectra relative intensity vs.  $m/z$  with a mass resolution of  $\sim 10,000$ . In (B) standard error bars were used to demonstrate overlapping CCS values vs. retention times and are within the scale of the marker for most values ( $n = 3$  intraday technical replicates).

## 4.2. *Experimental Methods*

### 4.2.1. *Standards and Chemicals*

Steroids utilized in this study are presented in **Table 4.1**. Epitestosterone S (4-androsten-17 $\alpha$ -ol-3-one sulphate), 7-Keto DHEA-3 S (5-androsten-3 $\beta$ -ol-7,17-dione sulphate), 16 $\alpha$ -hydroxy DHEA S (5-androsten-3 $\beta$ , 16 $\alpha$ -diol-17-one-3 sulphate), Prednisolone 21-S (1,4-pregnadien-11,17,21-triol-3,20-dione 21-sulphate), 11-Ketoetiocholanolone S (5 $\beta$ -androstan-3 $\alpha$ -ol-11,17-dione sulphate), Prasterone S (3 $\beta$ ) (5-androsten-3 $\beta$ -OL-17-one sulphate), Epiandrosterone S (5 $\alpha$ -androstan-3 $\beta$ -ol-17-one sulphate), Prasterone (3 $\alpha$ ) S (5-androsten-3 $\alpha$ -OL-17-one sulphate), 5 $\alpha$ -androstan-3 $\beta$ -ol-one S, Etiocholanolone S (5 $\beta$ -androstan-3 $\alpha$ -ol-17-one sulphate), and Androsterone S (5 $\alpha$ -androstan-3 $\alpha$ -ol-17-one sulphate) were purchased from Steraloids Inc. (Newport, RI, USA). Drostanolone M1 G (2 $\alpha$ -methyl-5 $\alpha$ -androstan-3 $\alpha$ -ol-17-one-3- $\beta$ -D-glucuronic acid), Methenolone M1 G (1-methylene-5 $\alpha$ -androstan-3 $\alpha$ -ol-17-one-3- $\beta$ -D-glucuronic acid), Mesterolone M1 G (1 $\alpha$ -methyl-5 $\alpha$ -androstan-3 $\alpha$ -ol-17-one-3- $\beta$ -D-glucuronic acid), Mesterolone M2 G (1 $\alpha$ -methyl-5 $\alpha$ -androstan-3 $\alpha$ ,17 $\beta$ -diol-3- $\beta$ -D-glucuronic acid), Boldenone G (1,4-adrostadien-17 $\beta$ -diol-3-one-17- $\beta$ -D-glucuronic acid), Bolasterone M1 G (7 $\alpha$ ,17 $\alpha$ -dimethyl-5 $\beta$ -androstan-3 $\alpha$ ,17 $\beta$ -diol-3- $\beta$ -D-glucuronic acid), Stanozolol 3'OH G (5 $\alpha$ -androstan-[3,2-c]pyrazole-3',17 $\beta$ -diol-17 $\alpha$ -methyl-3'- $\beta$ -glucuronic acid), Nandrolone G (4-estren-17 $\beta$ -ol-3-one-17- $\beta$ -D-glucuronic acid), Epinandrolone S (17 $\alpha$ -sulfoxy-4-estren-3-one), 19-norandrosterone D4 G (2,2,4,4-d4-5 $\alpha$ -Estran-3 $\alpha$ -ol-17-one-3- $\beta$ -D-glucuronic acid), Testosterone D3 S (16,16,17 $\alpha$ -d3-17 $\beta$ -sulfoxy-androst-4-en-3-one) were purchased from The National Measurement Institute of Australia (NMIA). Epi-THMT S3 (3 $\alpha$ -sulfoxy-17 $\beta$ -methyl-5 $\beta$ -androstan-17 $\alpha$ -ol) was a kind gift from the Institute Hospital del Mar d'Investigacions Mèdiques (IMIM) (Barcelona, Spain).

**Table 4.1.** AASs separated by isomer groups, neutral formulas, neutral exact mass, adduct exact mass, retention time (RT) using the 15 minute method, elution order annotation, RT CV%, collision cross sections ( $\text{\AA}^2$ ), and CCS CV% ( $n = 3$  technical replicates over 3 different days at 5  $\mu\text{g/mL}$ ). The color coordination is for isomer types described throughout this manuscript.

| <u>AAS</u>                                   | <u>Formula</u>  | <u>Exact Mass</u> | <u>[M-H]<sup>-</sup></u> | <u>Elution #</u> | <u>RT (min)</u> | <u>RT CV%</u> | <u>CCS</u> | <u>CCS CV%</u> |
|--|---|-------------------|--------------------------|------------------|-----------------|---------------|------------|----------------|
| Epi-THMT S3                                  | C <sub>20</sub> H <sub>34</sub> O <sub>5</sub> S              | 386.213           | 385.205                  | 22               | 9.5             | 0.2           | 200.9      | 0.1            |
| Methenolone M1 G                             | C <sub>26</sub> H <sub>38</sub> O <sub>8</sub>                | 478.257           | 477.249                  | 18               | 6.4             | 0.2           | 217.5      | 0.2            |
| 7-Keto DHEA-3 S                              | C <sub>19</sub> H <sub>26</sub> O <sub>6</sub> S              | 382.145           | 381.137                  | 1                | 1.4             | 2.1           | 194.9      | 0.2            |
| Bolasterone M1 G                             | C <sub>27</sub> H <sub>44</sub> O <sub>8</sub>                | 496.304           | 495.296                  | 19               | 6.4             | 0.5           | 212.1      | 0.1            |
| EpiNandrolone S                              | C <sub>18</sub> H <sub>26</sub> O <sub>5</sub> S              | 354.150           | 353.142                  | 7                | 3.1             | 2.3           | 189.3      | 0.1            |
| Boldenone G                                  | C <sub>25</sub> H <sub>34</sub> O <sub>8</sub>                | 462.225           | 461.218                  | 5                | 2.8             | 2.3           | 217.4      | 0.1            |
| Prednisolone 21-S                            | C <sub>21</sub> H <sub>28</sub> O <sub>8</sub> S              | 440.151           | 439.143                  | 3                | 2.1             | 3.2           | 196.9      | 0.1            |
| Mesterolone M2 G                             | C <sub>26</sub> H <sub>42</sub> O <sub>8</sub>                | 482.288           | 481.280                  | 17               | 6.3             | 0.3           | 220.0      | 0.2            |
| Nandrolone G                                 | C <sub>24</sub> H <sub>34</sub> O <sub>8</sub>                | 450.225           | 449.218                  | 6                | 2.8             | 2.5           | 215.3      | 0.1            |
| Stanozolol 1'N – G                           | C <sub>27</sub> H <sub>40</sub> N <sub>2</sub> O <sub>7</sub> | 504.284           | 503.276                  | 10               | 4.1             | 1.4           | 230.9      | 0.2            |
| Stanozolol 3'OH G                            | C <sub>27</sub> H <sub>40</sub> N <sub>2</sub> O <sub>8</sub> | 520.279           | 519.271                  | 14               | 5               | 0.6           | 229.6      | 0.1            |
| <u>Constitutional Isomers</u>                |   |                   |                          |                  |                 |               |            |                |
| 16 $\alpha$ -hydroxy DHEA 3-S                | C <sub>19</sub> H <sub>28</sub> O <sub>6</sub> S              | 384.161           | 383.153                  | 2                | 1.9             | 1.0           | 199.0      | 0.1            |
| 11-Ketoetiocholanolone S                     | C <sub>19</sub> H <sub>28</sub> O <sub>6</sub> S              | 384.161           | 383.153                  | 4                | 2.5             | 1.8           | 188.4      | 0.1            |
| 5 $\alpha$ -androstan-3 $\beta$ -ol-16-one S | C <sub>19</sub> H <sub>30</sub> O <sub>5</sub> S              | 370.181           | 369.174                  | 13               | 4.7             | 1.6           | 197.1      | 0.1            |
| Epitestosterone S                            | C <sub>19</sub> H <sub>28</sub> O <sub>5</sub> S              | 368.166           | 367.158                  | 9                | 4.1             | 2.1           | 192.9      | 0.1            |
| Mesterolone M1 G                             | C <sub>26</sub> H <sub>40</sub> O <sub>9</sub>                | 480.272           | 479.265                  | 20               | 7.3             | 0.3           | 217.7      | 0.2            |
| Drostanolone M1 G                            | C <sub>26</sub> H <sub>40</sub> O <sub>8</sub>                | 480.272           | 479.265                  | 21               | 8.5             | 0.3           | 218.6      | 0.2            |
| <u>Stereoisomers</u>                         |   |                   |                          |                  |                 |               |            |                |
| Prasterone S (3 $\alpha$ )                   | C <sub>19</sub> H <sub>28</sub> O <sub>5</sub> S              | 368.166           | 367.158                  | 12               | 4.6             | 1.9           | 194.6      | 0.1            |
| Prasterone S (3 $\beta$ )                    | C <sub>19</sub> H <sub>28</sub> O <sub>5</sub> S              | 368.166           | 367.158                  | 8                | 3.9             | 1.1           | 196.3      | 0.1            |
| Etiocholanolone S                            | C <sub>19</sub> H <sub>30</sub> O <sub>5</sub> S              | 370.181           | 369.174                  | 15               | 5.4             | 1.2           | 196.1      | 0.1            |
| Androsterone S                               | C <sub>19</sub> H <sub>30</sub> O <sub>5</sub> S              | 370.181           | 369.174                  | 16               | 5.5             | 0.6           | 195.5      | 0.1            |
| Epiandrosterone S                            | C <sub>19</sub> H <sub>30</sub> O <sub>5</sub> S              | 370.181           | 369.174                  | 11               | 4.5             | 2.1           | 197.4      | 0.2            |

Stanozolol 1'-N-G ( $5\alpha$ -androstan-[3,2-c] pyrazole-3',17 $\beta$ -diol-17 $\alpha$ -methyl-1'-N-glucuronic acid) was provided by Seibersdorf Laboratories (Austria). All 22 AAS chemical structures are shown in **Figure 4.2.**, with sections depicting constitutional isomer and stereoisomer groups along with CCS values for interday ( $n = 3$  technical replicates over 3 different days) analyses in this study. Optima LC/MS grade water, methanol, formic acid, and ammonium formate were obtained from Fisher Scientific (Hampton, NH, USA).

#### ***4.2.2. Human Urine Extraction and Preparation***

For urine samples analyzed in **Figure 4.1.** (Epi-THMT S3 as an example), a solid-phase extraction (SPE-C<sub>18</sub> Cartridges) was carried out. Briefly, 2 mL of methanol and 2 mL of water were used for cartridge conditioning. Afterward, the cartridge was loaded with 5 mL of human urine samples. The cartridges were washed with a mixture of methanol/water 10%. The steroid metabolites were eluted with 100% methanol. The solvent was evaporated under a nitrogen stream at 40°C for 40 min. The final extract was reconstituted with 100  $\mu$ L of mobile phase buffer before analyses.

#### ***4.2.3. Chromatographic Conditions***

For the LC-IMS-MS method, steroid standards were analyzed using a 2.1 x 75 mm (1.7  $\mu$ m) reverse phase column, Waters ACQUITY BEH C18 (Waters Corporation, Milford, MA) with a 2.1 x 5 mm 1.7  $\mu$ m Waters ACQUITY BEH C18 Vanguard precolumn (Waters Corporation, Milford, MA), maintained at 45°C for separation by Ultra High-Pressure Liquid Chromatography (UHPLC, Agilent 1290 Infinity I system, Agilent Technologies, Santa Clara, CA).

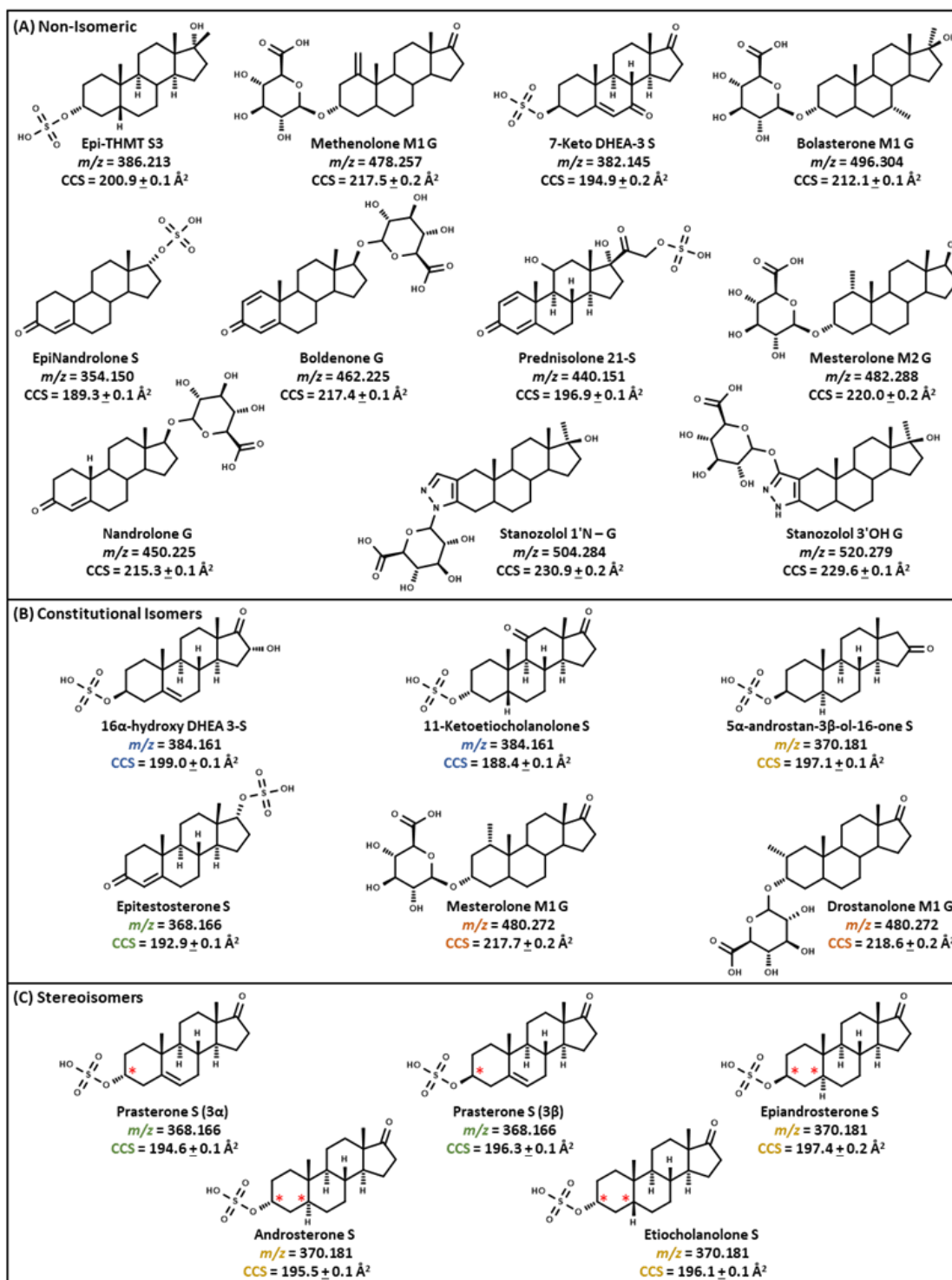


**Figure 4.2.** Chemical structures of 22 phase II steroids categorized as (A) non-isomeric, (B) constitutional isomers, and (C) stereoisomers. Reported CCS measurements represent  $n = 3$  technical replicates over 3 different days at  $5 \mu\text{g/mL}$ . The color coordination is for isomer groups and the red stars indicate positions of stereochemistry that differentiate stereoisomers.

Mobile phase A consisted of water with 0.1% formic acid and 1 mM ammonium formate. Mobile Phase B consisted of methanol with 0.1% formic acid and 1 mM ammonium formate. The UHPLC was directly coupled online to a commercial DTIMS-MS (6560, Agilent Technologies, Santa Clara, Ca). A 10  $\mu$ L sample was injected at a flow rate of 400  $\mu$ L/min and was analyzed using the following chromatographic conditions (15 minute runtime including purge and equilibration times): mobile phase B was maintained at 45% for the first 1 minute for an initial isocratic hold, linearly increased from 45% to 70% over 8.5 minutes, linearly increased again from 70% to 100% over 1 minute, and held at 100% for 1.5 minutes. Mobile phase B returned to 45% by 13 minutes and was held at 45% for 2 minutes to re-equilibrate the column. **Figure 4.1.** shows a 10 min LC method used for human urine samples to increase throughput (**Table D.1.**). In these methods, the initial isocratic hold, final purge, and re-equilibration times were performed to ensure efficient cleaning, minimize carryover, and preserve column integrity. A representative chromatogram of the 22 AASs and mobile phase B gradient for the 15 min LC method is shown in **Figure 4.3.A.**

#### **4.2.4. DTIMS-MS Conditions**

AASs were analyzed in negative ionization mode using the Jet Stream ESI source (Agilent Technologies, Santa Clara, CA) coupled with a drift tube IMS mass spectrometer (6560, Agilent Technologies) using settings similar to previously described instrumental methods.<sup>38,44,46,47,50,78</sup> Ionization source conditions were optimized (e.g., gas temperature, drying gas, nebulizer pressure, sheath gas temperature, sheath gas flow, capillary voltage, and nozzle voltage in **Table D.1.**) by flow injection analysis (FIA) to maximize sensitivity. Briefly, the LC-IMS-MS method consisted of a single-field drift time analyses using nitrogen drift gas with the drift tube at a temperature of 30°C, a pressure of 4.0 Torr, and an electric field of 17.3 V/cm.

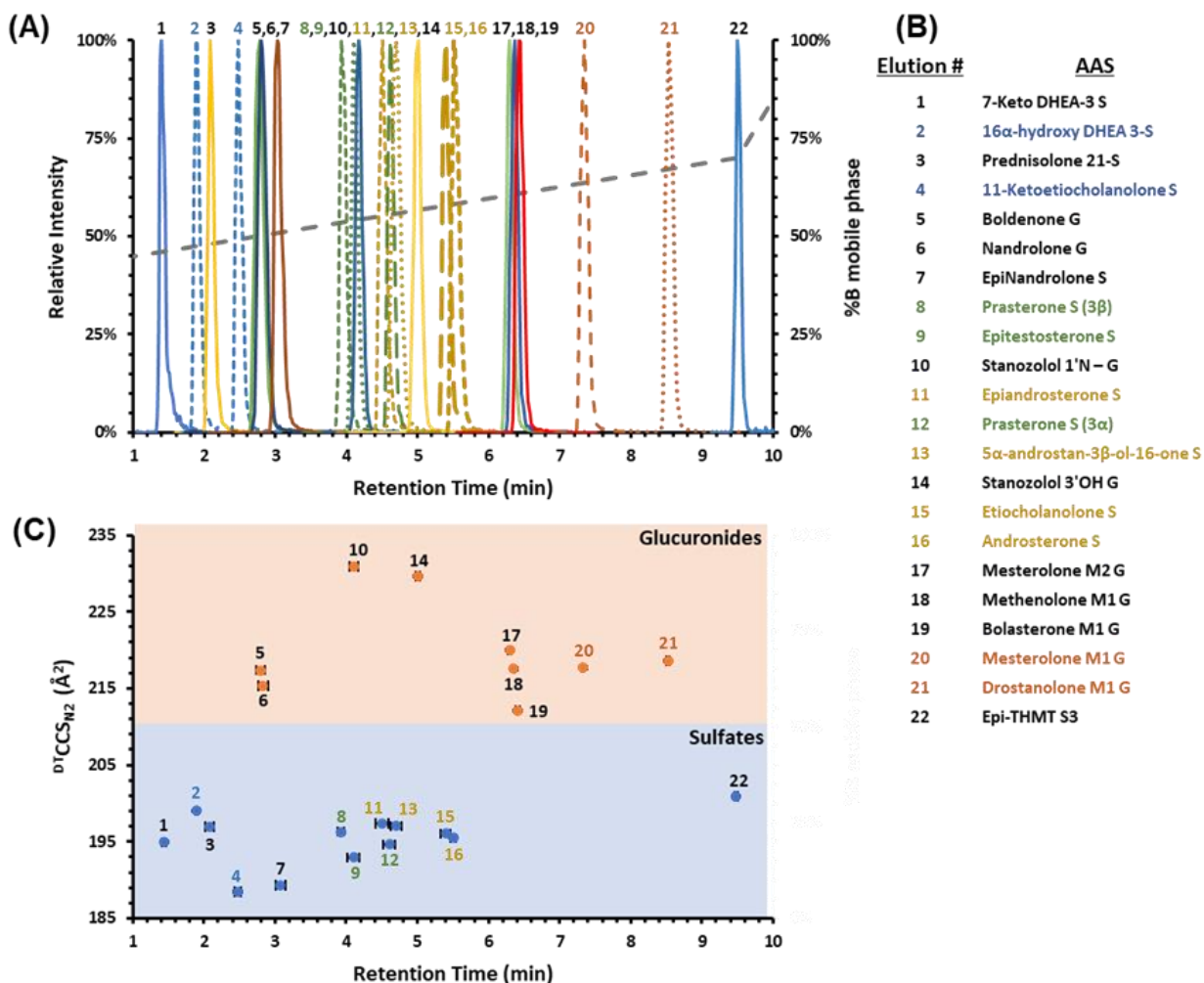


**Figure 4.3.** (A) LC-IMS-MS analysis showing an LC chromatogram of 22 phase II AAS. Dashed chromatograms are isomer groups. The dotted grey line represents %B mobile phase gradient. (B) The elution order of the 22 phase II AAS where the color coordination designates isomer groups. (C) Correlation of LC retention times and CCS values to specific types of phase II steroids (glucuronic acids are in orange and sulfonic acids are in blue). Error bars for both variation in retention times and CCS are shown and are for most values within the scale of the marker ( $n = 3$  technical replicates over 3 different days at 5  $\mu\text{g/mL}$ ).



A calibrated single field CCS method was used to calculate CCS values via the Mason-Schamp equation.<sup>46</sup> Data were acquired using Agilent's MassHunter Workstation Data Acquisition software. Data were analyzed using Agilent's MassHunter Qualitative Analysis software, Agilent's MassHunter IM-MS Browser, and Skyline (MacCoss Lab).<sup>79,80</sup> A representative CCS vs. retention time plot of the 22 AAS IMS and LC profiles is shown in **Figure 4.3.C**. **Table 4.1** also denotes AAS formulas, exact masses, isomer groups, [M-H]<sup>-</sup> measured masses, retention times (RT), RT coefficient of variations (CV%), CCS, and CCS CV%. CCS and *m/z* correlations are shown in **Figure 4.4.** and **Figure D.2.**

### **4.3. Results and Discussion**

#### **4.3.1. LC-IMS-MS**

The range of retention times (min) and ion mobility CCS values from LC-IMS-MS are shown in **Figure 4.3**. These data collectively demonstrate the structural diversity among the AAS phase II steroids outlined in this study even though there are many isomer groups (**Table 4.1.** and **Figure 4.2**). Chromatographically, most AAS were shown to display statistically different separation with some overlapping retention times (based on CV% in **Table 4.1.** and standard error bars in **Figure 4.3.A**). For AASs that did not exhibit baseline separation chromatographically, the data show that there were statistically distinct CCS values for most AASs (difference based on standard error bars in **Figure 4.3.**). Also, HRMS was able to resolve non-isomeric AAS coelution (**Figure 4.4.**).

Through combining LC, IMS, and MS data, nearly all AASs examined were separated in either chromatographic or CCS values except for Epiandrosterone S and

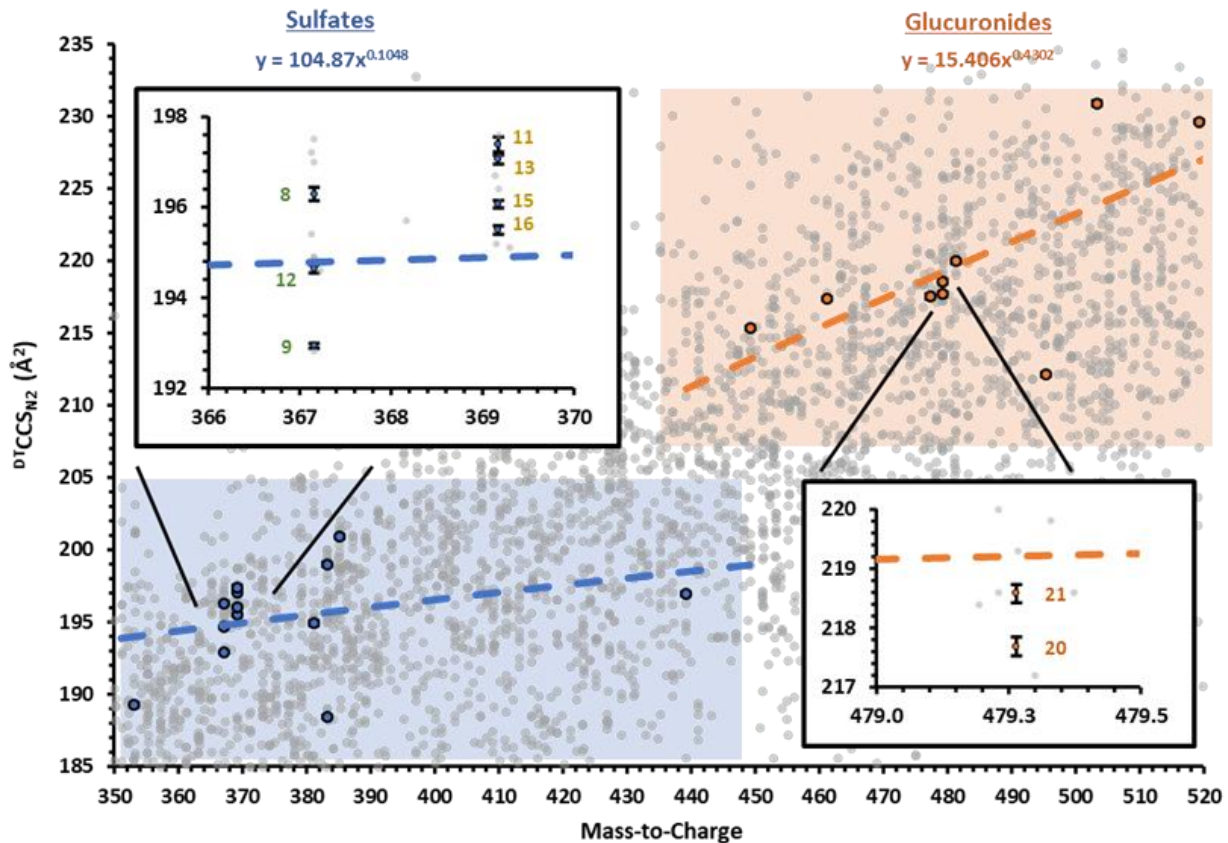


**Figure 4.4.** Conformational space analyses showing CCS values for the phase II steroids investigated using LC-IMS-MS with neat standards. Included is a blue dashed trendline, fit to a power function, representing the best fit line of the sulfate data and the orange trendline represents glucuronide data. The boxes are for isomer groups. Error bars represent standard errors and are for most values within the scale of the marker ( $n = 3$  technical replicates over 3 different days at 5  $\mu\text{g/mL}$ ). The gray data points represent  $\sim 5000$ - $9000$  entries from blank human urine.

5 $\alpha$ -androstan-3 $\beta$ -ol-16-one S (font colors represent AAS isomers in **Table 4.1**, **Figure 4.2**, and **Figure 4.3**). Separation of isomeric AAS via LC-IMS-MS can also be observed in **Figure 4.4** and **Figure D.2**. The data in **Figure D.2** exemplify the presence of unique mass-mobility correlations with  $\pm 10\%$  deviation from the best fit line for 13 sulfate AASs and for 9 glucuronide AASs. This differentiation demonstrates the structural properties of AAS and lays the groundwork for using CCS measurements as an identifier in untargeted and/or targeted AAS studies.<sup>49</sup> Taken together, LC-IMS-MS data strengthen the confidence in identifying AAS in a complex biological matrix and offers a characterization strategy of potentially unknown or known structurally similar steroids or steroid-like compounds in urine as chromatographically coeluting interferences. Interferences in complex biological matrixes can complicate accurate identification in anti-doping analyses, which ultimately may lead to disciplinary decisions for an athlete that might be different with improved analytical accuracy and precision.

#### **4.3.2. Isomer Separation**

To assess the utility of the LC-IMS-MS method for separating isomeric AASs (**Table 4.1** and **Figure 4.2**), we analyzed 11 analytes belonging to 4 isomeric sets including 16 $\alpha$ -hydroxy DHEA 3-S (in blue), 11-ketoetiocholoanolone S (in blue), Prasterone S (3 $\beta$ ) (in green), Epitestosterone S (in green), Prasterone S (3 $\alpha$ ) (in green), Epiandrosterone S (in gold), 5 $\alpha$ -androstan-3 $\beta$ -ol-16-one S (in gold), Etiocholanolone S (in gold), Androsterone S (in gold), Mesterolone M1 G (in orange), and Drostanolone M1 G (in orange). Because isomers have the same chemical formula, this presents challenges for mass separation alone. However, LC-IMS-MS analyses give the most accurate results (Mesterolone M1 G and Drostanolone M1 G in **Figure 4.3**). In the IMS dimension, statistically different separation was readily obtained for all isomer

sets except for Epiandrosterone S and 5 $\alpha$ -androstan-3 $\beta$ -ol-16-one S (difference based on standard error bars in **Figure 4.4.** and **Figure D.2.**). The IMS single-peak resolving power ( $R_p$ ) values and FWHM peak widths for Epiandrosterone S were 40.2 and 0.68 ms, respectively. The IMS  $R_p$  values and FWHM peak widths for 5 $\alpha$ -androstan-3 $\beta$ -ol-16-one S were 42.3 and 0.65 ms, respectively. These two AAS phase II metabolites would benefit from high resolution IMS techniques such as extended path-length traveling wave IMS (cyclic TWIMS), Structures for Lossless Ion Manipulation (SLIM), or ion multiplexing using DTIMS.<sup>81–86</sup> Structural analyses of the stereoisomers (in green, **Table 4.1.** and **Figure 4.2.**), Prasterone S (3 $\alpha$ ), and Prasterone S (3 $\beta$ ) along with their constitutional isomer, Epitestosterone S, showed that stereochemistry of the stereoisomers yielded both statistically different CCS and RT values from each other (in green, difference based on standard error bars in **Figure 4.3.C**). Epitestosterone S exhibited statistically different CCS and RT values from its two isomers mentioned previously (in green, difference based on standard error bars in **Figure 4.3.C**). The stereoisomers structural analysis (in gold, **Table 4.1.**), Epiandrosterone S, Etiocholanolone S, and Androsterone S do not all have statistically different RT values but do have statistically different CCS values (in gold, difference based on standard error bars in **Figure 4.3.** and **Figure 4.4.**). The constitutional isomer, 5- $\alpha$ -androstan-3 $\beta$ -ol-16-one S, yielded statistically different RT but not CCS values when compared to Epiandrosterone S (in gold, difference based on standard error bars in **Figure 4.3.C**, **Figure 4.4.**, and **Figure D.2.**). Each of the constitutional isomer sets (in blue and orange, **Table 4.1.**), 16 $\alpha$ -hydroxy DHEA 3-S (in blue), 11-ketoetiocholanolone S (in blue), Mesterolone M1 G (in orange), and Drostanolone M1 G (in orange) all have statistically different RT and CCS values (difference based on standard error bars in **Figure 4.3.**).

### 4.3.3. Mass-Mobility Correlations

This study's primary objectives were to determine CCS values of known AAS standards and develop correlations between mass and CCS values for two of the main AAS phase II metabolite groups (sulfonic acid and glucuronic acid). The fused ring sterol core, common to these AAS, has no rotational freedom. Therefore, the variability in CCS values is introduced by ketones, double bonds, a pyrazole ring, and stereochemistry of proton, methyl, hydroxyl, sulfate, and glucuronide functional groups. AASs cluster in CCS vs.  $m/z$  conformational space based on their structural similarity (**Figure 4.4.** and **Figure D.2.**). The AAS sulfate-conjugates exhibited the smaller CCS values, likely resulting from this group possessing a smaller sulfonic acid functional group than the glucuronides. The IMS resolving power was able to show statistically different CCS values between most compounds within isomer sets (color coordinating in **Table 4.1.** and **Figure 4.2.**). The AAS glucuronide-conjugates exhibited larger CCS values, likely because of the larger glucuronic acid functional groups.

Utilizing the CCS values reported here, we can develop correlations similar to those used by Picache et al. in the Unified CCS Compendium by mapping expected mobility-mass space for AAS phase II metabolites.<sup>49</sup> Our AAS data is plotted using a power fit. This correlation is representative of AAS phase II metabolites (sulfate and glucuronide). By reporting an AAS correlation generated from standard reference materials (**Figure 4.4.** and **Figure D.2.**) and using it to identify known and unknown AAS in human samples CCS values in future studies, we can increase AAS annotation confidence.<sup>75</sup> Utilizing the information gained from the trendline classification of AAS phase II metabolites shows great promise for identifying new and emerging AASs by plotting their  $m/z$  and CCS values. All values fall within  $\pm 10\%$  of the calculated

correlation, demonstrating its use for potentially identifying AAS phase II metabolite unknowns (**Figure D.2.**).

#### **4.3.4. Relationships Between CCS, Retention Time, and Mass-to-Charge**

Sulfate and glucuronide AAS phase II metabolites were characterized using both RT and CCS values to examine the complementary separation of each dimension (**Figure 4.3.**). There was no consistent trend in the LC elution order as both sulfate and glucuronide AAS phase II metabolites eluted at different times throughout the chromatographic method. However, in the IMS analyses, the sulfate metabolites' CCS values are smaller than the glucuronide metabolites. By combining approaches, most of the isomers can be resolved cooperatively using LC-IMS-MS.

This study has four isomeric groups consisting of both constitutional isomers and stereoisomers analyzed individually and in a mixture. The LC and IMS separations in **Figure 4.3.** illustrate the power of orthogonal separation mechanisms of polarity (LC) and molecular size in the gas phase (IMS). Although not all the isomeric AAS phase II metabolites could be resolved by the LC or MS dimension alone, coupling these two techniques provides a more comprehensive example of isomer separation in 3-dimensional space (LC-IMS-MS).

#### **4.3.5. AAS in Human Urine**

To evaluate the fitness for purpose of our LC-IMS-MS method, urine samples spiked with Epi-THMT S3 were tested after the SPE extraction protocol described in the Methods section (**Figure D.1.**). This metabolite was assessed at several low concentration levels to demonstrate analytical figures of merit, such as limits of detection and quantification limits in human urine, shown in **Figure D.1.** In addition to ppb level quantification/linearity, high mass measurement

accuracy, and retention time alignment afforded by our instrument setup, observed CCS values for Epi-THMT S3 in the human urine samples are in good agreement with CCS values from neat standards analyzed on different days (typically <0.5% difference) as shown in **Figure D.1**. These results illustrate the potential benefits of adding the IMS separation to current analytic workflows in routine testing laboratories performing urine analyses, especially for anti-doping purposes.

#### **4.4. Conclusions**

Overall, our results show that the use of IMS as a molecular descriptor in addition to accurate mass and retention time alignment in AAS phase II metabolite analyses has great potential for characterizing phase II metabolite groups and identifying various legacy and emerging AAS species. In the trendline assessments relating CCS to  $m/z$ , each subclass was separated from the others based on their structural properties. These separations provide additional descriptors for the molecules and can point to new species in biological samples. For the future, CCS prediction using machine learning algorithms will be necessary to populate the numerous possible AAS CCS values with high speed and accuracy (DeepCCS).<sup>87</sup> It should be noted that the results in this manuscript are a proof of concept to demonstrate that measured CCS values in human urine samples can be matched to pre-existing CCS values from neat standards to increase confidence in annotated features. In this analytical workflow, we did not evaluate explicit concentration levels for all AAS. Instead, this sampling provides qualitative measurements of AAS detection and CCS reproducibility. The results also highlight positive benefits of adding IMS dimension, such as the fact that while LC retention time precision can be influenced by a number of factors including system void volume, variations in solvent composition, or changes in pH. On the other hand, CCS

is an intrinsic molecular descriptor of gas-phase surface area and is generally thought to be less affected by experimental variables.

Moreover, the CCS values for AAS measured in this work will be readily incorporated into existing CCS libraries for inclusion into LC-IMS-MS workflows. Often, CCS values are highly reproducible (often less than 1.0% different between laboratories).<sup>46</sup> Anti-doping analyses can significantly benefit from database CCS matching with unknown analytes for additional molecular confidence in annotating unknown features in untargeted studies, especially in cases where reference materials are not available.

#### **4.5. Acknowledgements**

This chapter contains the submitted research article: Don E. Davis, Jr., Katrina L. Leaprot, David C. Koomen, Jody C. May, Gustavo de A. Cavalcanti, Monica C. Padilha, Henrique M.G. Pereira, and John A. McLean, “Multidimensional Separations of Intact Phase II Steroid Metabolites Utilizing LC-Ion Mobility-MS,” *Analytical Chemistry*, **2021** (submitted February 25).

I would like to thank Nadjali A. Chung and Bailey S. Rose for contributions in various stages for advice and technical expertise. Financial support for aspects of this research was provided by The National Institutes of Health (National Cancer Institute R03CA222452). Financial support was also provided by Partnership for Clean Competition (PCC) and in part using the resources of the Center for Innovative Technology at Vanderbilt University.

#### **4.6. References**

- (1) Stojanovic, B. J.; Göschl, L.; Forsdahl, G.; Günter, G. Metabolism of Steroids and Sport Drug Testing. *Bioanalysis*. **2020**, 12 (9), 561–563.  
<https://doi.org/10.4155/bio-2020-0077>



- (2) Parr, M. K.; Flenker, U.; Schänzer, W. The Assay of Endogenous and Exogenous Anabolic Androgenic Steroids. *Hormone Use and Abuse by Athletes*. **2011**, 121–130.  
[https://doi.org/10.1007/978-1-4419-7014-5\\_13](https://doi.org/10.1007/978-1-4419-7014-5_13)
- (3) World Anti-Doping Agency (WADA) International Standard Prohibited List 2021  
[https://www.wada-ama.org/sites/default/files/resources/files/2021list\\_en.pdf](https://www.wada-ama.org/sites/default/files/resources/files/2021list_en.pdf)
- (4) World Anti-Doping Agency (WADA) World Anti-Doping Code 2021  
[https://www.wada-ama.org/sites/default/files/resources/files/2021\\_wada\\_code.pdf](https://www.wada-ama.org/sites/default/files/resources/files/2021_wada_code.pdf)
- (5) Gómez, C.; Pozo, O. J.; Marcos, J.; Segura, J.; Ventura, R. Alternative Long-Term Markers for the Detection of Methyltestosterone Misuse. *Steroids*. **2013**, 78 (1), 44–52.  
<https://doi.org/10.1016/j.steroids.2012.10.008>
- (6) Gomez, C.; Fabregat, A.; Pozo, Ó. J.; Marcos, J.; Segura, J.; Ventura, R. Analytical Strategies Based on Mass Spectrometric Techniques for the Study of Steroid Metabolism. *TrAC - Trends Anal. Chem.* **2014**, 53, 106–116.  
<https://doi.org/10.1016/j.trac.2013.08.010>
- (7) Narciso, J.; Luz, S.; Bettencourt Da Silva, R. Assessment of the Quality of Doping Substances Identification in Urine by GC/MS/MS. *Anal. Chem.* **2019**, 91 (10), 6638–6644.  
<https://doi.org/10.1021/acs.analchem.9b00560>
- (8) Pozo, O. J.; Van Eenoo, P.; Deventer, K.; Delbeke, F. T. Ionization of Anabolic Steroids by Adduct Formation in Liquid Chromatography Electrospray Mass Spectrometry. *J. Mass Spectrom.* **2007**, 42 (4), 497–516.  
<https://doi.org/10.1002/jms.1182>
- (9) Rannulu, N. S.; Cole, R. B. Novel Fragmentation Pathways of Anionic Adducts of Steroids Formed by Electrospray Anion Attachment Involving Regioselective Attachment, Regiospecific Decompositions, Charge-Induced Pathways, and Ion-Dipole Complex Intermediates. *J. Am. Soc. Mass Spectrom.* **2012**, 23 (9), 1558–1568.  
<https://doi.org/10.1007/s13361-012-0422-y>

- (10) Forsdahl, G.; Zanitzer, K.; Erceg, D.; Gmeiner, G. Quantification of Endogenous Steroid Sulfates and Glucuronides in Human Urine after Intramuscular Administration of Testosterone Esters. *Steroids*. **2020**, *157*, 108614.  
<https://doi.org/10.1016/j.steroids.2020.108614>
- (11) Balcells, G.; Pozo, O. J.; Esquivel, A.; Kotronoulas, A.; Joglar, J.; Segura, J.; Ventura, R. Screening for Anabolic Steroids in Sports: Analytical Strategy Based on the Detection of Phase I and Phase II Intact Urinary Metabolites by Liquid Chromatography Tandem Mass Spectrometry. *J. Chromatogr. A*. **2015**, *1389*, 65–75. <https://doi.org/10.1016/j.chroma.2015.02.022>
- (12) Fabregat, A.; Pozo, O. J.; Marcos, J.; Segura, J.; Ventura, R. Use of LC-MS/MS for the Open Detection of Steroid Metabolites Conjugated with Glucuronic Acid. *Anal. Chem.* **2013**, *85* (10), 5005–5014. <https://doi.org/10.1021/ac4001749>
- (13) Lee, S. H.; Lee, N.; Hong, Y.; Chung, B. C.; Choi, M. H. Simultaneous Analysis of Free and Sulfated Steroids by Liquid Chromatography/Mass Spectrometry with Selective Mass Spectrometric Scan Modes and Polarity Switching. *Anal. Chem.* **2016**, *88* (23), 11624–11630.  
<https://doi.org/10.1021/acs.analchem.6b03183>
- (14) Kotronoulas, A.; Gomez-Gomez, A.; Segura, J.; Ventura, R.; Joglar, J.; Pozo, O. J. Evaluation of Two Glucuronides Resistant to Enzymatic Hydrolysis as Markers of Testosterone Oral Administration. *J. Steroid Biochem. Mol. Biol.* **2017**, *165*, 212–218.  
<https://doi.org/10.1016/j.jsbmb.2016.06.006>
- (15) Athanasiadou, I.; Angelis, Y. S.; Lyris, E.; Georgakopoulos, C. Chemical Derivatization to Enhance Ionization of Anabolic Steroids in LC-MS for Doping-Control Analysis. *TrAC – Trends Anal. Chem.* **2013**, *42*, 137–156.  
<https://doi.org/10.1016/j.trac.2012.10.003>
- (16) Thevis, M.; Walpurgis, K.; Thomas, A. Analytical Approaches in Human Sports Drug Testing: Recent Advances, Challenges, and Solutions. *Anal. Chem.* **2019**, *92* (1), 506-523  
<https://doi.org/10.1021/acs.analchem.9b04639>

- (17) Sobolevsky, T.; Rodchenkov, G. Detection and Mass Spectrometric Characterization of Novel Long-Term Dehydrochloromethyltestosterone Metabolites in Human Urine. *J. Steroid Biochem. Mol. Biol.* **2012**, *128*, 121–127.  
<https://doi.org/10.1016/j.jsbmb.2011.11.004>
- (18) Kratena, N.; Enev, V. S.; Gmeiner, G.; Gärtner, P. Synthesis of 17 $\beta$ -Hydroxymethyl-17 $\alpha$ -Methyl-18-Norandrosta-1,4,13-Trien-3-One: A Long-Term Metandienone Metabolite. *Steroids*, **2016**, *115*, 75–79.  
<https://doi.org/10.1016/j.steroids.2016.08.013>
- (19) Forsdahl, G.; Geisendorfer, T.; Göschl, L.; Pfeffer, S.; Gärtner, P.; Thevis, M.; Gmeiner, G. Unambiguous Identification and Characterization of a Long-Term Human Metabolite of Dehydrochloromethyltestosterone. *Drug Test. Anal.* **2018**, *10* (8), 1244–1250.  
<https://doi.org/10.1002/dta.2385>
- (20) Liu, J.; Chen, L.; Joseph, J. F.; Naß, A.; Stoll, A.; de la Torre, X.; Botrè, F.; Wolber, G.; Parr, M. K.; Bureik, M. Combined Chemical and Biotechnological Production of 20 $\beta$ OH-NorDHCMT, a Long-Term Metabolite of Oral-Turinabol (DHCMT). *J. Inorg. Biochem.* **2018**, *183*, 165–171.  
<https://doi.org/10.1016/j.jinorgbio.2018.02.020>
- (21) Kratena, N.; Pilz, S. M.; Weil, M.; Gmeiner, G.; Enev, V. S.; Gärtner, P. Synthesis and Structural Elucidation of a Dehydrochloromethyltestosterone Metabolite. *Org. Biomol. Chem.* **2018**, *16* (14), 2508–2521.  
<https://doi.org/10.1039/c8ob00122g>
- (22) Balcells, G.; Pozo, O. J.; Garrosta, L.; Esquivel, A.; Matabosch, X.; Kotronoulas, A.; Joglar, J.; Ventura, R. Detection and Characterization of Clostebol Sulfate Metabolites in Caucasian Population. *J. Chromatogr. B Anal. Technol. Biomed. Life Sci.* **2016**, *1022*, 54–63.  
<https://doi.org/10.1016/j.jchromb.2016.03.028>

- (23) Polet, M.; Van Gansbeke, W.; Albertsdóttir, A. D.; Coppieters, G.; Deventer, K.; Van Eenoo, P. Gas Chromatography–mass Spectrometry Analysis of Non-Hydrolyzed Sulfated Steroids by Degradation Product Formation. *Drug Test. Anal.* **2019**, *11* (11–12), 1656–1665.  
<https://doi.org/10.1002/dta.2606>
- (24) Hernández-Mesa, M.; Le Bizec, B.; Monteau, F.; García-Campaña, A. M.; Dervilly-Pinel, G. Collision Cross Section (CCS) Database: An Additional Measure to Characterize Steroids. *Anal. Chem.* **2018**, *90* (7), 4616–4625.  
<https://doi.org/10.1021/acs.analchem.7b05117>
- (25) Gouveia, M. J.; Brindley, P. J.; Santos, L. L.; Correia Da Costa, J. M.; Gomes, P.; Vale, N. Mass Spectrometry Techniques in the Survey of Steroid Metabolites as Potential Disease Biomarkers: A Review. *Metabolism: Clinical and Experimental.* **2013**, *62* (9), 1206–1217.  
<https://doi.org/10.1016/j.metabol.2013.04.003>
- (26) Polet, M.; Van Gansbeke, W.; Geldof, L.; Deventer, K.; Van Eenoo, P. Identification and Characterization of Novel Long-Term Metabolites of Oxymesterone and Mesterolone in Human Urine by Application of Selected Reaction Monitoring GC-CI-MS/MS. *Drug Test. Anal.* **2017**, *9* (11–12), 1673–1684.  
<https://doi.org/10.1002/dta.2183>
- (27) Wang, Z.; Zhou, X.; Liu, X.; Dong, Y.; Zhang, J. A Novel HPLC-MRM Strategy to Discover Unknown and Long-Term Metabolites of Stanozolol for Expanding Analytical Possibilities in Doping-Control. *J. Chromatogr. B Anal. Technol. Biomed. Life Sci.* **2017**, *1040*, 250–259.  
<https://doi.org/10.1016/j.jchromb.2016.11.006>
- (28) Balcells, G.; Matabosch, X.; Ventura, R. Detection of Stanozolol O- and N-Sulfate Metabolites and Their Evaluation as Additional Markers in Doping Control. *Drug Test. Anal.* **2017**, *9* (7), 1001–1010.  
<https://doi.org/10.1002/dta.2107>

- (29) Rzeppa, S.; Viet, L. Analysis of Sulfate Metabolites of the Doping Agents Oxandrolone and Danazol Using High Performance Liquid Chromatography Coupled to Tandem Mass Spectrometry. *J. Chromatogr. B Anal. Technol. Biomed. Life Sci.* **2016**, *1029–1030*, 1–9.  
<https://doi.org/10.1016/j.jchromb.2016.06.028>
- (30) World Anti-Doping Agency (WADA) 2018 Anti-Doping Testing Figures  
[https://www.wada-ama.org/sites/default/files/resources/files/2018\\_testing\\_figures\\_report.pdf](https://www.wada-ama.org/sites/default/files/resources/files/2018_testing_figures_report.pdf)
- (31) Liu, Y.; Lu, J.; Yang, S.; Zhang, Q.; Xu, Y. New Drostanolone Metabolites in Human Urine by Liquid Chromatography Time-of-Flight Tandem Mass Spectrometry and Their Application for Doping Control. *Steroids* **2016**, *108*, 61–67.  
<https://doi.org/10.1016/j.steroids.2016.01.013>
- (32) Piper, T.; Schänzer, W.; Thevis, M. Revisiting the Metabolism of 19-Nortestosterone Using Isotope Ratio and High Resolution/High Accuracy Mass Spectrometry. *J. Steroid Biochem. Mol. Biol.* **2016**, *162*, 80–91.  
<https://doi.org/10.1016/j.jsbmb.2015.12.013>
- (33) World Anti-Doping Agency (WADA) Technical Letter 21: In Situ Formation of 4-Androstene-3,6,17-Trione (6-oxo) and Metabolites  
[https://www.wada-ama.org/sites/default/files/resources/files/tl21\\_6oxo.pdf](https://www.wada-ama.org/sites/default/files/resources/files/tl21_6oxo.pdf)
- (34) Polet, M.; Van Gansbeke, W.; Van Eenoo, P.; Deventer, K. Efficient Approach for the Detection and Identification of New Androgenic Metabolites by Applying SRM GC-CI-MS/MS: A Methandienone Case Study. *J. Mass Spectrom.* **2016**, *51* (7) 524–534.  
<https://doi.org/10.1002/jms.3781>
- (35) Polet, M.; Van Gansbeke, W.; Van Eenoo, P.; Deventer, K. Gas Chromatography/Chemical Ionization Triple Quadrupole Mass Spectrometry Analysis of Anabolic Steroids: Ionization and Collision-Induced Dissociation Behavior. *Rapid Commun. Mass Spectrom.* **2016**, *30* (4), 511–522.  
<https://doi.org/10.1002/rcm.7472>

- (36) Marcos, J.; Pozo, O. J. Derivatization of Steroids in Biological Samples for GC-MS and LC-MS Analyses. *Bioanalysis*. **2015**, 7 (19), 2515–2536.  
<https://doi.org/10.4155/bio.15.176>
- (37) Nicoli, R.; Guillarme, D.; Leuenberger, N.; Baume, N.; Robinson, N.; Saugy, M.; Veuthey, J. L. Analytical Strategies for Doping Control Purposes: Needs, Challenges, and Perspectives. *Anal. Chem.* **2016**, 88 (1), 508–523.  
<https://doi.org/10.1021/acs.analchem.5b03994>
- (38) Dodds, J. N.; Hopkins, Z. R.; Knappe, D. R. U.; Baker, E. S. Rapid Characterization of Per- And Polyfluoroalkyl Substances (PFAS) by Ion Mobility Spectrometry-Mass Spectrometry (IMS-MS). *Anal. Chem.* **2020**, 92 (6), 4427–4435.  
<https://doi.org/10.1021/acs.analchem.9b05364>
- (39) Viehland, L. A.; Mason, E. A. Gaseous Ion Mobility in Electric Fields of Arbitrary Strength. *Ann. Phys.* **1975**, 91 (2), 499–533.  
[https://doi.org/10.1016/0003-4916\(75\)90233-X](https://doi.org/10.1016/0003-4916(75)90233-X)
- (40) Giles, K.; Williams, J. P.; Campuzano, I. Enhancements in Travelling Wave Ion Mobility Resolution. *Rapid Communications in Mass Spectrometry*. **2011**, 25 (11), 1559–1566.  
<https://doi.org/10.1002/rcm.5013>
- (41) Pu, Y.; Ridgeway, M. E.; Glaskin, R. S.; Park, M. A.; Costello, C. E.; Lin, C. Separation and Identification of Isomeric Glycans by Selected Accumulation-Trapped Ion Mobility Spectrometry-Electron Activated Dissociation Tandem Mass Spectrometry. *Anal. Chem.* **2016**, 88 (7), 3440–3443.  
<https://doi.org/10.1021/acs.analchem.6b00041>
- (42) Bijlsma, L.; Berntssen, M. H. G.; Merel, S. A Refined Nontarget Workflow for the Investigation of Metabolites through the Prioritization by in Silico Prediction Tools. *Anal. Chem.* **2019**, 91 (9), 6321–6328.  
<https://doi.org/10.1021/acs.analchem.9b01218>

- (43) Poland, J. C.; Schrimpe-Rutledge, A. C.; Sherrod, S. D.; Flynn, C. R.; McLean, J. A. Utilizing Untargeted Ion Mobility-Mass Spectrometry to Profile Changes in the Gut Metabolome Following Biliary Diversion Surgery. *Anal. Chem.* **2019**, *91* (22), 14417–14423.  
<https://doi.org/10.1021/acs.analchem.9b02924>
- (44) May, J. C.; Goodwin, C. R.; Lareau, N. M.; Leaptrot, K. L.; Morris, C. B.; Kurulugama, R. T.; Mordehai, A.; Klein, C.; Barry, W.; Darland, E.; Overney, G.; Imatani, K.; Stafford, G. C.; Fjeldsted, J. C.; McLean, J. A. Conformational Ordering of Biomolecules in the Gas Phase: Nitrogen Collision Cross Sections Measured on a Prototype High Resolution Drift Tube Ion Mobility-Mass Spectrometer. *Anal. Chem.* **2014**, *86* (4), 2107–2116.  
<https://doi.org/10.1021/ac4038448>
- (45) May, J. C.; Dodds, J. N.; Kurulugama, R. T.; Stafford, G. C.; Fjeldsted, J. C.; McLean, J. A. Broadscale Resolving Power Performance of a High Precision Uniform Field Ion Mobility-Mass Spectrometer. *Analyst.* **2015**, *140* (20), 6824–6833.  
<https://doi.org/10.1039/c5an00923e>
- (46) Stow, S. M.; Causon, T. J.; Zheng, X.; Kurulugama, R. T.; Mairinger, T.; May, J. C.; Rennie, E. E.; Baker, E. S.; Smith, R. D.; McLean, J. A.; Hann, S.; Fjeldsted, J. C. An Interlaboratory Evaluation of Drift Tube Ion Mobility-Mass Spectrometry Collision Cross Section Measurements. *Anal. Chem.* **2017**, *89* (17), 9048–9055.  
<https://doi.org/10.1021/acs.analchem.7b01729>
- (47) Dodds, J. N.; May, J. C.; McLean, J. A. Investigation of the Complete Suite of the Leucine and Isoleucine Isomers: Toward Prediction of Ion Mobility Separation Capabilities. *Anal. Chem.* **2017**, *89* (1), 952–959.  
<https://doi.org/10.1021/acs.analchem.6b04171>
- (48) Nichols, C. M.; Dodds, J. N.; Rose, B. S.; Picache, J. A.; Morris, C. B.; Codreanu, S. G.; May, J. C.; Sherrod, S. D.; McLean, J. A. Untargeted Molecular Discovery in Primary Metabolism:

- Collision Cross Section as a Molecular Descriptor in Ion Mobility-Mass Spectrometry. *Anal. Chem.* **2018**, *90* (24), 14484–14492.  
<https://doi.org/10.1021/acs.analchem.8b04322>
- (49) Picache, J. A.; Rose, B. S.; Balinski, A.; Leaptrot, K. L.; Sherrod, S. D.; May, J. C.; McLean, J. A. Collision Cross Section Compendium to Annotate and Predict Multi-Omic Compound Identities. *Chem. Sci.* **2019**, *10* (4), 983–993.  
<https://doi.org/10.1039/c8sc04396e>
- (50) May, J. C.; McLean, J. A. Ion Mobility-Mass Spectrometry: Time-Dispersive Instrumentation. *Anal. Chem.* **2015**, *87* (3), 1422–1436.  
<https://doi.org/10.1021/ac504720m>
- (51) Leaptrot, K. L.; May, J. C.; Dodds, J. N.; McLean, J. A. Ion Mobility Conformational Lipid Atlas for High Confidence Lipidomics. *Nat. Commun.* **2019**, *10* (1), 1–9.  
<https://doi.org/10.1038/s41467-019-08897-5>
- (52) Chouinard, C. D.; Wei, M. S.; Beekman, C. R.; Kemperman, R. H. J.; Yost, R. A. Ion Mobility in Clinical Analysis: Current Progress and Future Perspectives. *Clinical Chemistry.* **2016**, *62* (1), 124–133.  
<https://doi.org/10.1373/clinchem.2015.238840>
- (53) Harris, R. A.; Leaptrot, K. L.; May, J. C.; McLean, J. A. New Frontiers in Lipidomics Analyses Using Structurally Selective Ion Mobility-Mass Spectrometry. *TrAC - Trends Anal. Chem.* **2019**, *116*, 316–323.  
<https://doi.org/10.1016/j.trac.2019.03.031>
- (54) Maddox, S. W.; Fraser Caris, R. H.; Baker, K. L.; Burkus-Matesevac, A.; Peverati, R.; Chouinard, C. D. Ozone-Induced Cleavage of Endocyclic C=C Double Bonds within Steroid Epimers Produces Unique Gas-Phase Conformations. *J. Am. Soc. Mass Spectrom.* **2020**, *31* (2), 411–417.  
<https://doi.org/10.1021/jasms.9b00058>



- (55) Harris, R. A.; May, J. C.; Stinson, C. A.; Xia, Y.; McLean, J. A. Determining Double Bond Position in Lipids Using Online Ozonolysis Coupled to Liquid Chromatography and Ion Mobility-Mass Spectrometry. *Anal. Chem.* **2018**, *90* (3), 1915–1924.  
<https://doi.org/10.1021/acs.analchem.7b04007>
- (56) Sherrod, S. D.; McLean, J. A. Systems-Wide High-Dimensional Data Acquisition and Informatics Using Structural Mass Spectrometry Strategies. *Clinical Chemistry.* **2016**, *62* (1), 77–83.  
<https://doi.org/10.1373/clinchem.2015.238261>
- (57) Schrimpe-Rutledge, A. C.; Codreanu, S. G.; Sherrod, S. D.; McLean, J. A. Untargeted Metabolomics Strategies—Challenges and Emerging Directions. *J. Am. Soc. Mass Spectrom.* **2016**, *27* (12), 1897–1905.  
<https://doi.org/10.1007/s13361-016-1469-y>
- (58) Gabelica, V.; Shvartsburg, A. A.; Afonso, C.; Barran, P.; Benesch, J. L. P.; Bleiholder, C.; Bowers, M. T.; Bilbao, A.; Bush, M. F.; Campbell, J. L.; Campuzano, I. D. G.; Causon, T.; Clowers, B. H.; Creaser, C. S.; De Pauw, E.; Far, J.; Fernandez - Lima, F.; Fjeldsted, J. C.; Giles, K.; Groessl, M.; Hogan, C. J.; Hann, S.; Kim, H. I.; Kurulugama, R. T.; May, J. C.; McLean, J. A.; Pagel, K.; Richardson, K.; Ridgeway, M. E.; Rosu, F.; Sobott, F.; Thalassinos, K.; Valentine, S. J.; Wyttenbach, T. Recommendations for Reporting Ion Mobility Mass Spectrometry Measurements. *Mass Spectrom. Rev.* **2019**, *38* (3), 291–320.  
<https://doi.org/10.1002/mas.21585>
- (59) Dodds, J. N.; Baker, E. S. Ion Mobility Spectrometry: Fundamental Concepts, Instrumentation, Applications, and the Road Ahead. *J. Am. Soc. Mass Spectrom.* **2019**, *30* (11), 2185–2195.  
<https://doi.org/10.1007/s13361-019-02288-2>
- (60) Hines, K. M.; Ballard, B. R.; Marshall, D. R.; McLean, J. A. Structural Mass Spectrometry of Tissue Extracts to Distinguish Cancerous and Non-Cancerous Breast Diseases. *Mol. Biosyst.* **2014**, *10* (11), 2827–2837.

- <https://doi.org/10.1039/c4mb00250d>
- (61) Fenn, L. S.; McLean, J. A. Biomolecular Structural Separations by Ion Mobility-Mass Spectrometry. *Anal. Bioanal. Chem.* **2008**, *391* (3), 905–909.  
<https://doi.org/10.1007/s00216-008-1951-x>
- (62) Goodwin, C. R.; Fenn, L. S.; Derewacz, D. K.; Bachmann, B. O.; McLean, J. A. Structural Mass Spectrometry: Rapid Methods for Separation and Analysis of Peptide Natural Products. *J. Nat. Prod.* **2012**, *75* (1), 48–53.  
<https://doi.org/10.1021/np200457r>
- (63) Hines, K. M.; Ross, D. H.; Davidson, K. L.; Bush, M. F.; Xu, L. Large-Scale Structural Characterization of Drug and Drug-Like Compounds by High-Throughput Ion Mobility-Mass Spectrometry. *Anal. Chem.* **2017**, *89* (17), 9023–9030.  
<https://doi.org/10.1021/acs.analchem.7b01709>
- (64) Mairinger, T.; Causon, T. J.; Hann, S. The Potential of Ion Mobility–Mass Spectrometry for Non-Targeted Metabolomics. *Curr. Opin. Chem. Biol.* **2018**, *42*, 9–15.  
<https://doi.org/10.1016/j.cbpa.2017.10.015>
- (65) Zhang, X.; Quinn, K.; Cruickshank-Quinn, C.; Reisdorph, R.; Reisdorph, N. The Application of Ion Mobility Mass Spectrometry to Metabolomics. *Current Opinion in Chemical Biology.* **2018**, *42*, 60–66.  
<https://doi.org/10.1016/j.cbpa.2017.11.001>
- (66) May, J. C.; Gant-Branum, R. L.; McLean, J. A. Targeting the Untargeted in Molecular Phenomics with Structurally-Selective Ion Mobility-Mass Spectrometry. *Current Opinion in Biotechnology.* **2016**, *39*, 192–197.  
<https://doi.org/10.1016/j.copbio.2016.04.013>
- (67) Maddox, S. W.; Olsen, S. S. H.; Velosa, D. C.; Burkus-Matesevac, A.; Peverati, R.; Chouinard, C. D. Improved Identification of Isomeric Steroids Using the Paternò-Büchi Reaction with Ion Mobility-Mass Spectrometry. *J. Am. Soc. Mass Spectrom.* **2020**, *31* (10), 2086–2092.

- <https://doi.org/10.1021/jasms.0c00215>
- (68) Hernández-Mesa, M.; D’Atri, V.; Barknowitz, G.; Fanuel, M.; Pezzatti, J.; Dreolin, N.; Ropartz, D.; Monteau, F.; Vigneau, E.; Rudaz, S.; Stead, S.; Rogniaux, H.; Guillarme, D.; Dervilly, G.; Le Bizec, B. Interlaboratory and Interplatform Study of Steroids Collision Cross Section by Traveling Wave Ion Mobility Spectrometry. *Anal. Chem.* **2020**, *92* (7), 5013–5022.
- <https://doi.org/10.1021/acs.analchem.9b05247>
- (69) Hernández-Mesa, M.; Monteau, F.; Le Bizec, B.; Dervilly-Pinel, G. Potential of Ion Mobility-Mass Spectrometry for Both Targeted and Non-Targeted Analysis of Phase II Steroid Metabolites in Urine. *Anal. Chim. Acta X.* **2019**, *1*.
- <https://doi.org/10.1016/j.acax.2019.100006>
- (70) Chouinard, C. D.; Cruzeiro, V. W. D.; Roitberg, A. E.; Yost, R. A. Experimental and Theoretical Investigation of Sodiated Multimers of Steroid Epimers with Ion Mobility-Mass Spectrometry. *J. Am. Soc. Mass Spectrom.* **2017**, *28* (2), 323–331.
- <https://doi.org/10.1007/s13361-016-1525-7>
- (71) Wei, M. S.; Kemperman, R. H. J.; Palumbo, M. A.; Yost, R. A. Separation of Structurally Similar Anabolic Steroids as Cation Adducts in FAIMS-MS. *J. Am. Soc. Mass Spectrom.* **2020**, *31* (2), 355–365.
- <https://doi.org/10.1021/jasms.9b00127>
- (72) Plachká, K.; Pezzatti, J.; Musenga, A.; Nicoli, R.; Kuuranne, T.; Rudaz, S.; Nováková, L.; Guillarme, D. Ion Mobility-High Resolution Mass Spectrometry in Anti-Doping Analysis. Part I: Implementation of a Screening Method with the Assessment of a Library of Substances Prohibited in Sports. *Anal. Chim. Acta.* **2021**, *1152*.
- <https://doi.org/10.1016/j.aca.2021.338257>
- (73) Cumeras, R.; Figueras, E.; Davis, C. E.; Baumbach, J. I.; Gràcia, I. Review on Ion Mobility Spectrometry. Part 1: Current Instrumentation. *Analyst.* **2015**, *140* (5), 1376–1390.
- <https://doi.org/10.1039/c4an01100g>

- (74) Cumeras, R.; Figueras, E.; Davis, C. E.; Baumbach, J. I.; Gràcia, I. Review on Ion Mobility Spectrometry. Part 2: Hyphenated Methods and Effects of Experimental Parameters. *Analyst*. **2015**, *140* (5), 1391–1410.  
<https://doi.org/10.1039/c4an01101e>
- (75) Davis, D. E.; Sherrod, S. D.; Gant-Branum, R. L.; Colby, J. M.; McLean, J. A. Targeted Strategy to Analyze Antiepileptic Drugs in Human Serum by LC-MS/MS and LC-Ion Mobility-MS. *Anal. Chem.* **2020**, *92* (21), 14648–14656.  
<https://doi.org/10.1021/acs.analchem.0c03172>
- (76) May, J. C.; Goodwin, C. R.; McLean, J. A. Ion Mobility-Mass Spectrometry Strategies for Untargeted Systems, Synthetic, and Chemical Biology. *Current Opinion in Biotechnology*. **2015**, *31*, 117–121. <https://doi.org/10.1016/j.copbio.2014.10.012>
- (77) Dodds, J. N.; May, J. C.; McLean, J. A. Correlating Resolving Power, Resolution, and Collision Cross Section: Unifying Cross-Platform Assessment of Separation Efficiency in Ion Mobility Spectrometry. *Anal. Chem.* **2017**, *89* (22), 12176–12184.  
<https://doi.org/10.1021/acs.analchem.7b02827>
- (78) May, J. C.; McLean, J. A. Advanced Multidimensional Separations in Mass Spectrometry: Navigating the Big Data Deluge. *Annu. Rev. Anal. Chem.* **2016**, *9* (1), 387–409.  
<https://doi.org/10.1146/annurev-anchem-071015-041734>
- (79) MacLean, B.; Finney, G. L.; Chambers, M.; MacCoss, M. J.; Liebler, D. C.; Shulman, N.; Tomazela, D. M.; Tabb, D. L.; Kern, R.; Frewen, B.; et al. Skyline: An Open Source Document Editor for Creating and Analyzing Targeted Proteomics Experiments. *Bioinformatics*. **2010**, *26* (7), 966–968.  
<https://doi.org/10.1093/bioinformatics/btq054>
- (80) Henderson, C. M.; Shulman, N. J.; MacLean, B.; MacCoss, M. J.; Hoofnagle, A. N. Skyline Performs as Well as Vendor Software in the Quantitative Analysis of Serum 25-Hydroxy Vitamin D and Vitamin D Binding Globulin. *Clin. Chem.* **2017**, *64* (2), 408–410.

- <https://doi.org/10.1373/clinchem.2017.282293>
- (81) Giles, K.; Ujma, J.; Wildgoose, J.; Pringle, S.; Richardson, K.; Langridge, D.; Green, M. A. Cyclic Ion Mobility-Mass Spectrometry System. *Anal. Chem.* **2019**, *91* (13), 8564–8573.  
<https://doi.org/10.1021/acs.analchem.9b01838>
- (82) May, J. C.; Knochenmuss, R.; Fjeldsted, J. C.; McLean, J. A. Resolution of Isomeric Mixtures in Ion Mobility Using a Combined Demultiplexing and Peak Deconvolution Technique. *Anal. Chem.* **2020**, *92* (14), 9482–9492.  
<https://doi.org/10.1021/acs.analchem.9b05718>
- (83) Kirk, A. T.; Bohnhorst, A.; Raddatz, C. R.; Allers, M.; Zimmermann, S. Ultra-High-Resolution Ion Mobility Spectrometry—Current Instrumentation, Limitations, and Future Developments. *Analytical and Bioanalytical Chemistry.* **2019**, *411* (24), 6229–6246.  
<https://doi.org/10.1007/s00216-019-01807-0>
- (84) Hollerbach, A. L.; Li, A.; Prabhakaran, A.; Nagy, G.; Harrilal, C. P.; Conant, C. R.; Norheim, R. V.; Schimelfenig, C. E.; Anderson, G. A.; Garimella, S. V. B.; Smith, R. D.; Ibrahim, Y. M. Ultra-High-Resolution Ion Mobility Separations over Extended Path Lengths and Mobility Ranges Achieved Using a Multilevel Structures for Lossless Ion Manipulations Module. *Anal. Chem.* **2020**, *92* (11), 7972–7979.  
<https://doi.org/10.1021/acs.analchem.0c01397>
- (85) Deng, L.; Ibrahim, Y. M.; Hamid, A. M.; Garimella, S. V. B.; Webb, I. K.; Zheng, X.; Prost, S. A.; Sandoval, J. A.; Norheim, R. V.; Anderson, G. A.; Tolmachev, A. V.; Baker, E. S.; Smith, R. D. Ultra-High Resolution Ion Mobility Separations Utilizing Traveling Waves in a 13 m Serpentine Path Length Structures for Lossless Ion Manipulations Module. *Anal. Chem.* **2016**, *88* (18), 8957–8964.  
<https://doi.org/10.1021/acs.analchem.6b01915>

- (86) Ibrahim, Y. M.; Hamid, A. M.; Deng, L.; Garimella, S. V. B.; Webb, I. K.; Baker, E. S.; Smith, R. D. New Frontiers for Mass Spectrometry Based upon Structures for Lossless Ion Manipulations. *Analyst*. **2017**, *142* (7), 1010–1021.  
<https://doi.org/10.1039/c7an00031f>
- (87) Plante, P. L.; Francovic-Fontaine, É.; May, J. C.; McLean, J. A.; Baker, E. S.; Laviolette, F.; Marchand, M.; Corbeil, J. Predicting Ion Mobility Collision Cross-Sections Using a Deep Neural Network: DeepCCS. *Anal. Chem.* **2019**, *91* (8), 5191–5199.  
<https://doi.org/10.1021/acs.analchem.8b05821>

## CHAPTER 5

### PERSPECTIVES ON EMERGING AND FUTURE DIRECTIONS

#### 5.1. *Summary*

Routine small molecule quantification in the clinical setting is challenging. Some methods, such as immunoassays and liquid chromatography with ultraviolet (UV) detection, may not exhibit the selectivity or low limits of detection and quantification required. Chapter 1 of the dissertation reports a reversed-phase liquid chromatography-tandem mass spectrometry (RPLC-MS/MS) method to detect and quantify 14 anti-epileptic drugs (AEDs) in human serum as an example of method development, validation, and application workflows. The optimized method was validated under the FDA bioanalytical method validation and CLSI C62-A guidance documents evaluating analyte recovery, matrix effects, precision, accuracy, selectivity, stability, and carryover.<sup>1,2</sup> This method can provide clinical laboratories with a robust and selective quantitative protocol for measuring analytes in serum and better optimizing dosing or response to therapy.

Recent research regarding amino acid metabolism has shown that there may be a link between obesity and Alzheimer's Disease (AD). Chapter 2 reports a metabolomics study using targeted and untargeted strategies. Targeted liquid chromatography-triple quadrupole mass spectrometry (LC-MS/MS) and untargeted liquid chromatography-high resolution tandem mass spectrometry (LC-HRMS/MS) assays analyzed the metabolic changes that occur in AD and obesity. APP<sub>Swe</sub>/PS1<sub>ΔE9</sub> (APP/PSEN1) transgenic mice (to represent familial or early-onset AD) and wild-type litter mater controls were fed either a high-fat diet (HFD, 60% kcal from lard), low-fat diet (LFD, 10% kcal from lard) from 2 months of age, or reversal diet (REV, high fat followed by low fat from 9.5 months). For the targeted analysis, we applied the guidelines outlined in the

Clinical and Laboratory Standards Institute (CLSI) LC-MS C62-A document and the U.S. Food and Drug Administration (FDA) Bioanalytical Method Validation Guidance for Industry to evaluate the assay's figures of merit, and these include linearity, analyte recovery, matrix effects, precision, and accuracy.<sup>1,2</sup> Our targeted and untargeted metabolomics results suggest that numerous peripheral pathways, specifically amino acid metabolism, were significantly affected by AD and diet. The same trends in individual amino acids were observed in both strategies, highlighting the results' biological trueness. More substantial effects and more changes were observed in the APP/PSEN1 mice, suggesting that they were more sensitive to an HFD. Taken together, these data suggest that there are independent and combinatorial effects of AD and HFD on metabolic dysregulation.

Routine small molecule analysis needs high selectivity and/or low limits of quantification. Chapter 3 reports a liquid chromatography-tandem mass spectrometry (LC-MS/MS) method to quantify 14 anti-epileptic drugs (AEDs) in human serum. For the optimized LC-MS/MS method described herein, we applied the guidelines outlined in the Clinical and Laboratory Standards Institute (CLSI) LC-MS C62-A document and the U.S. Food and Drug Administration (FDA) Bioanalytical Method Validation Guidance for Industry to evaluate the quality of the assay.<sup>1,2</sup> In these studies, AED linearity, analyte recovery, matrix effects, precision, and accuracy were assessed. Using liquid chromatography drift tube ion mobility mass spectrometry (LC-DTIMS-MS), a qualitative method was also used to increase AED identification confidence using accurate mass and collision cross section (CCS) measurements. The LC-DTIMS-MS method was also used to assess the ability of drift tube CCS measurements to aid in the separation and identification of AED structural isomers and other AEDs. These data show that another dimension of information, namely CCS measurements, provides an orthogonal dimension of structural information needed



for AED analysis. Multiplexed AED measurements using LC-MS/MS and LC-DTIMS-MS can enable better optimization of dosing due to the high precision capabilities available in these types of analytical studies. Taken together, these data also show the ability to increase confidence in small molecule identification and quantification using these analytical technologies.

The detection and unambiguous identification of anabolic-androgenic steroid metabolites are essential in clinical, forensic, and anti-doping analyses (Chapter 4). Recently, sulfate phase II steroid metabolites have received increased attention in steroid metabolism and drug testing. In large part, this is because phase II steroid metabolites are excreted for an extended time, making them a potential long-term chemical marker of choice for tracking steroid misuse in sports. Comprehensive analytical methods, such as liquid chromatography-tandem mass spectrometry (LC-MS/MS), have been used to detect and identify glucuronide and sulfate steroids in human urine with high sensitivity and reliability. However, LC-MS/MS identification strategies can be hindered because phase II steroid metabolites generate non-selective ion fragments across the different metabolite markers, limiting the confidence in metabolite identifications that rely on exact mass measurement and MS/MS information. Additionally, liquid chromatography-high resolution mass spectrometry (LC-HRMS) and LC-MS/MS are sometimes insufficient at fully resolving the analyte peaks from the sample matrix (commonly urine) chemical noise, further complicating accurate identification efforts. Therefore, we developed a liquid chromatography-ion mobility-mass spectrometry (LC-IMS-MS) method to demonstrate the potential use of drift tube ion mobility to derive collision cross section (CCS) values as an additional molecular descriptor in steroid analyses.

## **5.2. Future Directions**

### **5.2.1. Elucidating Peripheral Amino Acid Changes in Obesity and Alzheimer's Disease Using Metabolomics Based LC-MS/MS and LC-HRMS/MS**

Future work should now focus on studying larger classes of biomolecules involved in mitochondrial dysfunction, such as lipids and carnitines. Also, utilizing LC-IMS-MS to identify isomeric compounds with high accuracy should be the next step.

### **5.2.2. Targeted Strategy to Analyze Anti-Epileptic Drugs in Human Serum by LC-MS/MS and LC-Ion Mobility-MS**

To gain a better insight into small molecule analysis with fragmentation utilizing LC-IMS-MS/MS, fragmentation patterns can be validated on the DTIMS platform with pre- and post-IMS fragments according to FDA and CLSI guidelines.<sup>1,2</sup> This can be performed in a single injection by performing a novel interleaved high/low energy CID experiment. These types of experiments would allow the investigation of isomeric compounds to a degree not yet explored.

### **5.2.3. Multidimensional Separations of Intact Phase II Steroid Metabolites Utilizing LC-Ion Mobility-MS**

The reported work in this study for AAS phase II metabolites will be used to evaluate targeted and untargeted human urine analyses. The orthogonality of IMS provides an extra feature for AAS phase II steroids identification besides the HRMS and LC dimensions. This extra analytical information is of utmost importance for structure elucidation, mainly for those phase II metabolites without reference material commercially available. Currently, AAS structure elucidation can only be assumed due to their ambiguous ESI MS<sup>2</sup> spectra. The data in this

manuscript demonstrates the utility of the reported CCS values for annotating and identifying metabolites in LC-IMS-MS data sets.

A comparison of a single pulse reconstructed (standard demultiplexed) and high resolution demultiplexed (HRdm) LC-IMS-MS spectra can be seen in **Figure 5.1.** for Epi-THMT S3. This ion multiplexing analytical workflow is described in detail elsewhere.<sup>3</sup> In contrast to the conventional single pulse spectrum (**Figure 5.1.A**), the standard demultiplex (**Figure 5.1.B**) is qualitatively similar to the singly pulse spectrum, except that the signal intensity is significantly higher for the demultiplexed spectrum. Note here that the overall signal does not change when processing the data with HRdm (**Figure 5.1.C**). While some gain in resolving power might be expected from ion multiplexing due to the transmission of low-density ion pulses that are less prone to space charge broadening, in practice, the IMS resolution differences between single pulse and standard demultiplexed data are not significant. This can be observed by comparing the IMS spectra of Epi-THMT S3 in single pulse (**Figure 5.1.A**) and standard demultiplexed (**Figure 5.1.B**) modes, where the  $R_p$  value for the standard demultiplexed data was less than the single peak resolution ( $R_p$ ) of the single pulse measurement. For Epi-THMT S3 data processed with HRdm, a single and significantly narrower IMS peak is observed. Future studies will entail analyzing AAS isomer sets in human urine with HRdm and high resolution IMS techniques such as extended path-length traveling wave IMS (cyclic TWIMS), Structures for Lossless Ion Manipulation (SLIM), or ion multiplexing using DTIMS to ascertain whether analytical benefits arise from the increased IMS resolution for routine urine analyses.<sup>3-8</sup> Also, CCS prediction using machine learning algorithms will be necessary to populate the multiple possible AAS CCS values with high speed and accuracy (DeepCCS).<sup>9</sup>

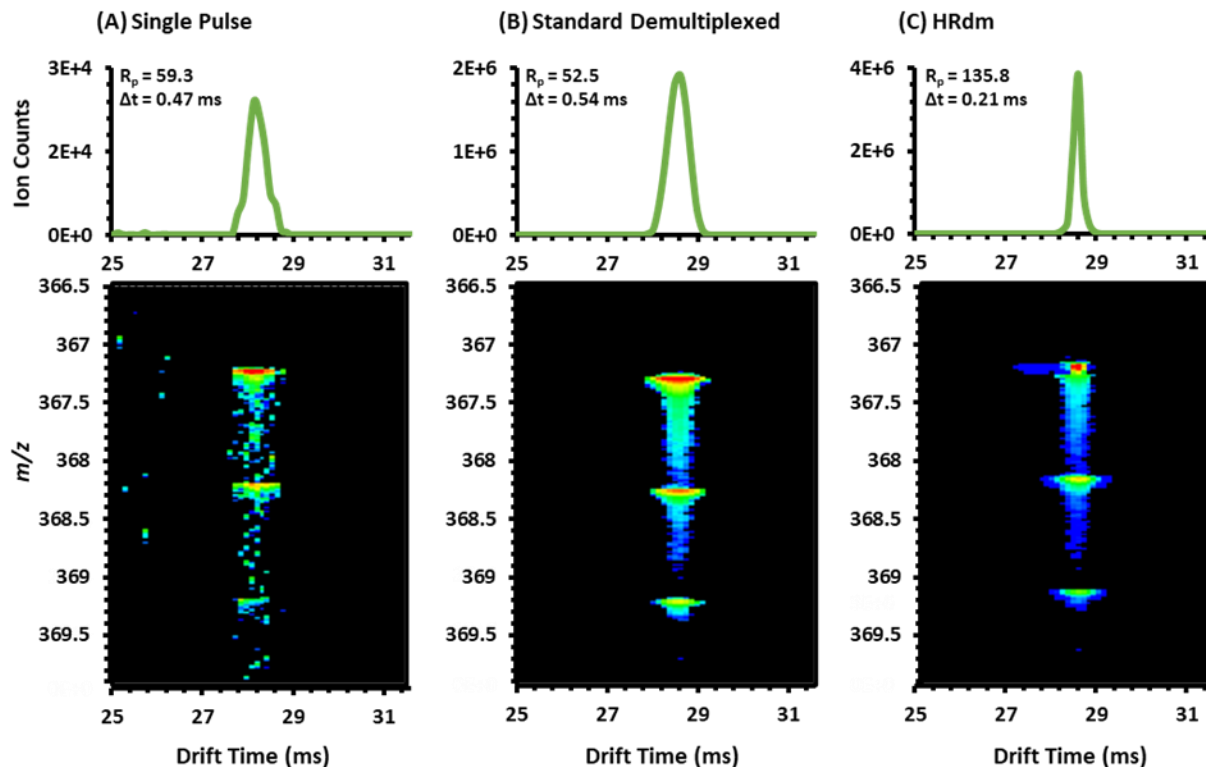


**Figure 5.1.** Example 2D LC-IMS-MS spectra (LC not shown) of Epi-THMT S3 as a pure standard obtained from (A) conventional single pulse IM experiment at 0.5 ppb, (B) demultiplexed LC-IMS-MS spectrum at 500 ppb, and (C) HRdm processed ion multiplex data at 500 ppb. The single-peak resolving power values and FWHM peak widths are listed next to each IMS peak. May and co-workers have previously described DTIMS-MS ion multiplexing experiments where this figure was in part adapted.<sup>3</sup>

### **5.3. Concluding Remarks**

Many different biological applications utilize all sorts of analytical platforms and have been increasing in analytical utility over the years. With this fact in mind, my graduate studies have primarily been devoted to benchmarking gold standard analytical methods with IMS methods to create cohesive workflows that include IMS but do not ultimately change or hinder current analytical workflows.<sup>1,2,10</sup> Studies using method validation are provided in Chapters 1, 2, and 3 of this dissertation, more specifically applied to routine clinical therapeutic drug management programs that often use quantitative immunoassays, LC-UV, and/or by LC-MS/MS (Chapters 1 and 3). Also, routine analysis of anabolic-androgenic steroids (AAS) is often performed using GC-MS/MS or LC-MS/MS. However, we have developed an LC-IMS-MS method for routine AAS analysis (Chapter 4).<sup>11-15</sup> Using IMS for real-world applications; the works compiled in this dissertation demonstrated IMS's utility in analytical settings like academia, clinical, industry, government, and any other routine testing environments that depend on analytical workflows to produce accurate results when analyzing complex biological matrices. Using workflows like these to supplement currently existing analytical workflows allows researchers to confidently identify isomeric species that may have been causing issues or questionable analytical results leading to troublesome auditing processes. Advances found in this dissertation will push the field of ion mobility forward in the mass spectrometry community and help any scientific community that depends on reliable data from analytical chemistry.

#### 5.4. References

- (1) FDA. Guidance for Industry: Bioanalytical Method Validation. **2018**, No. FDA-2013-D-1020, pp 1-41.
- (2) CLSI. Liquid Chromatography-Mass Spectrometry Methods; Approved Guidelines (C62-A). **2014**, No. I-56238-977-7, pp 1-71.
- (3) May, J. C.; Knochenmuss, R.; Fjeldsted, J. C.; McLean, J. A. Resolution of Isomeric Mixtures in Ion Mobility Using a Combined Demultiplexing and Peak Deconvolution Technique. *Anal. Chem.* **2020**, 92 (14), 9482–9492.  
<https://doi.org/10.1021/acs.analchem.9b05718>
- (4) Giles, K.; Ujma, J.; Wildgoose, J.; Pringle, S.; Richardson, K.; Langridge, D.; Green, M. A Cyclic Ion Mobility-Mass Spectrometry System. *Anal. Chem.* **2019**, 91 (13), 8564–8573.  
<https://doi.org/10.1021/acs.analchem.9b01838>
- (5) Kirk, A. T.; Bohnhorst, A.; Raddatz, C. R.; Allers, M.; Zimmermann, S. Ultra-High-Resolution Ion Mobility Spectrometry—Current Instrumentation, Limitations, and Future Developments. *Analytical and Bioanalytical Chemistry*. **2019**, pp 6229–6246.  
<https://doi.org/10.1007/s00216-019-01807-0>
- (6) Hollerbach, A. L.; Li, A.; Prabhakaran, A.; Nagy, G.; Harrilal, C. P.; Conant, C. R.; Norheim, R. V; Schimelfenig, C. E.; Anderson, G. A.; Garimella, S. V. B.; Smith, R. D.; Ibrahim, Y. M. Ultra-High-Resolution Ion Mobility Separations over Extended Path Lengths and Mobility Ranges Achieved Using a Multilevel Structures for Lossless Ion Manipulations Module. *Anal. Chem.* **2020**, 92 (11), 7972–7979.  
<https://doi.org/10.1021/acs.analchem.0c01397>
- (7) Deng, L.; Ibrahim, Y. M.; Hamid, A. M.; Garimella, S. V. B.; Webb, I. K.; Zheng, X.; Prost, S. A.; Sandoval, J. A.; Norheim, R. V; Anderson, G. A.; Tolmachev, A. V; Baker, E. S.; Smith, R. D. Ultra-High Resolution Ion Mobility Separations Utilizing Traveling Waves in a 13 m Serpentine P

- ath Length Structures for Lossless Ion Manipulations Module. *Anal. Chem.* **2016**, 88 (18), 8957–8964.  
<https://doi.org/10.1021/acs.analchem.6b01915>
- (8) Ibrahim, Y. M.; Hamid, A. M.; Deng, L.; Garimella, S. V. B.; Webb, I. K.; Baker, E. S.; Smith, R. D. New Frontiers for Mass Spectrometry Based upon Structures for Lossless Ion Manipulations. *Analyst.* **2017**, pp 1010–1021.  
<https://doi.org/10.1039/c7an00031f>
- (9) Plante, P. L.; Francovic-Fontaine, É.; May, J. C.; McLean, J. A.; Baker, E. S.; Laviolette, F.; Marchand, M.; Corbeil, J. Predicting Ion Mobility Collision Cross-Sections Using a Deep Neural Network: DeepCCS. *Anal. Chem.* **2019**, 91 (8), 5191–5199.  
<https://doi.org/10.1021/acs.analchem.8b05821>
- (10) Davis, D. E.; Sherrod, S. D.; Gant-Branum, R. L.; Colby, J. M.; McLean, J. A. Targeted Strategy to Analyze Antiepileptic Drugs in Human Serum by LC-MS/MS and LC-Ion Mobility-MS. *Anal. Chem.* **2020**, 92 (21), 14648–14656.  
<https://doi.org/10.1021/acs.analchem.0c03172>
- (11) Stojanovic, B. J.; Göschl, L.; Forsdahl, G.; Günter, G. Metabolism of Steroids and Sport Drug Testing. *Bioanalysis.* **2020**, pp 561–563.  
<https://doi.org/10.4155/bio-2020-0077>
- (12) Narciso, J.; Luz, S.; Bettencourt Da Silva, R. Assessment of the Quality of Doping Substances Identification in Urine by GC/MS/MS. *Anal. Chem.* **2019**, 91 (10), 6638–6644.  
<https://doi.org/10.1021/acs.analchem.9b00560>
- (13) Forsdahl, G.; Zanitzer, K.; Erceg, D.; Gmeiner, G. Quantification of Endogenous Steroid Sulfates and Glucuronides in Human Urine after Intramuscular Administration of Testosterone Esters. *Steroids* **2020**, 157, 108614.  
<https://doi.org/10.1016/j.steroids.2020.108614>

- (14) Balcells, G.; Pozo, O. J.; Esquivel, A.; Kotronoulas, A.; Joglar, J.; Segura, J.; Ventura, R. Screening for Anabolic Steroids in Sports: Analytical Strategy Based on the Detection of Phase I and Phase II Intact Urinary Metabolites by Liquid Chromatography Tandem Mass Spectrometry. *J. Chromatogr. A* **2015**, 1389, 65–75.  
<https://doi.org/10.1016/j.chroma.2015.02.022>
- (15) Fabregat, A.; Pozo, O. J.; Marcos, J.; Segura, J.; Ventura, R. Use of LC-MS/MS for the Open Detection of Steroid Metabolites Conjugated with Glucuronic Acid. *Anal. Chem.* **2013**, 85 (10), 5005–5014.  
<https://doi.org/10.1021/ac4001749>



## APPENDIX A

Chapters in this dissertation were either previously published or will be published in the following articles:

### Chapter 1

**Davis, D. E.**; Sherrod, S. D.; Gant-Branum, R. L.; Colby, J. M.; McLean, J. A. Targeted Strategy to Analyze Antiepileptic Drugs in Human Serum by LC-MS/MS and LC-Ion Mobility-MS. *Anal. Chem.* **2020**, 92 (21), 14648–14656.  
<https://doi.org/10.1021/acs.analchem.0c03172>

### Chapter 2

Amelia L. Taylor, **Don E. Davis, Jr.**, Simona G. Codreanu, Stacy D. Sherrod, Fiona E. Harrison, and John A. McLean, “Elucidating Peripheral Amino Acid Changes in Obesity and Alzheimer’s Disease Using Metabolomics,” *Analytical Chemistry*, **2021**.

### Chapter 3

**Davis, D. E.**; Sherrod, S. D.; Gant-Branum, R. L.; Colby, J. M.; McLean, J. A. Targeted Strategy to Analyze Antiepileptic Drugs in Human Serum by LC-MS/MS and LC-Ion Mobility-MS. *Anal. Chem.* **2020**, 92 (21), 14648–14656.  
<https://doi.org/10.1021/acs.analchem.0c03172>

### Chapter 4

**Don E. Davis, Jr.**, Katrina L. Leaptrot, David C. Koomen, Jody C. May, Gustavo de A. Cavalcanti, Monica C. Padilha, Henrique M.G. Pereira, and John A. McLean, “Multidimensional Separations of Intact Phase II Steroid Metabolites Utilizing LC-Ion Mobility-MS,” *Analytical Chemistry*, **2021** (submitted February 25).

## APPENDIX B

### Supporting Information for Chapter 2

#### Elucidating Peripheral Amino Acid Changes in Obesity and Alzheimer's Disease Using Metabolomics

Amelia L. Taylor<sup>1</sup>, Don E. Davis, Jr.<sup>1</sup>, Simona G. Codreanu<sup>1,2</sup>, Stacy D. Sherrod<sup>1,2</sup>, Fiona E. Harrison<sup>3</sup>, and John A. McLean<sup>1,2</sup>

<sup>1</sup>Department of Chemistry, Vanderbilt University, Nashville, TN 37235 USA

<sup>2</sup>Center for Innovative Technology, Vanderbilt University, Nashville, TN 37235 USA

<sup>3</sup>Division of Diabetes, Endocrinology, and Metabolism, Vanderbilt University Medical Center, Nashville, TN 37235 USA

#### ***Comments on HILC-MS/MS Data and RPLC-HR MS/MS Data***

In this supporting information, we provide figures for targeted chromatograms, MRM transitions, linear dynamic ranges, quality control (QC) analysis and concentrations, significant compounds, and significant pathways.

**Figure B.1.** Extracted ion chromatograms from HILIC-MS/MS method for 11 amino acids studied in this work at quality control (QC) mid-level concentrations. This chromatographic method demonstrates the ability to separate isomeric amino acids (L-Leucine and L-Isoleucine), allowing them to be quantitated independently.

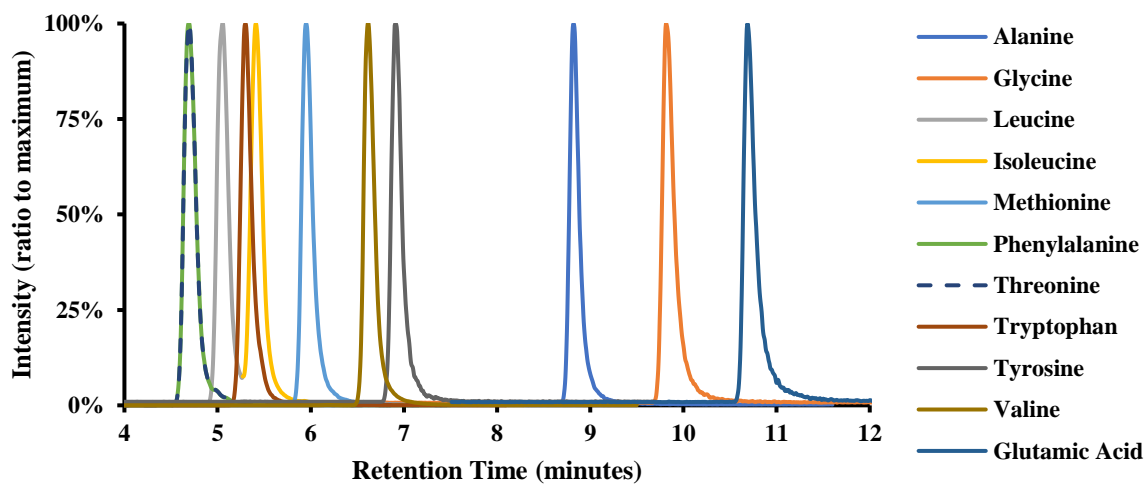


**Table B.1.** Amino acid MRM transitions, retention times (min), retention time windows, fragmentor voltages, collision energy voltages, polarity, and stable isotopically labeled internal standard assignments.

| Compound Name        | Precursor Ion | Product Ion | RT (min) | Delta Ret Time | Fragmentor | Collision Energy | Cell Accelerator Voltage | Polarity | Metabolite to normalize to |
|----------------------|---------------|-------------|----------|----------------|------------|------------------|--------------------------|----------|----------------------------|
| L-Alanine            | 90            | 44          | 8.6      | 6              | 70         | 11               | 3                        | Positive | L-Alanine (13C1)           |
| L-Alanine            | 90            | 44          | 8.6      | 6              | 70         | 11               | 3                        | Positive | L-Alanine (13C1)           |
| L-Alanine (13C1)     | 91            | 44          | 8.6      | 6              | 70         | 11               | 3                        | Positive | N/A                        |
| L-Glutamic Acid      | 148           | 130         | 10.5     | 6              | 75         | 7                | 3                        | Positive | L-Glutamic Acid (D5)       |
| L-Glutamic Acid      | 148           | 84          | 10.5     | 6              | 75         | 16               | 3                        | Positive | L-Glutamic Acid (D5)       |
| L-Glutamic Acid (D5) | 153           | 135         | 10.5     | 10             | 80         | 8                | 3                        | Positive | N/A                        |
| L-Glutamic Acid (D5) | 153           | 107         | 10.5     | 10             | 80         | 10               | 3                        | Positive | N/A                        |
| Glycine (D5)         | 78            | 50          | 9.6      | 10             | 85         | 4                | 3                        | Positive | N/A                        |
| Glycine (D5)         | 78            | 32          | 9.6      | 10             | 85         | 12               | 3                        | Positive | N/A                        |
| Glycine              | 76            | 30          | 9.6      | 6              | 70         | 11               | 3                        | Positive | Glycine (D5)               |
| L-Isoleucine         | 132           | 86          | 5.3      | 6              | 105        | 9                | 3                        | Positive | L-Isoleucine (D1)          |
| L-Isoleucine         | 132           | 69          | 5.3      | 6              | 105        | 19               | 3                        | Positive | L-Isoleucine (D1)          |
| L-Isoleucine         | 132           | 55          | 5.3      | 6              | 105        | 31               | 3                        | Positive | L-Isoleucine (D1)          |
| L-Isoleucine (D1)    | 133           | 87          | 5.3      | 10             | 90         | 10               | 3                        | Positive | N/A                        |
| L-Isoleucine (D1)    | 133           | 70          | 5.3      | 10             | 90         | 20               | 3                        | Positive | N/A                        |
| L-Leucine            | 132           | 86          | 4.9      | 6              | 105        | 9                | 3                        | Positive | L-Leucine (D2)             |
| L-Leucine            | 132           | 69          | 4.9      | 6              | 105        | 19               | 3                        | Positive | L-Leucine (D2)             |
| L-Leucine            | 132           | 55          | 4.9      | 6              | 105        | 31               | 3                        | Positive | L-Leucine (D2)             |
| L-Leucine (D2)       | 134           | 88          | 4.9      | 10             | 90         | 10               | 3                        | Positive | N/A                        |
| L-Leucine (D2)       | 134           | 71          | 4.9      | 10             | 90         | 20               | 3                        | Positive | N/A                        |
| L-Methionine         | 150           | 133         | 5.8      | 6              | 100        | 7                | 3                        | Positive | L-Methionine (D4)          |
| L-Methionine         | 150           | 104         | 5.8      | 6              | 100        | 9                | 3                        | Positive | L-Methionine (D4)          |
| L-Methionine (D4)    | 154           | 137         | 5.8      | 10             | 90         | 8                | 3                        | Positive | N/A                        |
| L-Methionine (D4)    | 154           | 108         | 5.8      | 10             | 90         | 10               | 3                        | Positive | N/A                        |
| L-Phenylalanine      | 166           | 103         | 4.5      | 6              | 80         | 33               | 3                        | Positive | L-Phenylalanine (D8)       |
| L-Phenylalanine      | 166           | 120         | 4.5      | 6              | 80         | 13               | 3                        | Positive | L-Phenylalanine (D8)       |

|                             |     |     |     |    |     |    |   |          |                   |
|-----------------------------|-----|-----|-----|----|-----|----|---|----------|-------------------|
| <b>L-Phenylalanine (D8)</b> | 174 | 109 | 4.5 | 6  | 80  | 33 | 3 | Positive | N/A               |
| <b>L-Threonine</b>          | 120 | 103 | 4.5 | 6  | 135 | 20 | 3 | Positive | L-Threonine (D2)  |
| <b>L-Threonine</b>          | 120 | 77  | 4.5 | 6  | 135 | 30 | 3 | Positive | L-Threonine (D2)  |
| <b>L-Threonine (D2)</b>     | 122 | 103 | 4.5 | 10 | 90  | 6  | 3 | Positive | N/A               |
| <b>L-Threonine (D2)</b>     | 122 | 75  | 4.5 | 10 | 90  | 12 | 3 | Positive | N/A               |
| <b>L-Tryptophan</b>         | 205 | 146 | 5.1 | 6  | 85  | 18 | 3 | Positive | L-Tryptophan (D3) |
| <b>L-Tryptophan</b>         | 205 | 188 | 5.1 | 6  | 85  | 8  | 3 | Positive | L-Tryptophan (D3) |
| <b>L-Tryptophan (D3)</b>    | 208 | 191 | 5.1 | 6  | 85  | 8  | 3 | Positive | N/A               |
| <b>L-Tryptophan (D3)</b>    | 208 | 147 | 5.1 | 6  | 85  | 18 | 3 | Positive | N/A               |
| <b>L-Tyrosine</b>           | 182 | 165 | 6.7 | 6  | 80  | 7  | 3 | Positive | L-Tyrosine (13C9) |
| <b>L-Tyrosine</b>           | 182 | 136 | 6.7 | 6  | 80  | 13 | 3 | Positive | L-Tyrosine (13C9) |
| <b>L-Tyrosine (13C9)</b>    | 192 | 174 | 6.7 | 6  | 80  | 7  | 3 | Positive | N/A               |
| <b>L-Tyrosine (13C9)</b>    | 192 | 145 | 6.7 | 6  | 80  | 13 | 3 | Positive | N/A               |
| <b>L-Valine</b>             | 118 | 72  | 6.5 | 6  | 85  | 9  | 3 | Positive | L-Valine (D8)     |
| <b>L-Valine</b>             | 118 | 55  | 6.5 | 6  | 85  | 25 | 3 | Positive | L-Valine (D8)     |
| <b>L-Valine (D8)</b>        | 126 | 80  | 6.5 | 6  | 80  | 12 | 3 | Positive | N/A               |
| <b>L-Valine (D8)</b>        | 126 | 62  | 6.5 | 6  | 80  | 28 | 3 | Positive | N/A               |

**Table B.2.** Quantification ranges for each amino acid (shown as limit of quantification (LOQ) to upper limit of quantification (ULOQ)) and linear correlation coefficients of the calibration curves for each analyte.

| Amino Acid             | Quantification Range (n=5) |              | Slope | Intercept | R <sup>2</sup> |
|------------------------|----------------------------|--------------|-------|-----------|----------------|
|                        | LOQ (µg/mL)                | ULOQ (µg/mL) |       |           |                |
| <b>L-Alanine</b>       | 1.17                       | 75           | 0.134 | 0.0982    | 0.9997         |
| <b>L-Glutamic Acid</b> | 0.1                        | 50           | 0.13  | 0.0032    | 0.9861         |
| <b>Glycine</b>         | 0.39                       | 100          | 0.028 | 0.0029    | 0.996          |
| <b>L-Isoleucine</b>    | 0.2                        | 100          | 0.258 | -0.0031   | 0.9995         |
| <b>L-Leucine</b>       | 0.2                        | 100          | 0.222 | -0.0065   | 0.983          |
| <b>D-Methionine</b>    | 0.2                        | 100          | 0.073 | -0.001    | 0.9821         |
| <b>L-Phenylalanine</b> | 0.2                        | 100          | 0.343 | -0.0044   | 0.9998         |
| <b>L-Threonine</b>     | 0.2                        | 100          | 0.182 | -0.0067   | 0.9994         |
| <b>L-Tryptophan</b>    | 0.2                        | 100          | 0.187 | -0.0024   | 0.9979         |
| <b>L-Tyrosine</b>      | 0.2                        | 100          | 0.137 | 0.00035   | 0.9987         |
| <b>L-Valine</b>        | 0.2                        | 100          | 0.22  | -0.0026   | 0.9997         |

**Table B.3.** The coefficient of variations (%CV) obtained for stable isotopically labeled internal standards used as QCs for the untargeted analysis in this project.

| Measurement                   | QC Sample          | % CV |
|-------------------------------|--------------------|------|
| <b>Process Variability</b>    | Biotin – D2        | 1.37 |
|                               | Phenylalanine – D8 | 2.86 |
| <b>Instrument Variability</b> | Tryptophan – D3    | 2.18 |
|                               | Valine – D8        | 2.23 |
|                               | Inosine – 4N15     | 9.05 |
|                               | Carnitine-D9       | 1.49 |

**Table B.4.** QC concentration for amino acids targeted in liver and plasma (shown as  $\mu\text{g/mL}$ ).

|                          | <b>Liver<br/>Low</b> | <b>Plasma<br/>Low</b> | <b>Liver<br/>Med</b> | <b>Plasma<br/>Med</b> | <b>Liver<br/>High</b> | <b>Plasma<br/>High</b> |
|--------------------------|----------------------|-----------------------|----------------------|-----------------------|-----------------------|------------------------|
| <b>Alanine</b>           | 11.4                 | 38.6                  | 41.4                 | 52.3                  | 68.7                  | 64.0                   |
| <b>Glutamic<br/>Acid</b> | 6.1                  | 3.9                   | 36.1                 | 5.9                   | 66.1                  | 8.0                    |
| <b>Glycine</b>           | 5.0                  | 19.2                  | 35.0                 | 32.9                  | 65.0                  | 45.3                   |
| <b>Isoleucine</b>        | 1.0                  | 7.5                   | 21.0                 | 15.9                  | 41.0                  | 26.5                   |
| <b>Leucine</b>           | 2.0                  | 12.6                  | 26.0                 | 19.6                  | 50.0                  | 30.8                   |
| <b>Methionine</b>        | 0.5                  | 2.9                   | 14.5                 | 10.5                  | 28.5                  | 20.4                   |
| <b>Phenylalanine</b>     | 1.0                  | 9.1                   | 19.0                 | 16.9                  | 37.0                  | 24.9                   |
| <b>Threonine</b>         | 1.1                  | 9.5                   | 31.1                 | 17.8                  | 61.1                  | 26.0                   |
| <b>Tryptophan</b>        | 0.3                  | 8.7                   | 30.3                 | 23.9                  | 60.3                  | 39.5                   |
| <b>Tyrosine</b>          | 2.2                  | 21.9                  | 32.2                 | 27.7                  | 62.2                  | 32.4                   |
| <b>Valine</b>            | 1.6                  | 31.3                  | 31.6                 | 47.6                  | 58.9                  | 63.7                   |



**Table B.5.** Number of significant compounds detected for each of the comparisons listed from untargeted analysis. Pairwise comparisons are performed between conditions A and B to give total number of significant compounds using the designated significance criteria.

| Pairwise Comparison |         | Total # of Significant Compounds<br>$p \leq 0.05$ | Total # of Significant Compounds<br>$p \leq 0.05$ and<br>$FC \geq  1.5 $ | Total # of Significant Compounds<br>$p \leq 0.05$ and<br>$FC \geq  2 $ | Total # of Compounds Observed<br>$CV < 25\%$ |
|---------------------|---------|---|--|--|--|
| Cond A              | Cond B  |   |  |  |  |
| WT_HFD              | WT_LFD  | 267   | 184  | 79   | 3172   |
| WT_HFD              | WT_REV  | 580   | 279  | 77   | 3172   |
| APP_HFD             | APP_LFD | 751   | 588  | 248  | 3172   |
| APP_HFD             | APP_REV | 749   | 572  | 248  | 3172   |

**Table B.6.** Affected pathways as predicted with Mummichog along with P-values for each pathway.

| Pathways   | WT_HFD_<br>LFD | WT_HFD_<br>REV | APP_HFD_<br>LFD | APP_HFD_<br>REV |
|--|----------------|----------------|-----------------|-----------------|
|  | p-value        | p-value        | p-value         | p-value         |
| <b>Androgen and estrogen biosynthesis and metabolism</b> | 0.407          | 0.557          | 0.047           | 0.034           |
| <b>Arachidonic acid metabolism</b>                       | 0.376          | 0.159          | 0.011           | 0.110           |
| <b>Aspartate and asparagine metabolism</b>               | 0.013          | 0.346          | 0.040           | 0.545           |
| <b>Bile acid biosynthesis</b>                            | 0.376          | 0.430          | 0.623           | 0.006           |
| <b>Butanoate metabolism</b>                              | 0.003          | 0.003          | 0.261           | 0.243           |
| <b>C21-steroid hormone biosynthesis and metabolism</b>   | 0.005          | 0.490          | 0.624           | 0.046           |
| <b>Carnitine shuttle</b>                                 | 0.363          | 0.357          | 0.438           | 0.046           |
| <b>Drug metabolism - cytochrome P450</b>                 | 0.407          | 0.035          | 0.624           | 0.318           |
| <b>Fatty acid activation</b>                             | 0.325          | 0.073          | 0.033           | 0.216           |
| <b>Glutamate metabolism</b>                              | 0.187          | 0.135          | 0.003           | 0.072           |
| <b>Glutathione Metabolism</b>                            | 0.407          | 0.383          | 0.015           | 0.243           |
| <b>Glycerophospholipid metabolism</b>                    | 0.397          | 0.452          | 0.019           | 0.545           |
| <b>Linoleate metabolism</b>                              | 0.407          | 0.430          | 0.483           | 0.001           |
| <b>Lipoate metabolism</b>                                | 0.407          | 0.010          | 0.624           | 0.614           |
| <b>Mono-unsaturated fatty acid beta-oxidation</b>        | 0.029          | 0.077          | 0.624           | 0.614           |
| <b>Nitrogen metabolism</b>                               | 0.140          | 0.306          | 0.023           | 0.404           |
| <b>Omega-6 fatty acid metabolism</b>                     | 0.029          | 0.077          | 0.624           | 0.614           |
| <b>Phytanic acid peroxisomal oxidation</b>               | 0.029          | 0.077          | 0.624           | 0.614           |
| <b>Propanoate metabolism</b>                             | 0.071          | 0.010          | 0.624           | 0.614           |
| <b>Prostaglandin formation from arachidonate</b>         | 0.400          | 0.068          | 0.002           | 0.177           |
| <b>Purine metabolism</b>                                 | 0.014          | 0.172          | 0.298           | 0.515           |
| <b>Pyrimidine metabolism</b>                             | 0.001          | 0.079          | 0.438           | 0.594           |
| <b>Saturated fatty acids beta-oxidation</b>              | 0.407          | 0.348          | 0.047           | 0.467           |
| <b>Tyrosine metabolism</b>                               | 0.371          | 0.393          | 0.002           | 0.464           |
| <b>Urea cycle/amino group metabolism</b>                 | 0.031          | 0.434          | 0.251           | 0.456           |
| <b>Valine, leucine and isoleucine degradation</b>        | 0.002          | 0.013          | 0.047           | 0.183           |

|  |       |       |       |       |
|--|-------|-------|-------|-------|
| <b>Vitamin B1 (thiamin) metabolism</b>                     | 0.071 | 0.010 | 0.624 | 0.614 |
| <b>Vitamin B2 (riboflavin) metabolism</b>                  | 0.029 | 0.077 | 0.624 | 0.614 |
| <b>Vitamin B3 (nicotinate and nicotinamide) metabolism</b> | 0.075 | 0.020 | 0.082 | 0.409 |
| <b>Vitamin B5 - CoA biosynthesis from pantothenate</b>     | 0.140 | 0.306 | 0.023 | 0.614 |
| <b>Vitamin D3 (cholecalciferol) metabolism</b>             | 0.407 | 0.494 | 0.624 | 0.024 |
| <b>Vitamin E metabolism</b>                                | 0.023 | 0.093 | 0.624 | 0.183 |
| <b>Vitamin H (biotin) metabolism</b>                       | 0.071 | 0.010 | 0.624 | 0.614 |
| <b>Vitamin K metabolism</b>                                | 0.029 | 0.557 | 0.624 | 0.105 |

**Table B.7.** P-values for significant amino acids from targeted analysis, as calculated by t-tests followed by Bonferroni correction. ns stands for not significant.

| <b>Amino Acids</b>   | <b>Comparison</b>     |                       |                      |                     |
|----------------------|-----------------------|-----------------------|----------------------|---------------------|
|                      | APP/HFD vs<br>APP/LFD | APP/REV vs<br>APP/HFD | WT/HFD vs<br>APP/LFD | WT/REV vs<br>WT/LFD |
| <b>Glutamic Acid</b> | 0.0077                | 0.0176                | 0.0132               | ns                  |
| <b>Glycine</b>       | ns                    | ns                    | ns                   | 0.044               |

**Table B.8.** P-values for amino acids in the untargeted study, calculated by ANOVA followed by corrections for multiple comparisons. ns stands for not significant.

| <b>Amino Acids</b>       | <b>Comparison</b>           |                             |                               |                                   |                               |
|--------------------------|-----------------------------|-----------------------------|-------------------------------|-----------------------------------|-------------------------------|
|                          | <b>WT/LFD vs<br/>WT/HFD</b> | <b>WT/LFD vs<br/>WT/REV</b> | <b>APP/LFD vs<br/>APP/HFD</b> | <b>APP/HFD<br/>vs<br/>APP/REV</b> | <b>APP/LFD vs<br/>APP/REV</b> |
| <b>Alanine</b>           | ns                          | ns                          | 0.012252796                   | ns                                | 0.033727279                   |
| <b>Glutamic<br/>Acid</b> | ns                          | ns                          | 0.000377238                   | 0.009938925                       | ns                            |
| <b>Glutamine</b>         | ns                          | ns                          | ns                            | ns                                | ns                            |
| <b>Glycine</b>           | ns                          | ns                          | ns                            | ns                                | ns                            |
| <b>Isoleucine</b>        | ns                          | ns                          | 0.000353444                   | ns                                | 0.017844578                   |
| <b>Leucine</b>           | ns                          | ns                          | 0.007377326                   | ns                                | 0.012011312                   |
| <b>Phenylalanine</b>     | ns                          | ns                          | 0.015554535                   | ns                                | 0.005725853                   |
| <b>Valine</b>            | 0.016686542                 | 0.045780936                 | ns                            | ns                                | ns                            |

## APPENDIX C

### Supporting Information for Chapter 3

#### Targeted Strategy to Analyze Anti-Epileptic Drugs in Human Serum by LC-MS/MS and LC-ion mobility-MS

Don E. Davis, Jr.,<sup>†</sup> Stacy D. Sherrod,<sup>†</sup> Randi L. Gant-Branum,<sup>†,1</sup> Jennifer M. Colby,<sup>‡</sup> and John A. McLean<sup>\*,†</sup>

<sup>†</sup>Center for Innovative Technology, Department of Chemistry, Institute of Chemical Biology, Institute for Integrative Biosystems Research and Education, Vanderbilt-Ingram Cancer Center, Vanderbilt University, Nashville, TN 37235 USA

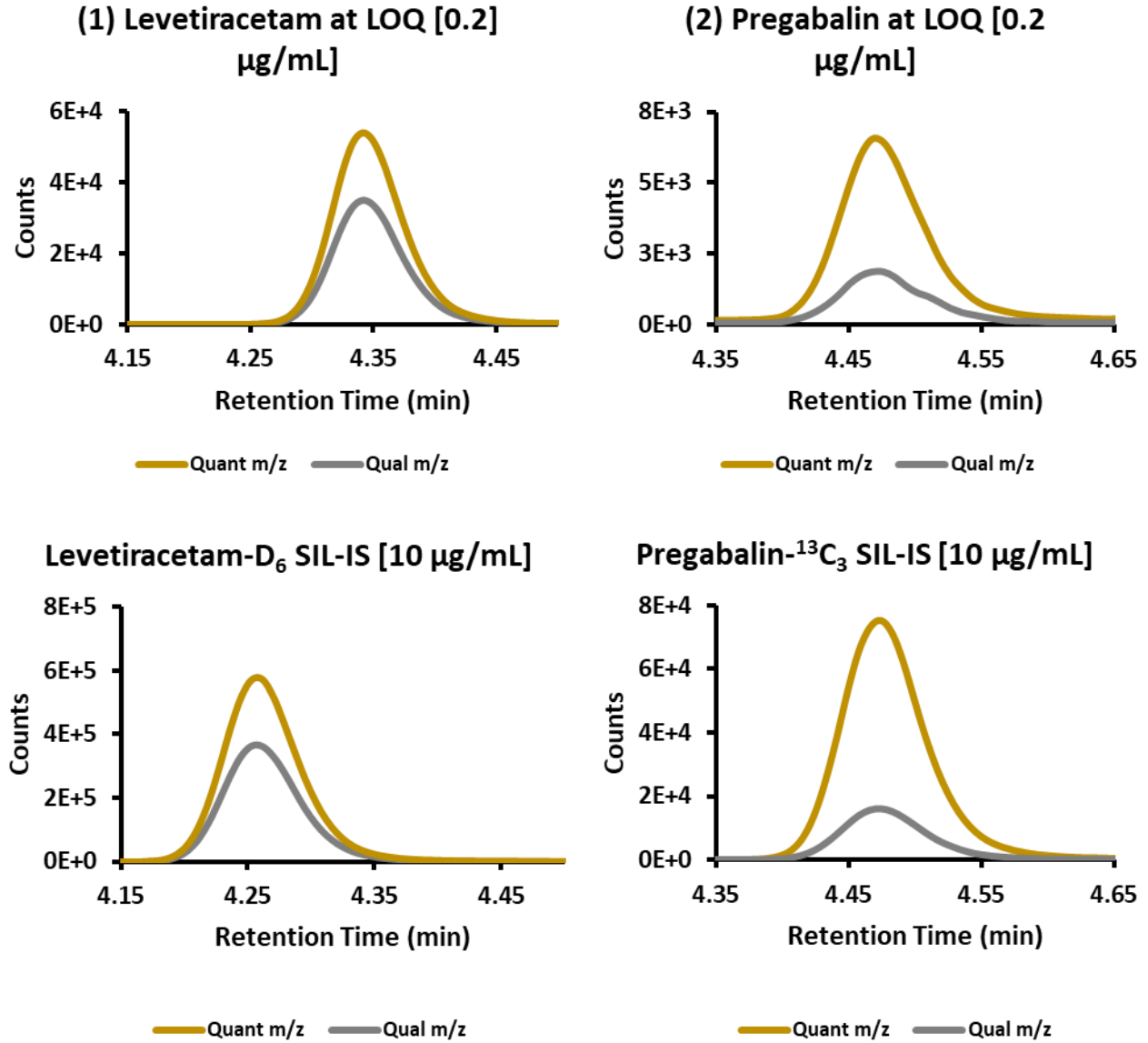
<sup>‡</sup>Department of Pathology, Microbiology, and Immunology; Vanderbilt University Medical Center, Nashville, TN 37235 USA

<sup>1</sup>Current location: HQ Air Force Drug Testing Laboratory (AFDTL), Lackland Air Force Base, San Antonio, TX, United States.

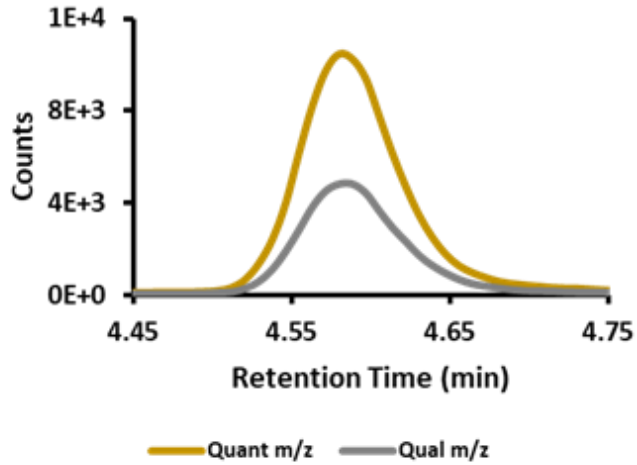
#### *Comments on LC-MS/MS Data, LC-DTIMS-MS Data, and samples presented in this work*

In this supporting information, we provide figures for limit of quantitation chromatograms (14 AEDs), patient sample analysis on both analytical platforms, validation studies, a table for human drug-free and 3<sup>rd</sup> party verified serum quality control material concentrations. We also include additional tables related to linearity study concentrations and calibrator concentrations.

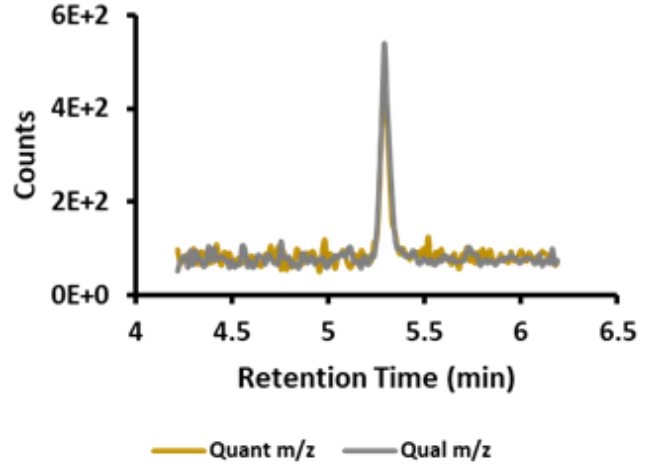
**Figure C.1.** Limit of quantitation (LOQ) chromatograms of 14 AEDs with their given stable isotopically labelled – internal standard (SIL-IS).



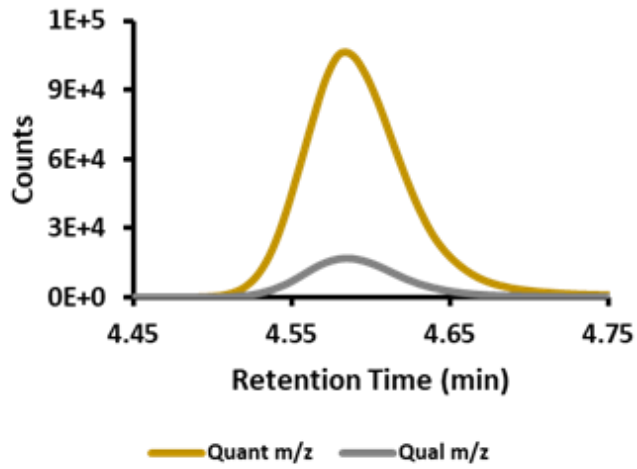
(3) Gabapentin at LOQ [0.2 µg/mL]



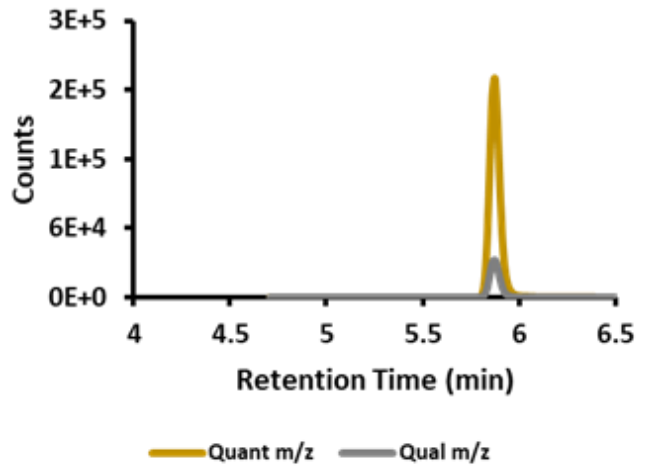
(4) Ethosuximide at LOQ [6.3 µg/mL]



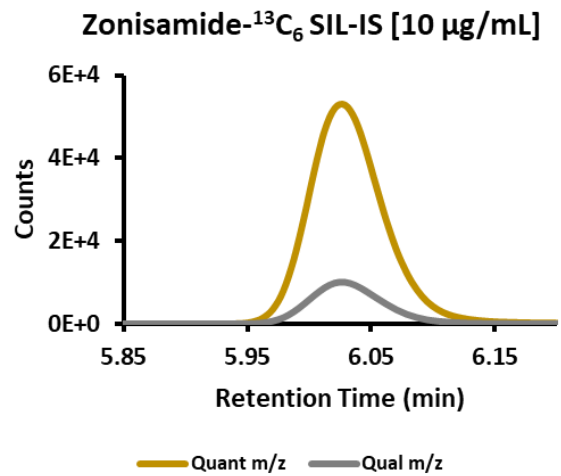
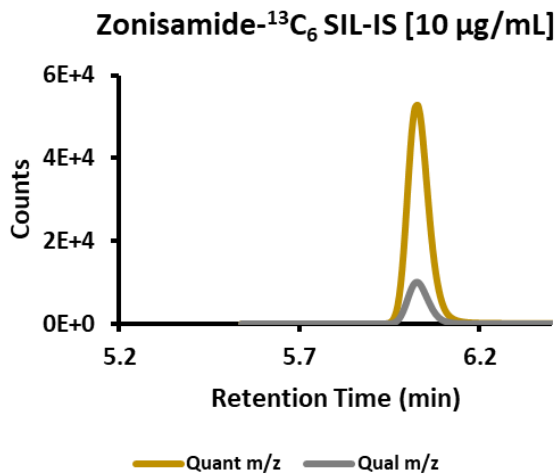
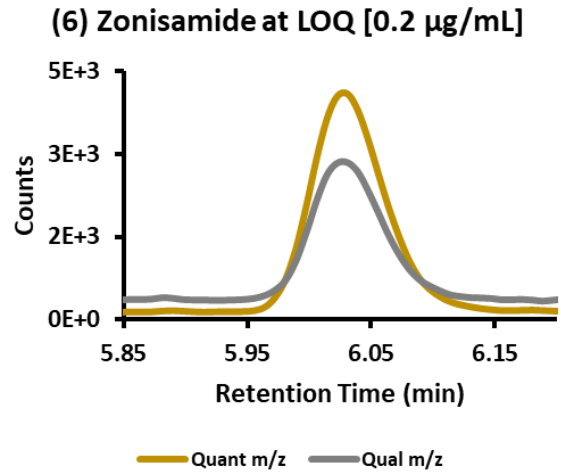
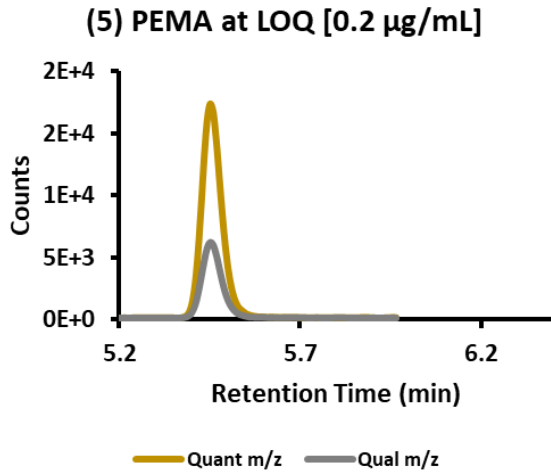
Gabapentin-<sup>13</sup>C<sub>3</sub> SIL-IS [10 µg/mL]

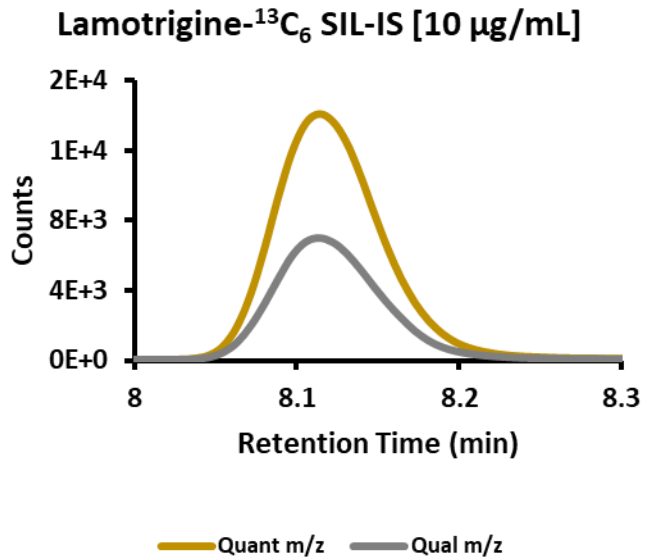
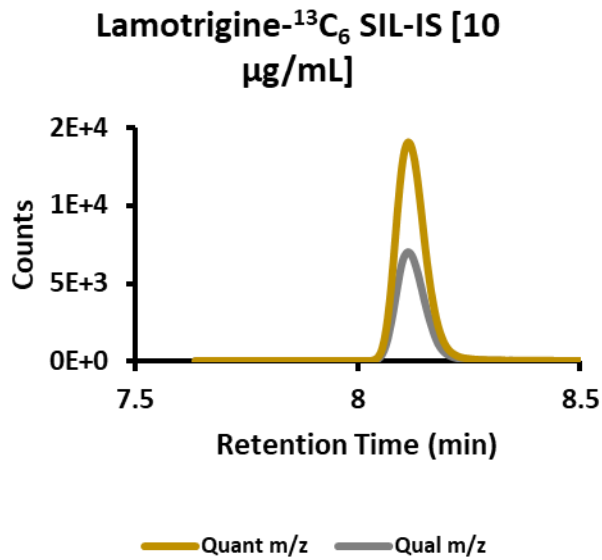
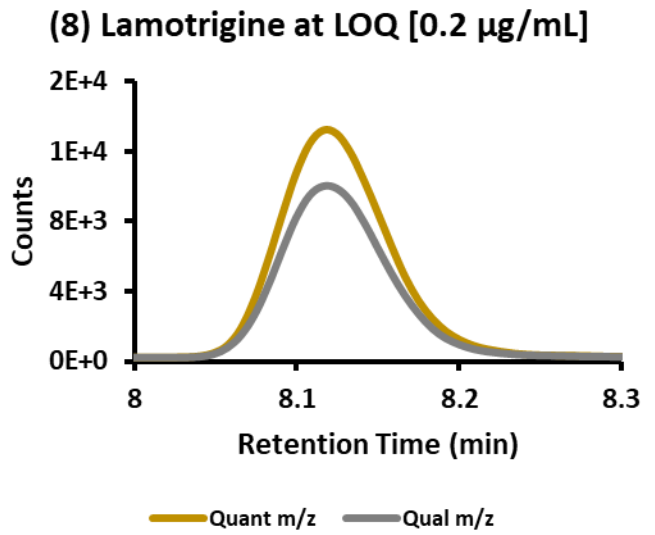
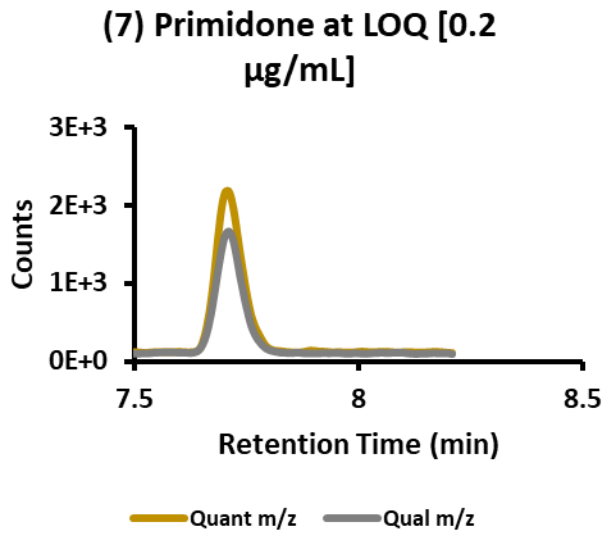


Zonisamide-<sup>13</sup>C<sub>6</sub> SIL-IS [10 µg/mL]

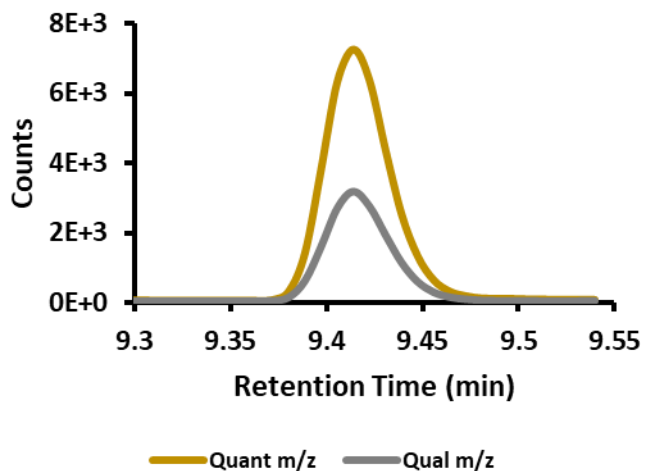




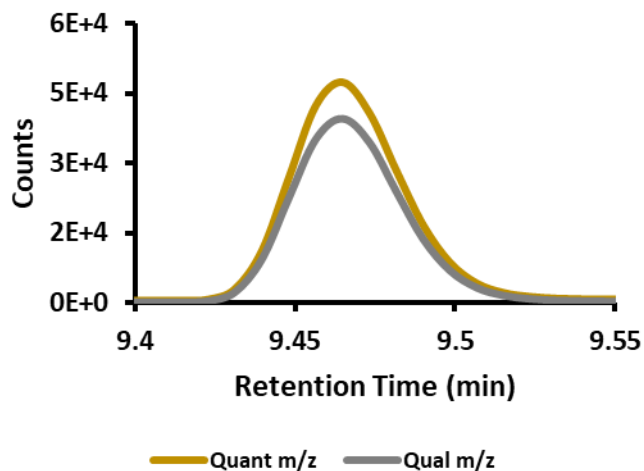




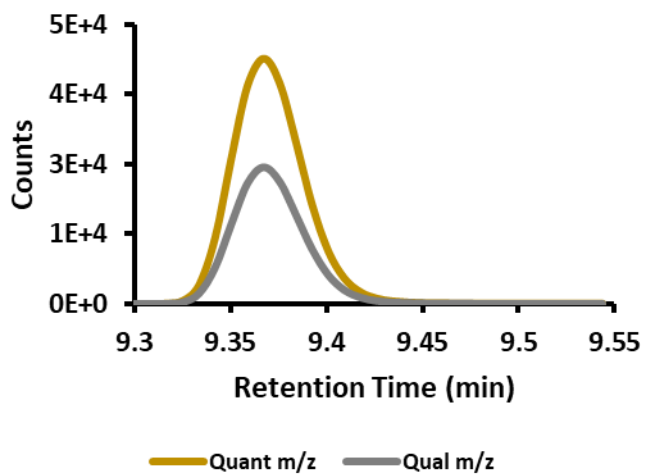
(9) Topiramate at LOQ [0.4 µg/mL]



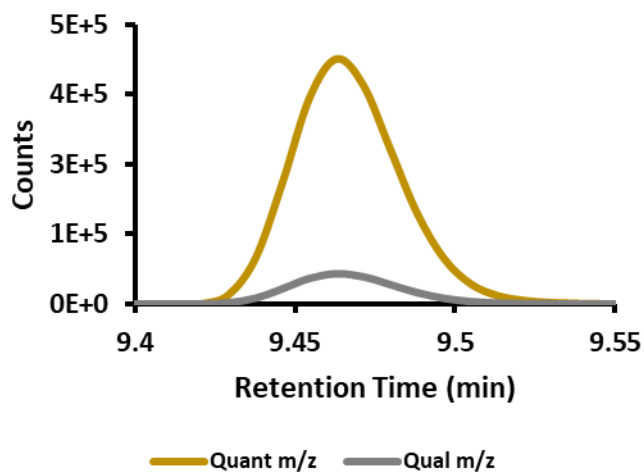
(10) MHD at LOQ [0.2 µg/mL]

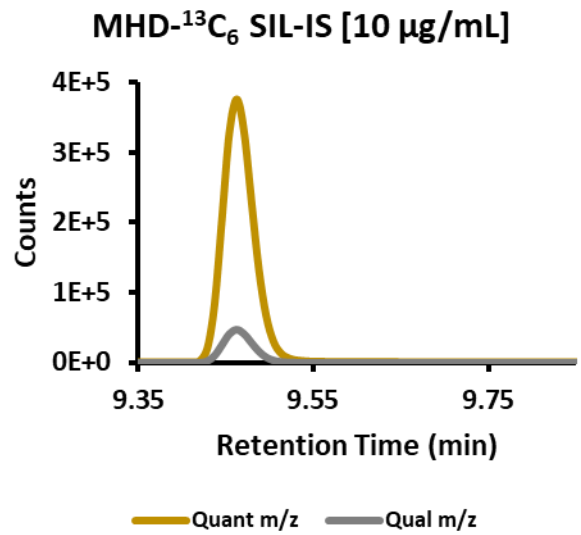
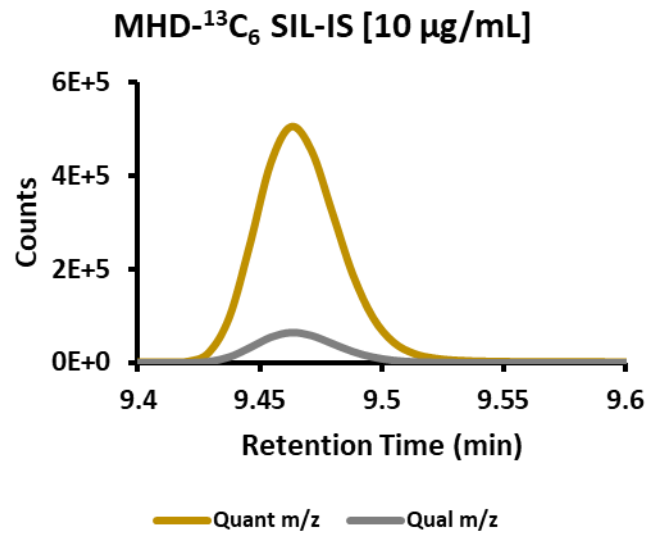
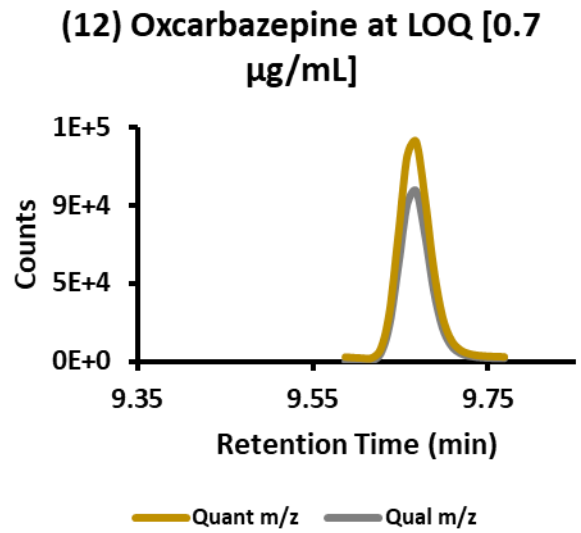
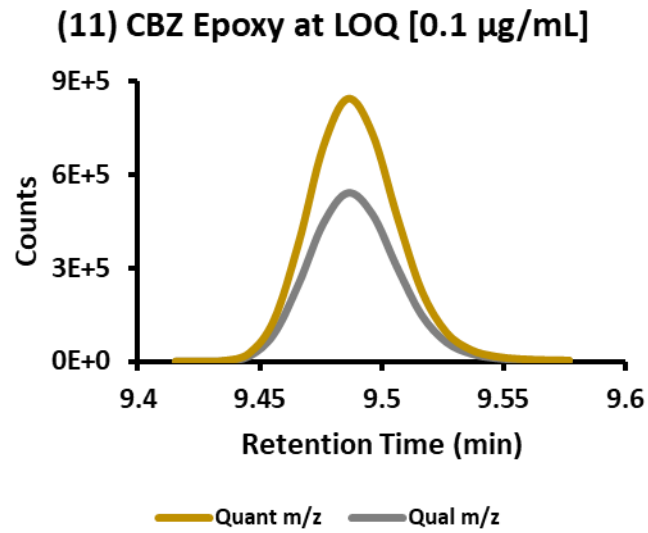


Topiramate-D<sub>12</sub> [10 µg/mL]

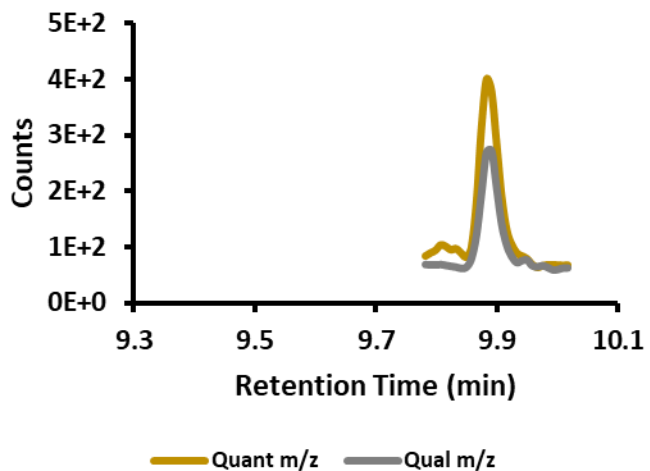


MHD-<sup>13</sup>C<sub>6</sub> SIL-IS [10 µg/mL]

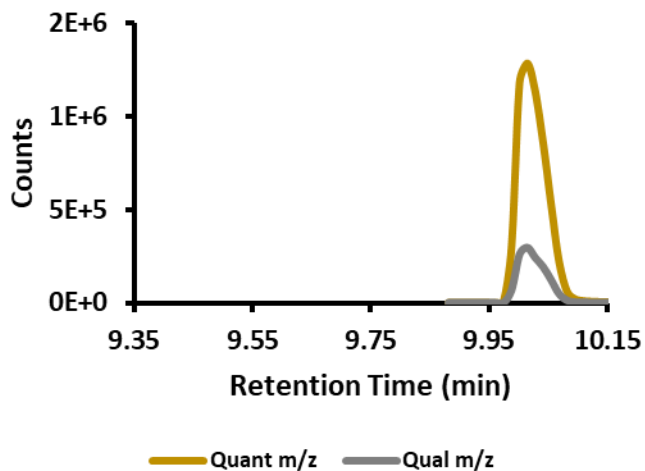




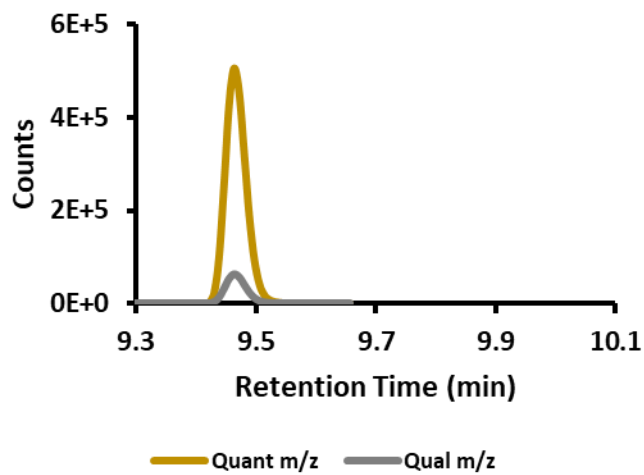
(13) Phenytoin at LOQ [0.8 µg/mL]



(14) CBZ at LOQ [0.1 µg/mL]



MHD-<sup>13</sup>C<sub>6</sub> SIL-IS [10 µg/mL]



MHD-<sup>13</sup>C<sub>6</sub> SIL-IS [10 µg/mL]

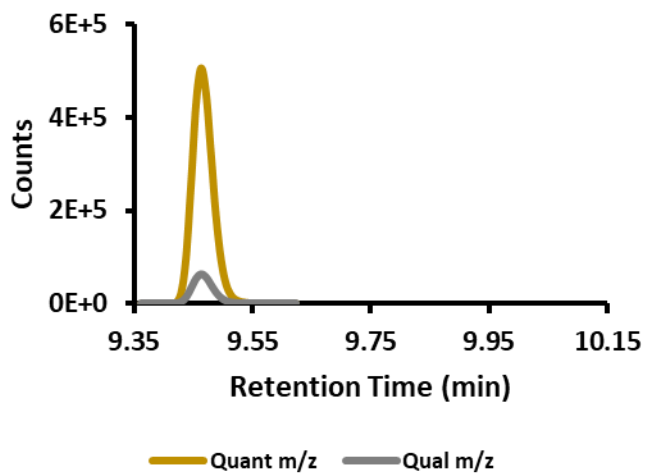


**Figure C.2.** AED between-day precision (A) and accuracy (B) analyses using LC-MS/MS. Samples ( $n = 5$  process replicates) were extracted and analyzed on 3 separate days. All data/replicates were combined for statistical analysis ( $n=15$  process replicates). (A) Precision is representative of experimental random error where the low, medium, and high averages for all AEDs were 5%, 3%, and 4%, respectively. The total average %CV for all AEDs was 4%. (B) Accuracy is representative of experimental systematic error where the low, medium, and high averages for all AEDs were 7%, 7%, and 9%, respectively. The total average %bias for all AEDs was 8%. Both random and systematic error is within the margin of error (15% as outlined in the FDA’s bioanalytical method validation guidelines) demonstrating the method’s precision and accuracy.

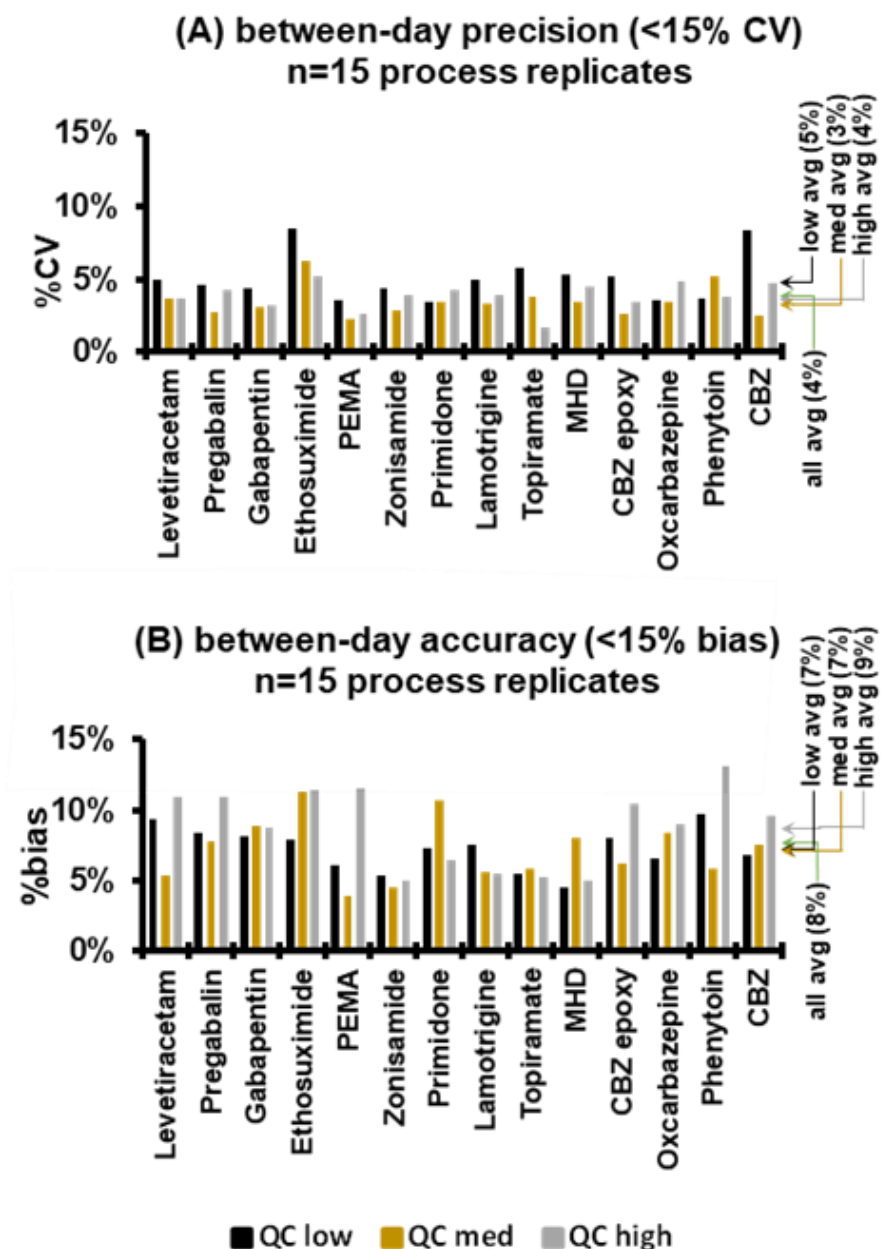


**Figure C.3.** (A) This was a blind study whereas the concentrations of the 21 patient samples received from the clinic were not given until LC-MS/MS analysis was finished. All patients underwent polypharmacy with multiple AEDs. LC-UV analysis was compared to LC-MS/MS analysis. (B) As an example of how LC-DTIMS-MS increases confidence in identifications, patient samples 3, 9, and 11 was highlighted to show CCS and drift time alignments of levetiracetam, lamotrigine, zonisamide, pregabalin, and MHD where the QCs ( $n = 3$ ) confirms the identifications of the patient samples ( $n = 1$ ). Standard error bars were used for QCs to demonstrate overlapping drift times where all 5 AEDs exhibit statistically significant drift times.

**(A) LC-MS/MS patient sample analysis**

| Patient Sample # | AEDs          | LC-UV ( $\mu\text{g/mL}$ ) | LC-MS/MS ( $\mu\text{g/mL}$ ) |
|------------------|---------------|----------------------------|-------------------------------|
| Patient 1        | Lamotrigine   | 12.2                       | 10.22                         |
|                  | Gabapentin    | NR                         | 6.47                          |
| Patient 2        | Lamotrigine   | 10.6                       | 4.96                          |
|                  | Levetiracetam | 32.3                       | 20.8                          |
| Patient 3        | Lamotrigine   | 5.80                       | 4.49                          |
|                  | Levetiracetam | NR                         | 20.7                          |
| Patient 4        | Lamotrigine   | 10.6                       | 8.02                          |
| Patient 5        | Lamotrigine   | 10.0                       | 8.04                          |
|                  | Levetiracetam | 61.5                       | 71.0                          |
| Patient 6        | Lamotrigine   | 14.2                       | 8.58                          |
|                  | Levetiracetam | 39.8                       | 52.1                          |
| Patient 7        | Lamotrigine   | 14.2                       | 11.7                          |
|                  | Levetiracetam | 39.8                       | 40.3                          |
| Patient 8        | Ethosuximide  | 145                        | 134.8                         |
|                  | Zonisamide    | 11.0                       | 5.94                          |
| Patient 9        | Levetiracetam | NR                         | 3.2                           |
|                  | Pregabalin    | NR                         | 1.75                          |
| Patient 10       | Ethosuximide  | 46.0                       | 44.2                          |
|                  | Lamotrigine   | NR                         | 5.18                          |
| Patient 11       | Zonisamide    | 51.0                       | 37.9                          |
|                  | Levetiracetam | NR                         | 43.9                          |
| Patient 12       | MHD           | NR                         | 19.3                          |
| Patient 12       | Lamotrigine   | 11.8                       | 6.66                          |
| Patient 13       | Lamotrigine   | 8.00                       | 5.74                          |
|                  | Zonisamide    | 14.0                       | 9.20                          |
| Patient 14       | Zonisamide    | 10.0                       | 6.35                          |
|                  | Carbamazepine | 4.00                       | 1.53                          |
| Patient 15       | MHD           | 24.0                       | 20.7                          |
|                  | Topiramate    | 17.2                       | 22.1                          |
| Patient 16       | Levetiracetam | < 3.00                     | 23.8                          |
| Patient 17       | Lamotrigine   | 32.7                       | 22.6                          |
|                  | Levetiracetam | 46.4                       | 39.7                          |
| Patient 18       | Lamotrigine   | < 1.00                     | < 1.00                        |
| Patient 18       | Levetiracetam | 37.7                       | 26.7                          |
|                  | Gabapentin    | 6.70                       | 4.03                          |
| Patient 19       | Ethosuximide  | 75.0                       | 73.9                          |
| Patient 20       | MHD           | 13.0                       | 10.5                          |
|                  | Gabapentin    | NR                         | 1.03                          |
| Patient 21       | MHD           | 39.0                       | 27.6                          |

**(B) LC-DTIMS-MS patient sample analysis**

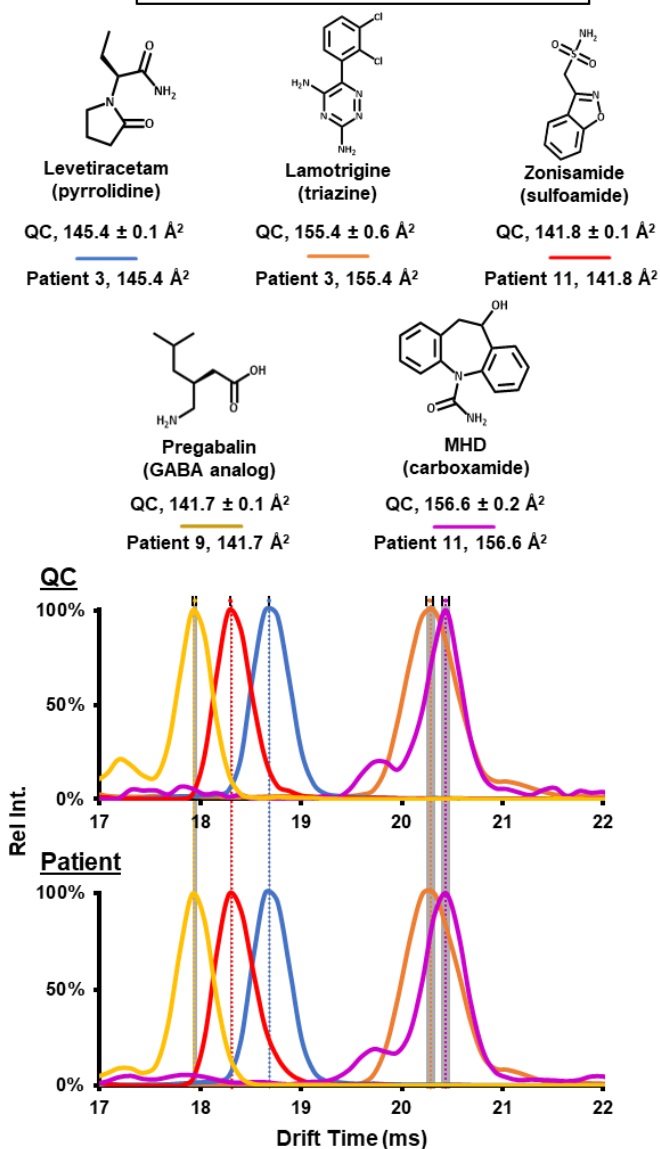


**Figure C.4.** Stability of AEDs in extracted serum at 4°C after 48 idle hours in autosampler ( $n = 3$  technical replicates).

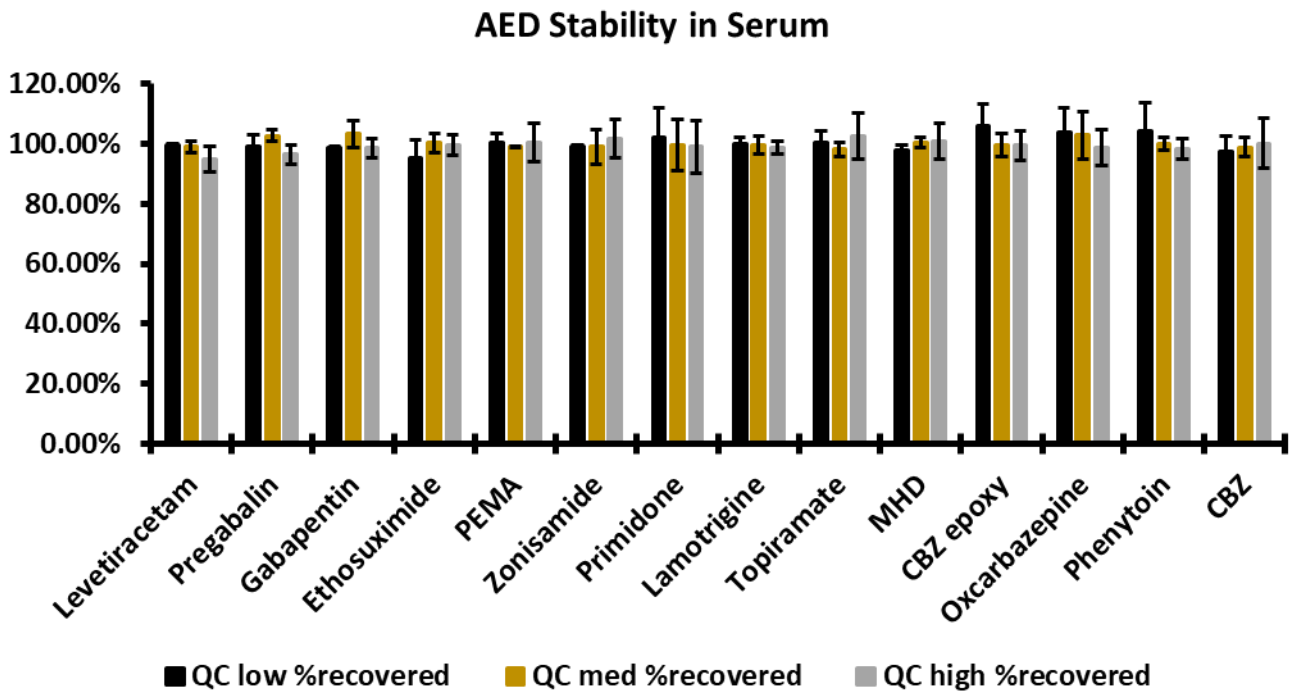




**Figure C.5.** Carry over of AEDs in extracted serum (n = 5 technical replicates). Carry over was determined by injecting an extracted negative sample after the QC high sample. The CLSI C62A recommendation is that the carryover limit should be the highest concentration that does not carry over to the negative sample at or above 25% of the QC low sample.<sup>1,2</sup> The FDA recommendation is 20%.<sup>3</sup>

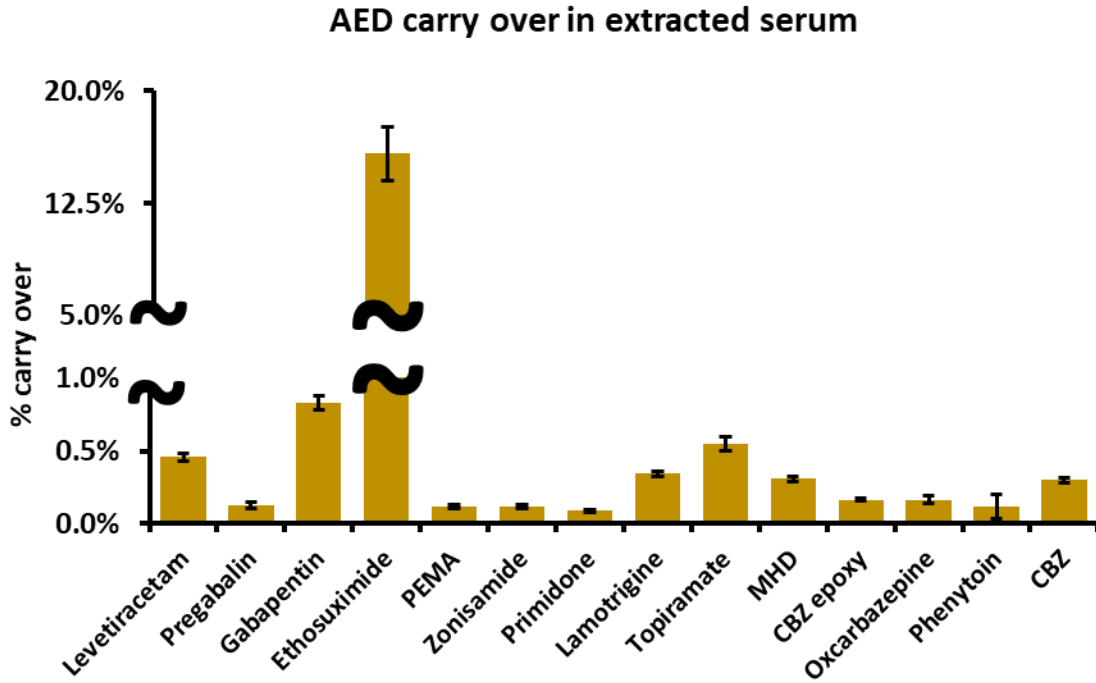


**Figure C.6:** Recovery and Matrix Effects Equations.

$$1) \% \text{Recovery} = \frac{\text{Peak Area (spike pre - extraction)}}{\text{Peak Area (spike post - extraction)}} \times 100$$

$$2) \% \text{Matrix effect} = \frac{\text{Peak Area (spike post - extraction)}}{\text{Peak Area (neat)}} \times 100$$

**Table C.1.** Serum 3rd party verified quality control (QC) material at low, medium, and high AED concentrations were purchased from UTAK Laboratories Inc, (Valencia, CA, USA).

| AED                   | ( $\mu\text{g/mL}$ ) |        |         |
|-----------------------|----------------------|--------|---------|
|                       | Low QC               | Med QC | High QC |
| Levetiracetam         | 5.00                 | 25.0   | 50.0    |
| Zonisamide            | 5.00                 | 25.0   | 50.0    |
| Topiramate            | 5.00                 | 15.0   | 30.0    |
| Lamotrigine           | 5.00                 | 15.0   | 30.0    |
| MHD                   | 5.00                 | 25.0   | 50.0    |
| Ethosuximide          | 15.0                 | 70.0   | 125     |
| Gabapentin            | 5.00                 | 15.0   | 30.0    |
| Pregabalin            | 5.00                 | 15.0   | 30.0    |
| Primidone             | 5.00                 | 15.0   | 30.0    |
| PEMA                  | 5.00                 | 15.0   | 30.0    |
| Carbamazepine         | 5.00                 | 15.0   | 30.0    |
| Carbamazepine Epoxide | 5.00                 | 15.0   | 30.0    |
| Oxcarbazepine         | 5.00                 | 15.0   | 30.0    |
| Phenytoin             | 5.00                 | 15.0   | 30.0    |

**Table C.2.** Linearity study concentrations and correlation coefficients ( $R^2$ ). These linearity calibrators were prepared in human drug free serum purchased from UTAK Laboratories Inc, (Valencia, CA, USA).

| AED           | Calibrator Concentration ( $\mu\text{g/mL}$ ) |      |      |      |      |      |      |      |      |      |      |      | $R^2$  |
|---------------|---|------|------|------|------|------|------|------|------|------|------|------|--------|
|               | 12  | 11   | 10   | 9    | 8    | 7    | 6    | 5    | 4    | 3    | 2    | 1    |        |
| Levetiracetam | 200   | 100  | 50.0 | 25.0 | 12.5 | 6.25 | 3.13 | 1.56 | 0.78 | 0.39 | 0.20 | 0.10 | >0.985 |
| Zonisamide    | 200   | 100  | 50.0 | 25.0 | 12.5 | 6.25 | 3.13 | 1.56 | 0.78 | 0.39 | 0.20 | 0.10 | >0.985 |
| Topiramate    | 100   | 50.0 | 25.0 | 12.5 | 6.25 | 3.13 | 1.56 | 0.78 | 0.39 | 0.20 | 0.10 | 0.05 | >0.985 |
| Lamotrigine   | 200   | 100  | 50.0 | 25.0 | 12.5 | 6.25 | 3.13 | 1.56 | 0.78 | 0.39 | 0.20 | 0.10 | >0.985 |
| MHD           | 200   | 100  | 50.0 | 25.0 | 12.5 | 6.25 | 3.13 | 1.56 | 0.78 | 0.39 | 0.20 | 0.10 | >0.985 |
| Ethosuximide  | 300   | 150  | 75.0 | 37.5 | 18.8 | 9.38 | 4.69 | 2.34 | 1.17 | 0.59 | 0.29 | 0.15 | >0.985 |
| Gabapentin    | 200   | 100  | 50.0 | 25.0 | 12.5 | 6.25 | 3.13 | 1.56 | 0.78 | 0.39 | 0.20 | 0.10 | >0.985 |
| Pregabalin    | 200   | 100  | 50.0 | 25.0 | 12.5 | 6.25 | 3.13 | 1.56 | 0.78 | 0.39 | 0.20 | 0.10 | >0.985 |
| Primidone     | 100   | 50.0 | 25.0 | 12.5 | 6.25 | 3.13 | 1.56 | 0.78 | 0.39 | 0.20 | 0.10 | 0.05 | >0.985 |
| PEMA          | 100   | 50.0 | 25.0 | 12.5 | 6.25 | 3.13 | 1.56 | 0.78 | 0.39 | 0.20 | 0.10 | 0.05 | >0.985 |
| Carbamazepine | 100   | 50.0 | 25.0 | 12.5 | 6.25 | 3.13 | 1.56 | 0.78 | 0.39 | 0.20 | 0.10 | 0.05 | >0.985 |
| CBZ Epoxy     | 50.0  | 25.0 | 12.5 | 6.3  | 3.13 | 1.56 | 0.78 | 0.39 | 0.20 | 0.10 | 0.05 | 0.02 | >0.985 |
| Oxcarbazepine | 100   | 50.0 | 25.0 | 12.5 | 6.25 | 3.13 | 1.56 | 0.78 | 0.39 | 0.20 | 0.10 | 0.05 | >0.985 |
| Phenytoin     | 50.0  | 25.0 | 12.5 | 6.3  | 3.13 | 1.56 | 0.78 | 0.39 | 0.20 | 0.10 | 0.05 | 0.02 | >0.985 |

**Table C.3.** Calibrator concentrations and correlation coefficients ( $R^2$ ). Calibrators are samples used for linearity and/or the calibration curve when analyzing patient samples. These calibrators were prepared in human drug free serum purchased from UTAK Laboratories Inc, (Valencia, CA, USA).

| AED           | Calibrator Concentration ( $\mu\text{g/mL}$ ) |     |    |     |      |     | $R^2$  |
|---------------|---|-----|----|-----|------|-----|--------|
|               | 6   | 5   | 4  | 3   | 2    | 1   |        |
| Levetiracetam | 60  | 30  | 15 | 7.5 | 3.8  | 1.9 | >0.985 |
| Zonisamide    | 60  | 30  | 15 | 7.5 | 3.8  | 1.9 | >0.985 |
| Topiramate    | 60  | 30  | 15 | 7.5 | 3.8  | 1.9 | >0.985 |
| Lamotrigine   | 60  | 30  | 15 | 7.5 | 3.8  | 1.9 | >0.985 |
| MHD           | 60  | 30  | 15 | 7.5 | 3.8  | 1.9 | >0.985 |
| Ethosuximide  | 200   | 100 | 50 | 25  | 12.5 | 6.3 | >0.985 |
| Gabapentin    | 60  | 30  | 15 | 7.5 | 3.8  | 1.9 | >0.985 |
| Pregabalin    | 60  | 30  | 15 | 7.5 | 3.8  | 1.9 | >0.985 |
| Primidone     | 60  | 30  | 15 | 7.5 | 3.8  | 1.9 | >0.985 |
| PEMA          | 60  | 30  | 15 | 7.5 | 3.8  | 1.9 | >0.985 |
| Carbamazepine | 60  | 30  | 15 | 7.5 | 3.8  | 1.9 | >0.985 |
| CBZ epoxy     | 60  | 30  | 15 | 7.5 | 3.8  | 1.9 | >0.985 |
| Oxcarbazepine | 60  | 30  | 15 | 7.5 | 3.8  | 1.9 | >0.985 |
| Phenytoin     | 60  | 30  | 15 | 7.5 | 3.8  | 1.9 | >0.985 |

**Table C.4.** The developed and validated RPLC-UV method was compared to VUMC’s pre-existing RPLC-UV method by parallel analysis of samples. The (-) indicates that the sample was not analyzed for the given AED.

| AED Parallel Samples Sample # | AED           | Expected (µg/mL) | LC - UV (µg/mL) | LC - MS/MS (µg/mL) | LC - UV (%bias) | LC - MS/MS (%bias) |
|-------------------------------|---------------|------------------|-----------------|--------------------|-----------------|--------------------|
| Parallel 1                    | Pregabalin    | 3.00             | -               | 2.50               | -               | -17%               |
|                               | Gabapentin    | 1.00             | -               | 1.18               | -               | 18%                |
| Parallel 2                    | Zonisamide    | 11.0             | 0.00            | 11.0               | -100%           | 0%                 |
|                               | Lamotrigine   | 2.00             | 2.40            | 2.30               | 20%             | 15%                |
|                               | Levetiracetam | 6.00             | 5.80            | 7.00               | -3%             | 17%                |
| Parallel 3                    | MHD           | 9.00             | 9.00            | 8.50               | 0%              | -6%                |
| Parallel 4                    | Pregabalin    | 11.0             | -               | 11.2               | -               | 2%                 |
|                               | Gabapentin    | 15.0             | -               | 13.8               | -               | -8%                |
| Parallel 5                    | Zonisamide    | 26.0             | 26.0            | 25.0               | 0%              | -4%                |
|                               | Lamotrigine   | 11.0             | 11.0            | 11.0               | 0%              | 0%                 |
|                               | Levetiracetam | 22.0             | 22.8            | 25.2               | 4%              | 15%                |
| Parallel 6                    | MHD           | 24.0             | 23.0            | 26.0               | -4%             | 8%                 |
| Parallel 7                    | Pregabalin    | 30.0             | -               | 29.6               | -               | -1%                |
|                               | Gabapentin    | 22.0             | -               | 21.9               | -               | 0%                 |
| Parallel 8                    | Zonisamide    | 50.0             | 50.2            | 52.7               | 0%              | 5%                 |
|                               | Lamotrigine   | 26.0             | 22.7            | 27.3               | -13%            | 5%                 |
|                               | Levetiracetam | 40.0             | 37.1            | 42.0               | -7%             | 5%                 |
| Parallel 9                    | MHD           | 45.0             | 45.0            | 50.0               | 0%              | 11%                |

References:

- (1) CLSI. Liquid Chromatography-Mass Spectrometry Methods; Approved Guidelines (C62-A). **2014**, No. 1-56238-977-7, pp 1-71.
- (2) Viswanathan, C. T.; Bansal, S.; Booth, B.; DeStefano, A. J.; Rose, M. J.; Sailstad, J.; Shah, V. P.; Skelly, J. P.; Swann, P. G.; Weiner, R. Quantitative Bioanalytical Methods Validation and Implementation: Best Practices for Chromatographic and Ligand Binding Assays. *Pharmaceutical Research*. **2007**, pp 1962–1973.
- (3) FDA. Guidance for Industry: Bioanalytical Method Validation. **2018**, No. FDA-2013-D-1020, pp 1-41.

## APPENDIX D

### Supporting Information for Chapter 4

#### Multidimensional Separations of Intact Phase II Steroid Metabolites Utilizing LC-Ion Mobility-MS

Don E. Davis, Jr.<sup>1</sup>, Katrina L. Leaptrot<sup>1</sup>, David C. Koomen<sup>1</sup>, Jody C. May<sup>1</sup>, Gustavo de A. Cavalcanti<sup>2</sup>, Monica C. Padilha<sup>2</sup>, Henrique M.G. Pereira<sup>2</sup>, and John A. McLean<sup>1</sup>

<sup>1</sup>Department of Chemistry, Center for Innovative Technology, Institute of Chemical Biology, Institute for Integrative Biosystems Research and Education, Vanderbilt-Ingram Cancer Center, Vanderbilt University, Nashville, Tennessee, United States

<sup>2</sup>Brazilian Doping Control Laboratory– LBCD – Chemistry Institute – Federal University of Rio de Janeiro – UFRJ, Rio de Janeiro, RJ, Brazil

#### *Comments on LC-IMS-MS instrument settings, data, and ion multiplexing data presented in this work*

In this supporting information, we provide tables for RPLC settings, source settings, DTIMS settings, figures for the novel/synthesized AAS investigated in human urine, LC-IMS-MS ion multiplexing, and conformational space analysis.

**Table D.1.** LC-IMS-MS parameters used to collect the steroid data in our work. Source settings for the Agilent Jet Stream ESI and chromatographic conditions were optimized specifically for this study using Agilent 1290 I (LC) and 6560 (DTIMS-MS) instruments.

| RPLC Settings    |                        |  |
|------------------|------------------------|--|
| Parameter        | Value                  | Units                                      |
| Column           | Waters ACQUITY BEH C18 | 2.1 x 75 mm (1.7 $\mu$ m)                  |
| Temperature      | 45                     | Celsius                                    |
| Injection Volume | 10                     | $\mu$ L                                    |
| Flow Rate        | 0.400                  | mL/min                                     |
| Mobile Phase (A) | H <sub>2</sub> O       | 1 mM ammonium formate/<br>0.1% formic acid |
| Mobile Phase (B) | MeOH                   | 1 mM ammonium formate/<br>0.1% formic acid |

| RPLC Settings |     |
|---------------|-----|
| Time (min)    | %B  |
| 0             | 45  |
| 1             | 45  |
| 9.5           | 70  |
| 10.5          | 100 |
| 12            | 100 |
| 13            | 45  |
| 15            | 45  |

| Source Settings                       |       |         |
|---------------------------------------|-------|---------|
| Parameter                             | Value | Units   |
| Gas Temp                              | 300   | Celsius |
| Drying Gas                            | 12    | L/min   |
| Nebulizer                             | 20    | psi     |
| Sheath Gas Temp                       | 300   | Celsius |
| Sheath Gas Flow                       | 12    | L/min   |
| Capillary Voltage (V <sub>Cap</sub> ) | 2000  | V       |
| Nozzle Voltage                        | 500   | V       |

| RPLC Settings |     |
|---------------|-----|
| Time (min)    | %B  |
| 0             | 50  |
| 1             | 50  |
| 5.5           | 100 |
| 7             | 100 |
| 8             | 50  |
| 10            | 50  |

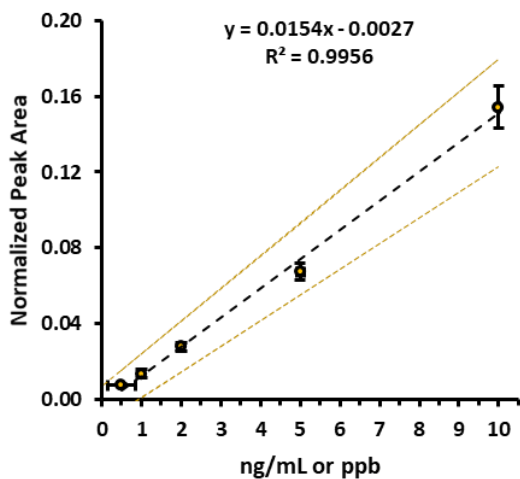
| DTIMS-MS Single Pulse Settings |         |                          |
|--------------------------------|---------|--------------------------|
| Parameter                      | Value   | Units                    |
| Mass Range                     | 50-1700 | m/z                      |
| Trap Fill Time                 | 20000   | $\mu$ s                  |
| Trap Release Time              | 180     | $\mu$ s                  |
| Frame Rate                     | 0.9     | Frames/sec               |
| IM Transient Rate              | 14      | IM Transients/Frame      |
| Max Drift Time                 | 60      | ms                       |
| TOF Transient Rate             | 600     | Transients/IM Transients |
| Drift Tube Entrance            | -1474   | V                        |
| Drift Tube Exit                | -224    | V                        |
| Rear Funnel Entrance           | -217.5  | V                        |
| Rear Funnel Exit               | -45     | V                        |

| DTIMS-MS Ion multiplexing Settings |         |                          |
|------------------------------------|---------|--------------------------|
| Parameter                          | Value   | Units                    |
| Mass Range                         | 50-1700 | m/z                      |
| Trap Fill Time                     | 3900    | $\mu$ s                  |
| Trap Release Time                  | 180     | $\mu$ s                  |
| Frame Rate                         | 0.9     | Frames/sec               |
| IM Transient Rate                  | 18      | IM Transients/Frame      |
| Max Drift Time                     | 60      | ms                       |
| TOF Transient Rate                 | 600     | Transients/IM Transients |
| Drift Tube Entrance                | -1474   | V                        |
| Drift Tube Exit                    | -224    | V                        |
| Rear Funnel Entrance               | -217.5  | V                        |
| Rear Funnel Exit                   | -45     | V                        |

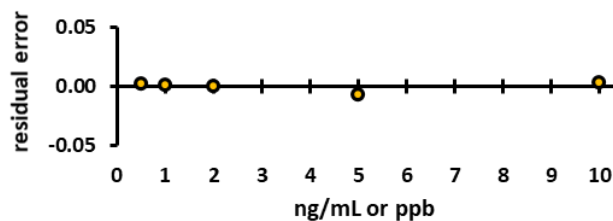


**Figure D.1.** Anabolic androgenic steroid investigated in human urine (top table). A calibration curve (left) showing the lower dynamic range from 0.5 ppb to 10 ppb with the gold dashed lines representing the 95% confidence interval. Standard error bars ( $n = 3$  intraday technical replicates) were used to demonstrate variation in both peak area and concentration. A table is provided to the right of the calibration curve to provide expected concentrations, normalized peak areas, standard deviations, calculated concentrations, and analytical figures of merit (e.g., precision by %CV, accuracy by %bias, and LOQ). Also, a residual error versus concentration plot was provided to evaluate the validity of the linear regression model.

| Analyte                          | LOQ (ng/mL) | Formula            | Exact m/z | Adduct         | Exp. m/z | Mass error (ppm) | IM drift time (ms) | CCS ( $\text{\AA}^2$ ) | CCS %diff standard vs sample |
|----------------------------------|-------------|--------------------|-----------|----------------|----------|------------------|--------------------|------------------------|------------------------------|
| Epi-THMT S3 (human urine sample) | 1           | $C_{20}H_{31}O_4S$ | 367.194   | $[M-H_2O-H]^-$ | 367.193  | -3.5             | 28.56              | 200.8                  | 0.3                          |



| [expected] (ppb) | normalized peak area | %CV  | [calculated] (ppb) | %bias |     |
|------------------|----------------------|------|--------------------|-------|-----|
| 0.5              | 0.0076               | 8.5% | 0.67               | -34%  | LOD |
| 1.0              | 0.0137               | 15%  | 1.06               | -6.4% | LOQ |
| 2.0              | 0.0279               | 7.6% | 1.99               | 0.7%  |     |
| 5.0              | 0.0673               | 6.6% | 4.55               | 9.1%  |     |
| 10               | 0.1541               | 7.2% | 10.2               | -1.8% |     |



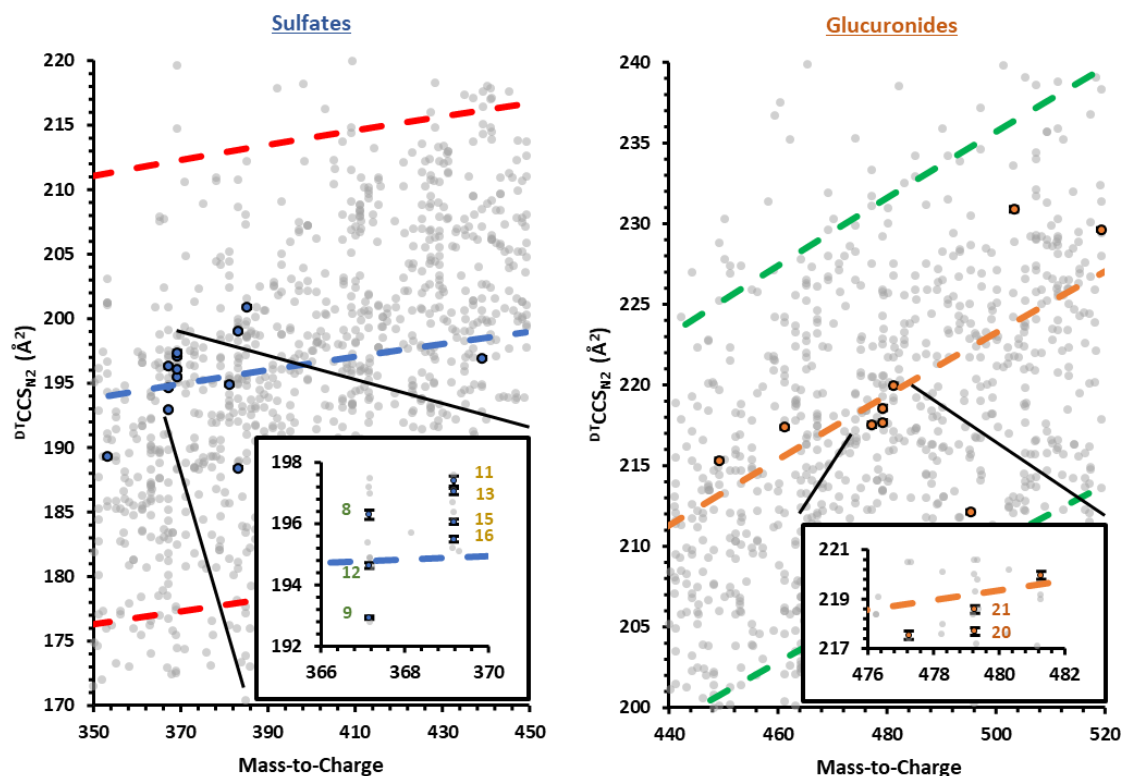


**Figure D.2.** Conformational space analysis showing CCS values for the phase II steroids investigated using LC-IMS-MS with neat standards. Included is a blue dashed trendline, fit to a power function, representing the best fit line of the sulfated data and the orange trendline represents glucuronide data. Also shown are red dashed lines representing  $\pm 10\%$  deviation from the best fit line for sulfated data and green dashed lines representing  $\pm 10\%$  deviation from the best fit line for glucuronide data. Measured phase II steroids were within  $\pm 10\%$  of the best fit line. Error bars represent standard errors and are for most values within the scale of the marker ( $n = 3$  technical replicates over 3 different days at  $5 \mu\text{g/mL}$ ). The gray data points represent  $\sim 5000$ - $9000$  entries from blank human urine.

Reference:

- (1) May, J. C.; Knochenmuss, R.; Fjeldsted, J. C.; McLean, J. A. Resolution of Isomeric Mixtures in Ion Mobility Using a Combined Demultiplexing and Peak Deconvolution Technique. *Anal. Chem.* **2020**, *92* (14), 9482–9492. <https://doi.org/10.1021/acs.analchem.9b05718>